Journal of Materials Chemistry C

ROYAL SOCIETY OF CHEMISTRY

REVIEW

View Article Online
View Journal | View Issue

Cite this: J. Mater. Chem. C, 2024, 12, 2662

Molecular design, synthesis, properties, and applications of organic triplet emitters exhibiting blue, green, red and white room-temperature phosphorescence

Mariia Stanitska, [a] Dmytro Volyniuk, [a] Boris Minaev, [bc] Hans Agren [c] and Juozas V. Grazulevicius *[a]

Received 8th December 2023,
Accepted 25th December 2023

DOI: 10.1039/d3tc04514e

rsc.li/materials-c

At room temperature, many organic compounds can emit light not only from singlet excited states but also from triplet excited states. This phenomenon is known as room-temperature phosphorescence (RTP). RTP has numerous potential applications in various areas, including industry, medicine, and daily life. RTP materials can be used in white light-emitting, memorising, sensing, bioimaging, semiconducting, 3D printing, microfluidic visualisation, quantum computing, X-ray detection, *etc.* They have advantages over fluorescent and metal-based phosphorescent materials. They are characterized by different emission spectra, longer lifetimes, and higher environmental sensitivity. However, challenges related to the tuning of emission colours, realization of dual emission, and meeting application-specific requirements still need to be overcome. Various molecular design strategies and synthetic approaches have been developed to overcome these challenges and to develop efficient RTP materials. This review article discusses recent advances in the synthesis and properties of RTP materials, focusing on emission colours and applications.

1. Introduction

With exponentially accelerating technological progress, the demand from humanity for efficient electroactive materials is rising since most modern electronic technologies that operate on integrated circuits require the utilization of semiconductors. A significant portion of semiconductors produced is employed in light-emitting devices, such as light-emitting diodes (LEDs) that have been proven to be the paramount light-generators in comparison to the alternative lighting sources. However, the most effective semiconductive materials up-to-date are inorganic, mainly consisting of silicon, germanium and binary compounds such as gallium arsenide.[1] The fabrication of semiconductors involves the usage of hazardous substances, *e.g.*, phosphorus, antimony, and arsenic.[2] This poses a bunch of challenges for researchers such as achieving high device performance by replacing the inorganic constituents of LEDs with organic ones, while minimizing environmental risks.

Researchers around the world try to make organic electroactive compounds compatible with inorganic ones in terms of efficiency. The main problem with organic light-emitting materials arises from spin-statistics: in simple fluorescent materials, emission can occur from only 25% of the formed excited states. The appealing solution to the problem was introduced by Forrest *et al.* in 1998[3] when they employed a platinum-centred phosphorescent organic complex in an electroluminescent device, thus taking a giant leap forward in lighting technology. Phosphorescent complexes usually consist of organic ligands that are coordinated by central heavy metal atoms, such as iridium, copper, platinum, *etc.* The presence of a transition metal makes phosphorescent emitters advantageous, as it enables the harvesting of 100% of the formed excited states. Strong spin–orbit coupling that is induced by a heavy metal atom facilitates intersystem crossing and promotes the harvesting of triplet excitons that are usually non-emissive in pure organic compounds. However, the presence of transition metal atoms in the molecules of emitters is quintessential and, at the same time, the most unwanted. Heavy metals such as iridium are expensive. Most of them, including copper and chromium, are environmentally unfriendly to the utmost degree. Once a sufficient amount of a compound containing such a metal is released into the environment, it disrupts the natural synthetic pathways of many bioactive compounds due to the strong complexing ability of the metal.[3] Thus, the development of organic compounds with the ability to "activate" dark triplet excitons has appeared to be the major focus of research.

[a] Department of Polymer Chemistry and Technology, Kaunas University of Technology, Barsausko 59, LT-51423, Kaunas, Lithuania. E-mail: juozas.grazulevicius@ktu.lt
[b] Bohdan Khmelnytsky National University of Cherkasy, Ukraine
[c] Department of Physics and Astronomy, Uppsala University, SE-751 20 Uppsala, Sweden

Thermally activated delayed fluorescence (TADF) allows gathering 75% of "dark" triplet excitons *via* non-radiative internal conversion of triplet excited states to singlet ones (reverse intersystem crossing[4]). However, this is not the only way to exploit triplet excitons in pure organic compounds. Room-temperature phosphorescence (further abbreviated as RTP) is another excellent mechanism of complete utilization of electro-generated excited states.[5]

When discussing RTP and TADF, it is important to differentiate between the various interpretations of the phosphorescence and luminescence phenomena. Throughout history, the term "phosphorescence" has been used to describe several mechanisms with distinct physical origins. The word "phosphorescence" comprises a distinction between long-lasting afterglow and fast emission (fluorescence) in a general optical sense. In such a phenomenological context, the term "phosphorescence" is still often used to describe different mechanistic photo-processes in adjacent fields of physics and chemistry. The distinction based on the lifetime of the fast and slow emission in solid-state physics concerning the luminescence of inorganic and organic materials leads to the "phosphorescence" notion assignment to electronic mechanisms of a completely different physical nature.[6] The long-lasting emission of inorganic solids is related to the trapping of excitons by lattice impurities, while organic RTP and TADF of organic compounds are determined by spin selection of spontaneous emissive and non-radiative processes. Organic RTP as well as a more general low-temperature phosphorescence phenomenon refer to the radiative transition from the first excited triplet (T_1) state to the ground singlet (S_0) state of a photo-chemically stable molecule. This spin-forbidden $T_1 \rightarrow S_0$ triplet–singlet emission typically has a lower transition moment and a rate constant *ca.* a million times lower than that of the spin-allowed S_1–S_0 transition, *i.e.*, fluorescence.

The growing research interest in organic compounds exhibiting RTP is depicted in Fig. 1a. Although TADF still remains the paramount strategy to utilize triplet excitons that has resulted in a number of scientific publications exceeding those related to RTP, the progress in the investigations of the RTP phenomenon is more rapid. For example, in 2019 RTP publications covered barely one-third of the number of papers about emission from triplet excitons whereas in 2020, this number increased up to one half. It is evident from Fig. 1b that in 2020 and in 2021, the number of publications on TADF increased by 1.09 and 1.16 times, respectively, while the number of articles on RTP increased by 1.5 times (here dividing the number of publications from the current year by the number from the previous year).

There are review articles on organic materials exhibiting RTP either covering a wide range of structural peculiarities and utility areas, or discussing narrow topics such as the work of metal-free polymer-based materials,[7] chiral organic materials[8] and co-crystals exhibiting RTP,[9] as well as boron-containing RTP compounds.[10] Despite the fact that the emission colours of organic compounds exhibiting RTP can significantly impact their potential applications, there is a lack of literature analysing and classifying them based on the emission colours. In this review, we have categorized the latest and most effective organic emitters exhibiting RTP based on the colour of their phosphorescence. Only low-molar-mass purely organic RTP compounds are discussed, excluding polymers, metalorganic complexes and quantum dots. We cover both theoretical and experimental approaches used for the development of organic RTP compounds, exhibiting blue, green, red, and white emissions. We also briefly discuss their potential applications.

2. Theory of room-temperature phosphorescence

The theoretical analysis of phosphorescence requires adiabatic calculations of the S and T excited states' structure and electronic wave functions with an obligatory account of internal magnetic interactions (spin–orbit coupling, SOC). Very often, it is sufficient to account for SOC through perturbation theory,[6,12] at least for the $T_1 \rightarrow S_0$ spontaneous emission lifetime estimation. For calculations involving non-radiative transition rates and quenching channels, the electronic–vibrational and spin–vibronic couplings should be taken into account as additional perturbations. The quadratic response (QR) formalism in terms of the Dalton code[11] is often used now in quantum-chemical calculations of phosphorescence.[6]

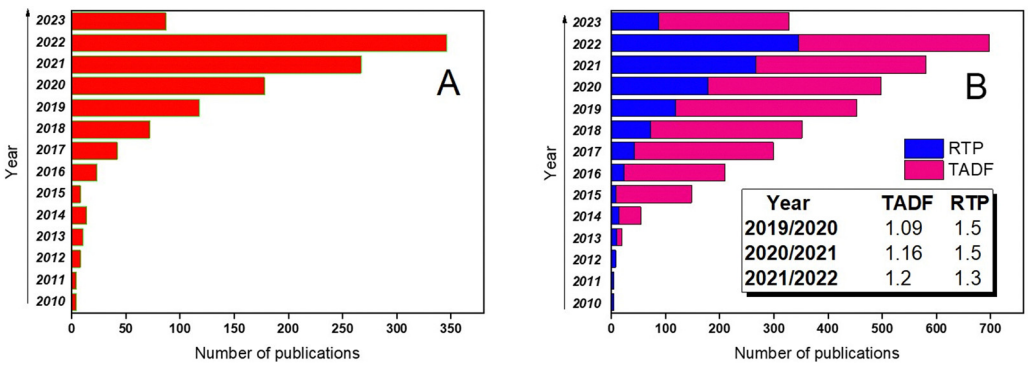

Fig. 1 (a) Progress in RTP scientific papers in the 2010–2023 timeframe and (b) comparative progress in TADF and RTP scientific papers in the same timeframe. Adapted from the Scopus database.

The phosphorescent T_1–S_0 transition can acquire the dipole activity by "intensity borrowing" from the spin-allowed S_0–S_n and T_1–T_m transitions calculated under the general nonrelativistic Born–Oppenheimer approximation[6] *via* spin–orbit coupling perturbation.

The RTP definition being applied until recent time resembles a "delayed luminescence that persists after the removal of the excitation source".[6] But according to the modern IUPAC rule, a significant number of processes of delayed luminescence of inorganic metal salt semiconductors should be excluded from our scope, even though they are considered originally as producing real genuine phosphorescence.[11] Several luminescence delay processes can follow the accumulation of the photochemical reaction products, thus tracking the chemical kinetics of photo-transformations. This luminescence delay could be connected with exciton migration between traps in crystals and does not depend on spin prohibition for optical transition. The white phosphorus in the moist air can be slowly oxidized to make it luminescent; such long-persistent emission erroneously contributed to the origin of the term "phosphorescence", although it has nothing in common with the modern RTP notion. Thus, the quite general RTP phenomenon of molecular spectroscopy was fallaciously connected with the particular inorganic reaction of slowly oxidized and glowing white phosphorus. In doped metal sulphides and some heated minerals, the electron–hole recombination in the p–n junctions of these semiconductors, which leads to long-lasting emission, has nothing in common with molecular phosphorescence.

According to the modified Jablonsky diagram (Fig. 2a), the lowest-lying triplet excited molecular state (T_1) could be populated through the sequence of the following processes:

(1) the starting incident UV light absorption ($S_0 \rightarrow S_k$) leads to the resonance excitation of a highly excited S_k state followed by

(2) a fast internal conversion (IC) to the lowest singlet excited state (S_1) with the rate constant (k_{IC}) which is typically high ($k_{IC} > 10^{12}$ s^{-1}) for numerous fluorophores; the k_{IC} rate constant usually follows the so-called Kasha rule, which posits that fluorescence emission ($S^* \rightarrow S_0$) more frequently originates from the S_1 state;

(3) additionally, the nonradiative transition $S_1 \sim \rightarrow T_1$ called intersystem crossing (ISC) produces the T_1 state population with the k_{ISC} rate constant;

(4) the ISC between the higher-lying singlet (S_k) and triplet (T_n) states followed by the subsequent internal conversion (T_n–T_1) with a high k_{IC} rate constant in some molecules could also lead to the T_1 state population and to the subsequent phosphorescent emission.

(5) the fluorescence channel ($S_0 \rightarrow S_k$) with the rate constant (k_f) is the main radiative process that competes with the $S_1 \sim \rightarrow T_1$ intersystem crossing k_{ISC} rate of relaxation leading to T_1 state production.

(6) besides such T_1 triplet state optical pumping, the lowest triplet can be produced by an electric current through an organic semiconductor solid as a result of electron–hole recombination in specially fabricated organic light-emitting diodes (OLEDs).

(7) after the optical or electrical T_1 state population, the nonradiative $T_1 \sim \rightarrow S_0$ relaxation (k_{nr}) rate strongly competes with the phosphorescent $T_1 \rightarrow S_0$ radiation (k_p) being dependent on temperature, crystal packing and vibrational modes.[11] The $T_1 \rightarrow S_0$ emissive transition is spin forbidden according to the electric dipole selection rule that renders the phosphorescence process less probable. This makes phosphorescence less intense than the fast spin-allowed fluorescent emission in pure organic fluorophores. For the nonradiative ISC relaxation $T_1 \sim \rightarrow S_0$, the electron–vibrational coupling plays a much more crucial role than for spontaneous phosphorescent light emission. The late ISC process strongly depends on the temperature and aggregation form of the environment (much more temperature dependent than the $S_1 \sim \rightarrow T_1$ intersystem crossing having a smaller energy gap). Thus, for the ISC relaxation $T_1 \sim \rightarrow S_0$ process the spin prohibition is not as severe as for light emission being of a different physical origin. Spin prohibition is based on Pauli's exclusion principle and the ISC rate still follows the general quantum mechanical trend and obeys the spin conservation law. Apparently, an additional SOC perturbation is necessary in both processes to violate spin selection since SOC induces S–T mixing. Non-radiative processes are more dependent on the rigidity of a large molecular environment around the particular phosphorescent chromophore and the vibrational activity of many degree of freedom including many phonons. Radiative transitions are "more localized" depending on the molecular symmetry point group

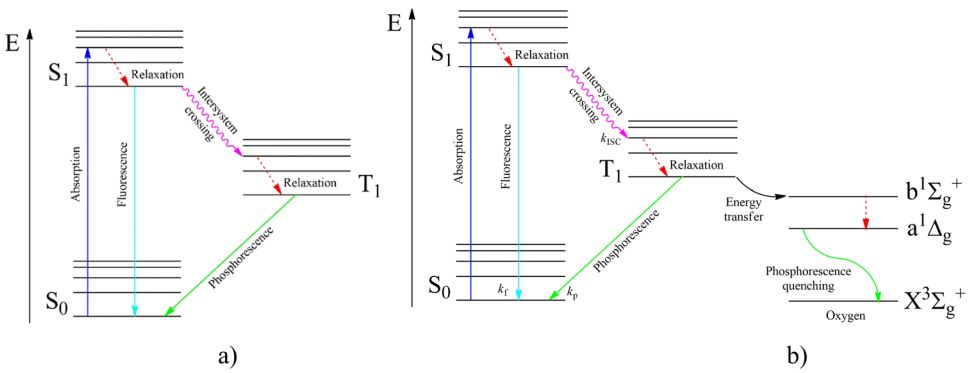

Fig. 2 Jablonsky diagram of fluorophores in an inert atmosphere (a) and in the presence of oxygen (b).

and local electronic wave functions. Spin–lattice relaxation and ISC processes provide vibrational energy flow and embrace many structural variables. Much more spin–vibronic perturbations are involved in ISC calculations than in radiative T–S transition calculations; thus, the selection rules for ISC relaxation are less severe. Both ''activating'' and ''promoting'' vibrational modes participate in the non-radiative energy flow during ISC processes. Taking them into account, one can see much greater possibility to add new SOC perturbations in order to reduce restrictions in the spin selection rule for the ISC transitions. SOC perturbations for radiative T–S transitions are much more limited by the smaller number of electronic and vibrational parameters.

In Fig. 2b, we present the influence of dissolved molecular oxygen on the photophysics of organic luminophores which shows blue or green phosphorescence; the T_1 state energy is larger than 1.63 eV, which is the second singlet state energy level of oxygen $O_2(^1\Sigma_g^+)$. The first excited singlet oxygen state $O_2(^1\Delta_g)$ level lies 0.98 eV above the ground triplet state $O_2(^3\Sigma_g^-)$. Paramagnetic triplet oxygen in the ground $O_2(^3\Sigma_g^-)$ state can effectively quench phosphorescence by colliding with the triplet-excited T_1 organic molecule in a solvent; the process is limited by diffusion since it is not forbidden by the spin selection rule. The energy transfer to the singlet excited $O_2(^1\Sigma_g^+)$ oxygen with simultaneous $T_1 \sim \rightarrow S_0$ quenching of the luminophore is a spin-allowed process

$$T_1\,(\uparrow\uparrow) + O_2(^3\Sigma_g^-)\,(\downarrow\downarrow) \rightarrow S_0\,(\uparrow\downarrow) + O_2(^1\Sigma_g^+)\,(\uparrow\downarrow)$$

since the total spin is zero for the reactants and products after collision. Quenching of triplet organic molecules and their phosphorescence by triplet oxygen from the air is well established through numerous experiments and strongly depends on the air pressure.[5,34] Nitrogen purge or oxygen out-pumping is widely used in phosphorescence studies.[34] The driving force for RTP quenching by triplet oxygen is determined by electronic exchange interactions in the collision complexes between two triplet molecules $T_1 + O_2(^3\Sigma_g^-)$. It simply follows from the above equation for the T_1 state quenching (relaxation to the ground S_0 state); one needs to exchange two spins between two molecules. Such a simple trick implies (in the quantum mechanics language) the necessity to calculate an exchange integral

$$(iu|\pi_x\pi_y) = \iint \psi_i^*(1)\psi_u(1)\left(e^2/r_{1,2}\right)\pi_{g,x}^*(2)\pi_{g,y}(2)\mathrm{d}v_1\mathrm{d}v_2, \quad (1)$$

which determines the rate of T_1 state quenching by O_2. Here, the $i \rightarrow u$ excitation determines the T_1 state wave function and $\pi_x\pi_y$ are degenerate MOs of the oxygen open shell in the ground $^3\Sigma_g^-$ state.[6,12]

The singlet–singlet internal relaxation in oxygen $O_2(^1\Sigma_g^+) \rightarrow O_2(^1\Delta_g)$ is very fast and UV excitation of the luminophore often leads to the singlet oxygen $O_2(^1\Delta_g)$ production which being very reactive can oxidize the singlet S_0 ground-state of organic molecules. In contrast to atmospheric oxygen $O_2(^3\Sigma_g^-)$, which shows sluggish chemical reactivity in the absence of fire (and radicals), the singlet oxygen $O_2(^1\Delta_g)$ molecule has no spin restrictions for interaction with diamagnetic organic substances.

Spin quantization and theoretical backgrounds of the Jablonsky diagram

All-electronic wave functions as solutions of the nonrelativistic Schrödinger equation for a molecule under Born–Oppenheimer approximation should be the eigen-functions of the total spin operator $\hat{\vec{S}} = \sum_i \hat{\vec{s}}_i$, where $\hat{\vec{s}}_i$ represents the single-electron Pauli matrices for the ith electron.[5]

$$\hat{s}_x = \frac{\hbar}{2}\begin{pmatrix}0 & 1\\ 1 & 0\end{pmatrix},\ \hat{s}_y = \frac{-i\hbar}{2}\begin{pmatrix}0 & 1\\ -1 & 0\end{pmatrix},\ \hat{s}_z = \frac{\hbar}{2}\begin{pmatrix}0 & 1\\ 0 & -1\end{pmatrix}$$

The single-electron Pauli functions $\alpha = \begin{pmatrix}1\\0\end{pmatrix}$ and $\beta = \begin{pmatrix}0\\1\end{pmatrix}$ are eigen-functions of the $\hat{s}_z$ and $\hat{\vec{s}}^{\,2} = \hat{s}_x^2 + \hat{s}_y^2 + \hat{s}_z^2$ operators. In a many-electron molecule, the total wave function satisfies the following equations for the total spin $\hat{\vec{S}}$ operator (of its square and z-projection operators)

$$\begin{aligned}\hat{\vec{S}}^2\Psi &= S(S+1)\hbar^2\Psi\\ \hat{S}_z\Psi &= M_s\hbar\Psi\end{aligned} \quad (2)$$

For one electron, eqn (2) describes the doublet state ($S = 1/2$, M_s is equal to $1/2$ and $-1/2$ for the α and β eigen-functions, respectively). In a more general case, S is the total spin quantum number that could be equal to zero $S = 0$ for the singlet state and $S = 1$ for the triplet state in the typical organic molecule with an even number of electrons. The main feature of the triplet (T) state is that it consists of three spin sublevels (T^x, T^y, and T^z) which are analogous to eigenstates with different M_s quantum numbers ($M_s = 0$ and ±1). The latter is typical for atoms and transition metal complexes with high spatial symmetry and degenerate irreducible representations, where three Cartesian axes are almost equivalent. In organic molecules with low symmetry and the absence of degeneracy, the three Cartesian axes are specifically connected with the molecular frame and determine the so-called zero-field splitting spin sublevels.[6] They are

$$\begin{aligned}T^z &= \frac{1}{\sqrt{2}}(\alpha^1\beta^2 + \alpha^2\beta^1) = T^0;\\ T^x &= \frac{1}{\sqrt{2}}(\beta^1\beta^2 - \alpha^1\alpha^2) = \frac{1}{\sqrt{2}}(T^{-1} - T^1);\\ T^y &= \frac{i}{\sqrt{2}}(\beta^1\beta^2 + \alpha^1\alpha^2) = \frac{1}{\sqrt{2}}(T^{-1} + T^1);\end{aligned} \quad (3)$$

where T^0, $T^1 = \alpha^1\alpha^2$, and $T^{-1} = \beta^1\beta^2$ are quantum numbers of dipole moments. Digits 1 and 2 at the α and β functions denote the spin variables of the first and second electrons; their exact kinematic nature is unknown, but the numeration of electron coordinates is still necessary. The main peculiarities of the Jablonsky scheme can be explained with the effective one-electron approach based on the molecular orbital (MO) method under the self-consistent field (SCF) approximation.[11] Thus, the S and T excited states can be presented by their open shells with the two-electron wave functions $^1\Psi_S = \Psi_+\Omega_-$ and $^3\Psi_T = \Psi_-\Omega_+$, respectively.[6] Here, the total wave functions are shown as

products of the spatial ($\Psi_{\pm}$) and spin ($\Omega_{\mp}$) parts; the signs refer to the permutation symmetry

$$\Psi_{\pm} = \frac{1}{\sqrt{2}}(\psi_i^1\psi_u^2 \pm \psi_i^2\psi_u^1) \text{ and } \Omega_{-} = \frac{1}{\sqrt{2}}(\alpha^1\beta^2 - \alpha^2\beta^1);$$
$$\Omega_{+} = \frac{1}{\sqrt{2}}(\alpha^1\beta^2 + \alpha^2\beta^1) \quad (4)$$

Ψ_+ and Ω_- represent symmetric and antisymmetric wave functions, respectively, with respect to the permutation of two-electron coordinates;[11] their product provides the singlet excited state produced by $\psi_i \rightarrow \psi_u$ excitation. This could be the highest occupied molecular orbital (HOMO) ψ_i and the lowest unoccupied molecular orbital (LUMO) ψ_u, in the typical example of the S_1 fluorescent state. All triplet state spin functions, eqn (3), are symmetric with respect to the permutation of two electrons. Thus, the total products $T = \Psi_-\Omega_+$ are antisymmetric with respect to the permutation; it means that this total wave function changes sign with the permutation of two electrons, as is required by the Pauli principle.[6] The same requirement applied to the singlet state leads to wave functions $S = \Psi_+\Omega_-$ also including the ground S_0 state with the closed-shell orbital $\Psi_+ = \psi_i^1\psi_i^2$ structure. Molecular symmetry point groups imply additional restrictions on the possible types of spatial wave functions; excited electronic states of the $\psi_i \rightarrow \psi_u$ type, which belong to the same irreducible representation as the $\psi_i \rightarrow \psi_u$ excitation, can be mixed by the configuration interaction (CI). However, this complication does not influence the general restrictions (1)–(4) implied by Pauli's exclusion principle and antisymmetric requirement with respect to the permutation of any two electronic coordinates.

In the framework of the electric-dipole approximation, the S–T transitions are strictly forbidden since the transition dipole moment is equal to

$$M_{S-T} = \langle \Psi_+\Omega_- | M | \Psi_-\Omega_+ \rangle = 0. \quad (5)$$

Integration by spatial variables in eqn (5) with the electric dipole operator $M = e(r_1 + r_2)$ produces zero results since this operator is symmetric to permutation; besides this, the S and T spin functions are orthogonal $\langle \Omega_- | \Omega_+ \rangle = 0$. Not only spin properties but also orbital selection produce this "double" forbiddance of the S–T transitions. Thus, it is very difficult to overcome such prohibition of phosphorescence emission. Weak SOC in organic molecules can induce essential perturbations in electronic wave functions (3) and (4) if the orbital parts of the S and T states differ in their MO spatial orientation like π and σ (or n-lone pair) orbitals. For example, the ground state $^1\Psi_S = \Psi_+\Omega_-$ with the closed-shell structure $\Psi_+ = \psi_i^1\psi_i^2$ and the $^3(n\pi^*)$ triplet $^3\Psi_T = \Psi_-\Omega_+$ state (where i is the HOMO n orbital) are mixed by the SOC operator $\hat{H}_{SO} = \sum_{i,A} \varsigma_A \vec{l}_{i,A}\vec{s}_i$. The wave function for two electrons can be presented in the following form:

$$\hat{H}_{SO} = \sum_A \varsigma_A(\vec{l}_{1,A}\vec{s}_1 + \vec{l}_{2,A}\vec{s}_2)$$
$$= \frac{1}{2}\sum_A \varsigma_A[(\vec{l}_{1,A} + \vec{l}_{2,A})(\vec{s}_1 + \vec{s}_2) + (\vec{l}_{1,A} - \vec{l}_{2,A})(\vec{s}_1 - \vec{s}_2)], \quad (6)$$

Here ς_A is a SOC constant for the valence shell of atom A, $\vec{l}_{i,A}$,$\vec{s}_i$ represent the orbital and spin angular momenta for the i-th electron, respectively. Eqn (6) includes artificial separation of the SOC operator into two parts: one being symmetrical with respect to permutation of two electrons, which can mix triplet states, and the other – is antisymmetric. The latter can mix S_0 and T(nπ*) states, each including different permutation symmetry for their orbital and spin functions. Thus, the SOC matrix element (ME) $\langle ^1\Psi_S | \hat{H}_{SO} | ^3\Psi_T \rangle$ is proportional to a single-electron orbital integral $\frac{1}{2}\left\langle n \middle| \vec{l} \middle| \pi^* \right\rangle$ between two molecular orbitals. Since the $\vec{l}$ operator produces rotation of the π* MO in the direction of the orthogonal n-orbital, the SOC ME is nonzero and includes large contribution from the heteroatom (the owner of the lone pare) which typically possesses larger internal SOC ς_A constants than carbon atoms. That is why the dyes with a low-lying $^3(n\pi^*)$ triplet state provide more intense phosphorescence than pure hydrocarbons. This is also a background for the well-known El-Sayed rule.[5] The SOC ME determines a mixture of the lowest singlet and triplet states according to perturbation theory

$$^3\tilde{\Psi}_T = {}^3\Psi_T + \left[\langle ^1\Psi_S | \hat{H}_{SO} | ^3\Psi_T \rangle / \left(^1E_S - {}^3E_T\right)\right] {}^1\Psi_S \quad (7)$$

$$^1\tilde{\Psi}_S = {}^1\Psi_S + \left[\langle ^3\Psi_T | \hat{H}_{SO} | ^1\Psi_S \rangle / \left(^3E_T - {}^1E_S\right)\right] {}^3\Psi_T \quad (8)$$

where symbol $\tilde{\Psi}$ determines the perturbed wave functions accounting for SOC perturbation. Since $\langle ^1\Psi_S | \hat{H}_{SO} | ^3\Psi_T \rangle^* = \langle ^3\Psi_T | \hat{H}_{SO} | ^1\Psi_S \rangle$ the electric-dipole transition moment (EDTM) between these states is equal

$$\left\langle ^3\tilde{\Psi}_T^* | M | ^1\tilde{\Psi}_S \right\rangle = \left[\langle ^1\Psi_S | \hat{H}_{SO} | ^3\Psi_T \rangle^* / \left(^1E_S - {}^3E_T\right)\right](M_S - M_T) \quad (9)$$

The square of the EDTM (9) determines the phosphorescence intensity, the spontaneous emission rate constant (k_p) and the radiative lifetime of the T state. This T–S optical transition gains intensity from the difference in the permanent dipole moments M_S–M_T, where $M_S = \left\langle ^1\Psi_S | M | ^1\Psi_S \right\rangle$ is the molecular ground state dipole moment. Besides this T_1–S_0 state mixing, eqn (7) and (8), all other closely lying T_n and S_m states can participate in similar SOC perturbations;[11] this will lead to the $T_1 \rightarrow S_0$ intensity borrowing from the EDTM-allowed S_0–S_m and T_1–T_n transitions. The $S_0 \rightarrow S_m$ transitions are usually well-known from the absorption spectra; thus, the RTP properties are often discussed in terms of their S–S intensity borrowing. However, direct *ab initio* calculations often indicate the importance of the contributions from the T_1–T_n transitions to the RTP rate constant.[6,12]

The larger the SOC ME and the smaller the energy gaps in eqn (7)–(9), the more intense the RTP intensity and the k_p rate. Adachi *et al.* have proposed that the T_1–S_1 energy gap can effectively regulate the TADF when the small T_1–S_1 gap is comparable with the SOC ME integral.[13] In such case, the $T_1 \leftarrow S_1$ reverse intersystem crossing (rISC) could be very fast and compete with the RTP, thus providing the TADF radiation.[4,13] The temperature dependence of the rISC rate and RTP intensity really indicates the TADF importance for specially synthesized chromophores with a charge transfer nature of the T_1–S_1 states and very low energy gaps.[12]

Comparison of singlet oxygen and organic phosphorescence

The singlet oxygen lifetime in solvents is comparable with that of organic RTP. The singlet oxygen emission $O_2(^1\Delta_g) \rightarrow O_2(^3\Sigma_g^-)$ ranging 1270–1060 nm represents the reverse phosphorescence according to the IUPAC definition[6] (since it is a transition between states of different multiplicity, $S_1 \rightarrow T_0$). Moreover, it is observed as weak RTP in solvents and matrices.[6,12] It is easy to show that SOC ME between triplet $O_2(^3\Sigma_g^-)$ and singlet $O_2(^1\Delta_g)$ states is equal to zero and the singlet oxygen relaxation is strictly forbidden in the electric dipole approach.[6,12] Both the states $O_2(^3\Sigma_g^-)$ and $O_2(^1\Delta_g)$ differ by the orbital angular momentum projection ($\Delta\Lambda = 2$); this selection rule strictly forbids their SOC mixing[12] and EDTM activity. The $O_2(^1\Delta_g)$ state radiative rate constant k_p in a free O_2 molecule is determined by a weak magnetic-dipole transition and its lifetime exceeds an hour. In contrast, the non-radiative ISC rate $O_2(^1\Delta_g) \rightarrow O_2(^3\Sigma_g^-)$ in organic solvents is rather fast and provides a τ_Δ lifetime in the μs[11] range. The radiative lifetime of oxygen phosphorescence $^1\Delta_g \rightarrow {}^3\Sigma_g^-$ is much longer in any solvent, even though this emission acquires an electric-dipole nature in the condensed phase.[6] The organic RTP quenching by O_2 is often accompanied by the generation of singlet oxygen. The observed τ_Δ lifetime strongly depends on SOC between $O_2(^3\Sigma_g^-)$ and $O_2(^1\Sigma_g^+)$ states and on charge-transfer interactions with the nearest environment.[6] One can see that the RTP quenching problem by environmental temperature-factors and the τ_Δ lifetime theory[11] both depend on the fine tuning between intramolecular and intermolecular SOC effects including spin–vibronic interactions and exciton and phonon dynamics in the vicinity of the RTP emitter. Because of this, the corresponding lifetimes are strongly reduced depending on the environment. Besides the k_p rate constant, the origin of RTP depends on other parameters connected with k_{nr}, k_{ISC}, and k_{rISC} and other photophysical processes rates which will be discussed below.

3. Blue RTP emitters

The first sources of blue lasting emission for colour TV pictures were developed with the implementation of noble metal atoms. The internal atomic SOC ς_A constants for heavy metals (A = Pt, Ir, and Au) exceed those for the first-row elements by two orders of magnitude; thus, the SOC ME integrals (6)–(9) in such metal–organic complexes with pronounced ''metal-to-ligand charge transfer effects'' provide strong mixing of S–T states and efficient RTP with short lifetime.[6] The k_p rate constant of RTP depends on the square of the SOC ME value; thus, the k_p rate is four orders of magnitude higher for metal complexes. The development of organic RTP materials containing no metal atoms that emit light in the short-wavelength region of the electromagnetic spectrum (with emission wavelengths up to 475 nm) is one of the most complicated tasks, because of the low k_p rate. After the discovery of the TADF phenomenon, researchers have encountered several problems related to the blue TADF emitters. For a long time, researchers could not overcome the problem of 20% external quantum efficiency for OLEDs based on blue TADF emitters. Such devices suffered from short operation lifetimes and colour aging that were caused by lower photostability of blue TADF-emitters compared to their green and red counterparts.[13] The major problem with blue RTP materials is that phosphorescence is usually red-shifted in comparison to fluorescence because the triplet-excited states usually have lower energy compared to the S_1 excited state, following the molecular analog of the Hund rule.[6] The S_1–T_1 energy gap of the $\psi_i \rightarrow \psi_u$ excitation is determined by the $2(iu|iu)$ expression, being twice the exchange integral between the HOMO and LUMO, eqn (1). In order to achieve blue RTP, the organic compounds have to possess triplet excitation energy levels of *ca.* 3 eV. High-lying triplets have a tendency to populate singlet excited states *via* reverse intersystem crossing resulting in TADF.[4] To avoid complete triplet upconversion and to afford RTP for a single compound k_{ISC} should be larger than k_{rISC}. The non-radiative loss of triplet excitation states can be prevented by embedding a luminophore into a rigid polymer matrix to reduce the non-radiative channels of energy dissipation or by crystallization of the luminophore.[14]

The latter concept was successfully implemented by Han *et al.*[15] They reported *N*-phenyl-substituted 9,10-dihydro-9,9-dimethylacridine **B1** (Fig. 5 and Table 1), which exhibits persistent luminescence in the blue area of the spectrum. Compared to its methyl and methoxy-containing analogues (**G1** and **G2**, Fig. 11 and Table 2) that showed green RTP, fluorescence and RTP maxima of **B1** were blue-shifted to 351 nm and 475 nm, respectively. The long-lived RTP of **B1** was explained by the peculiarities of the crystal structure. When two phenyl rings of triphenylamine are intramolecularly locked *via* an sp^3-hybridized carbon atom to afford *N*-phenyl-9,10-dihydro-9,9-dimethylacridine, the target compound exhibits a twisted conformation with a torsion angle of *ca.* 90° between acridine and the unlocked phenyl ring. DFT calculations revealed rather weak overlap between the HOMO and the LUMO of **B1** that leads to a low ΔE_{ST} gap, thereby promoting intersystem crossing.[15] X-ray analysis performed for B1 single crystals revealed the presence of intermolecular interactions of different types such as C···H and C···NH, whereas no π–π stacking was observed. In the case of methyl and methoxy-containing counterparts such interactions are more abundant, which sufficiently prolong the RTP lifetime compared to **B1**.

Deng *et al.* managed to achieve blue RTP by incorporating the phenyl fragment into the sulfone-locked triphenylamine heteroaromatic core.[16] Thorough investigations disclosed that the introduction of the phenyl fragment results in the rearrangement of its excited state energy levels thus providing more efficient ISC and strengthened SOC between the triplet excited states and first singlet excited state S_1. Embedding 5 wt% of compound B2 (Fig. 5 and Table 1) into a PMMA matrix resulted in the cessation of the non-radiative relaxation of triplex excitons. Steady-state PL spectra revealed a peak at 387 nm, which was attributed to fluorescence whereas RTP peaked at 460 nm with a τ_{RTP} of 542 ms. CIE colour coordinates of blue afterglow were (0.16, 0.27).

Xie *et al.* reported phase-dependent RTP of very simple bromine-containing biphenyl derivative **B3** ((Fig. 5 and Table 1)).[17] The authors managed to obtain two crystalline

Table 1 Photophysical parameters of blue RTP-agents **B1**–**B10**

Compound	λ_{FL}, nm	τ_{PL}, ns	FLQY, %	λ_{RTP}, nm	τ_{RTP}, ms	PHQY, %	Host	Ref.
B1	351	—	13.47	475	30	2.26	—	15
B2	387	0.89	4.2	460	542	11.7	PMMA	16
B3-1	373	3.82	0.9	467	3.5	9.1	—	17
B3-2	378	1.62	3	467	2.7	6	—	17
B3$^{gr.}$	334	1.6	7.6	467	2.1	1.4	—	17
B4	392	—	—	403	51.96	—	—	18
B5	338	—	—	471	1116.10	—	—	18
B6	379	—	—	409	60.75	—	—	18
B7	351	—	—	471	249.43	—	—	18
B8	—	—	—	465	580	—	—	19
B9	390, 410	4.46	—	434, 464	760	—	PVA	20
B10	405	5.44	—	434, 464, 494	87	—	PVA	20

λ_{FL} – the wavelength of fluorescence maxima, τ_{PL} – fluorescence lifetime, FLQY – fluorescence quantum yield, λ_{RTP} – the wavelength of room temperature phosphorescence maxima, τ_{RTP} – RTP lifetime, PHQY – phosphorescence quantum yield, and gr. – ground.

Table 2 Photophysical parameters of green RTP-agents **G1**–**G37**

Compound	λ_{FL}, nm	τ_{PL}, ns	FLQY, %	λ_{RTP}, nm	τ_{RTP}, ms	PHQY, %	Host	Ref.
G1	361	—	20.8	529	28	2.0	—	15
G2	386	—	83.5	508	18	—	—	15
G3	363	4.73	—	489	517	7.7	PVA	22
G4	491	10.19	—	502	229	19.6	PVA	22
G5	495	12.57	—	494	222	10.7	PVA	22
G6	—	—	—	515	32	25.6	DIPHOS	23
G7	447	—	—	510[a]	6.92	4.80	—	26
G7	—	—	—	567[b]	4.24	—	—	26
G8	453	1.08	3.8	500	1.62	44.3	PS	27
G8^{cr}	483	0.79	2.1	543	0.016	2.9	—	27
G9	441	1.35	11.8	487	10.38	10.1	PS	27
G9^{cr}	472	1.21	7.6	529	0.61	21.7	—	27
G10	424	1.91	0.5	497	3.09	66.7	PS	37
G11	—	—	—	536	0.67	7.7	—	28
G12	—	—	—	—	—	0	—	28
G13	393	1.79	21.3	486, 514	730, 747	10.6	PMMA	29
G14	380	1.34	14.2	485, 518	822, 760	11.6	PMMA	29
G15	358	3.28	29.4	510, 545	340, 284	7.4	PMMA	29
G16	387	1.08	7.5	477	818	20.2	PMMA	16
G17	409	1.97	8.5	480	380	15.6	PMMA	16
G18	450	2.37	7.3	499	87	16.8	PMMA	16
G19	430	7.1	16.3	476	96	—	—	30
G20	455	3.26	5.9	466, 539	125, 136	—	—	30
G21	423	1.03	2.9	—	—	—	—	30
G22	—	6.63	3.01	516	98	0.37	$OPPh_3$	30
G23	—	4.95	4.45	510	980	3.33	$OPPh_3$	30
G24	—	6.01	5.09	515	334	1.13	$OPPh_3$	30
G25	360	2.66	3.29	508	339	0.73	$OPPh_3$	30
G26	393	2.07	6.35	512	907	4.48	$OPPh_3$	30
G27	397	2.29	2.18	516	464	0.24	$OPPh_3$	30
G28	440	3.24	—	516	32[a]	11[a]	PMMA	32
G29	440	3.23	—	516	25[a]	20[a]	PMMA	32
G30	440	3.15	—	516	30[a]	22[c]	PMMA	32
G31	563	10.71 2×10^4	30.2	530	1.06, 5.48	3.8	PMMA	33
G31	590	25.96 3.36×10^3	14.7	532	2.03, 19.53	3.3	DPEPO	33
G32	558	11.33 12.82	25.5	530	1.1, 5.5	2.5	PMMA	33
G32	584	23.51 3.69×10^4	16.4	532	4.05, 23.07	3.6	DPEPO	33
G33	453	—	3	551	16.6	54	Zeonex	34
G34	456	11.81	—	533	0.001	—	Zeonex	35
G35	—	—	—	545	80.4	—	H35	36
G36	—	—	—	550	3.85	—	H36	36
G37	—	—	—	550	59.44	—	H37	36

λ_{FL} – the wavelength of fluorescence maxima, τ_{PL} – fluorescence lifetime, FLQY – fluorescence quantum yield, λ_{RTP} – the wavelength of room temperature phosphorescence maxima, τ_{RTP} – RTP lifetime, and PHQY – phosphorescence quantum yield. [a] Under ambient conditions. [b] At a pressure of 4.15 GPa. [c] After 30 s of 365 nm UV irradiation, and cr. – crystal.

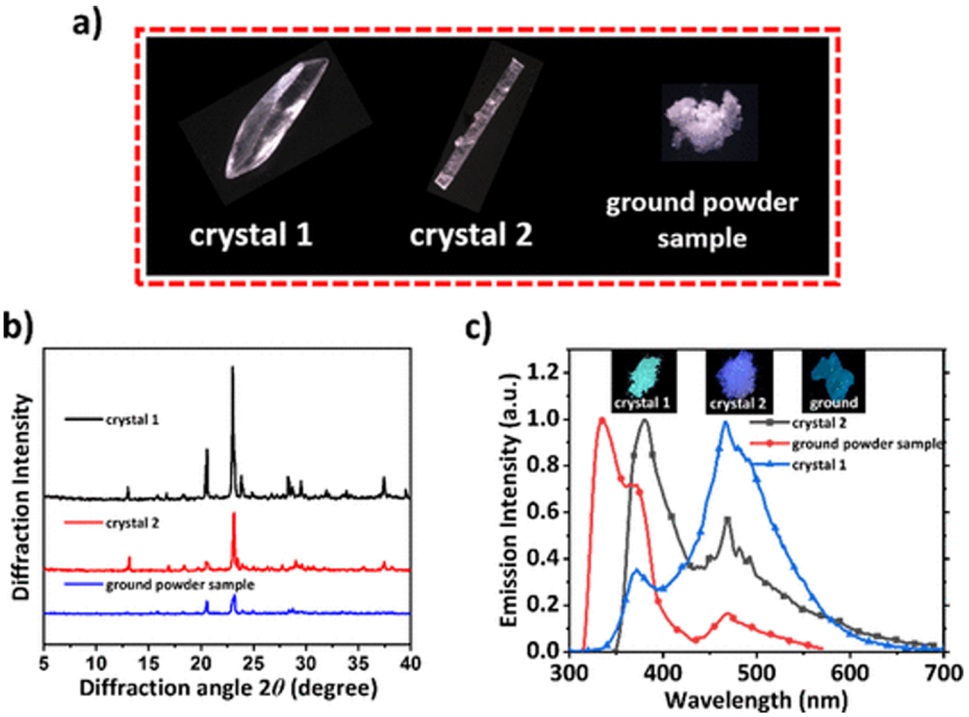

Fig. 3 (a) Photographs of **B3** different crystalline samples under a microscope; (b) PXRD patterns of **B3-1**, **B3-2**, and ground powder samples; and (c) PL spectra of **B3** in different solid states. Adapted with permission from ref. 17. Copyright 2023 American Chemical Society.

forms of compound **B3**. High-quality crystals of **B3-1** were obtained by vacuum gradient sublimation and low-quality crystals of **B3-2** were grown by quick solvent evaporation. The PL spectra of two crystalline forms revealed two peaks around 370 nm (τ of 3.82 ns) and 470 nm (τ of 3.5 ms) that were attributed to fluorescence and RTP. Interestingly, the ratios between the intensities of fluorescence and phosphorescence were different and strongly dependent on the quality of the crystal. The RTP of crystal **B3-1** was much more expressed than fluorescence whereas lower-quality crystalline form **B3-2** displayed the opposite behaviour. When compound **B3** was ground in a mortar, its RTP almost disappeared confirming that crystallization is the key factor in initiation of RTP in **B3** (Fig. 3). The phosphorescence quantum yields were 9.1%, 6% and 1.4% for **B3-1**, **B3-2** and the ground sample of **B3**, respectively. In the case of lower quality crystals and a thoroughly ground sample, the crystalline lattice is damaged to some degree as well as specific molecular arrangement, leading to less efficient RTP.

Cong and co-workers[18] recently studied the possibility of initiating blue RTP in the phenothiazine-5,5-dioxide moiety by the attachment of cycloalkane fragments with different sizes of the rings. Cycloalkyl groups have superiority above alkyl ones because the rotation of C–C single bonds is restricted in cyclic structures which is favourable for RTP. Having this in mind, the authors[18] synthesized a family of compounds with cycloalkyl rings varying from cyclopropyl to cycloheptyl and acyclic analogous compounds. All the compounds were obtained through a two-step synthetic pathway including the acylation of phenothiazine with the corresponding cycloalkyl or alkyl moiety and the following oxidation of phenothiazine to phenothiazine-5,5-dioxide. In the crystalline state, cyclopropyl- and cyclobutyl-containing materials demonstrated green RTP, whereas cyclopentyl–cycloheptyl containing ones **B4–B6** ((Fig. 5 and Table 1)) afforded blue afterglow, visible by the naked eye after turning off the excitation source. The most efficient blue afterglow was observed for compound **B5** having a cyclohexyl fragment linked with a phenothiazine-5,5-dioxide moiety, with a τ_{RTP} of 1116.1 ms and a RTP intensity maximum wavelength of 471 nm. This is reported to be the longest RTP lifetime among phenothiazine-5,5-dioxide derivatives. Among aliphatic analogues, only the butyl-containing compound **B7** (Fig. 5 and Table 1) showed blue RTP also peaking at 471 nm but with a sufficiently shortened lifetime of 249.43 ms.[18] After grinding the crystals to powder all the materials demonstrated much weaker afterglow with shortened decay lifetimes, which proves that RTP properties of this family are promoted by multiple intermolecular interactions in the crystalline phase.

Miao *et al.* found that under certain conditions, blue RTP can be initiated in widely used melamine **B8** (Fig. 5 and Table 1).[19] Excitation of the crystalline powder of **B8** with 310 nm resulted in blue RTP with the intensity maximum at 465 nm and a τ_{RTP} of 580 ms. The decrease in the excitation energy to 365 nm resulted in green RTP peaking at 490 nm. The authors[19] explained such a dynamic shift in the phosphorescence colour by the formation of H-aggregates between adjacent melamine molecules. Blue RTP of melamine originated from triplet excited-state radiative transition, and the excited S_1 exciton was converted into a T_1 exciton *via* intersystem crossing. Next, the T_1 exciton was trapped by the H-aggregates and stabilized by the

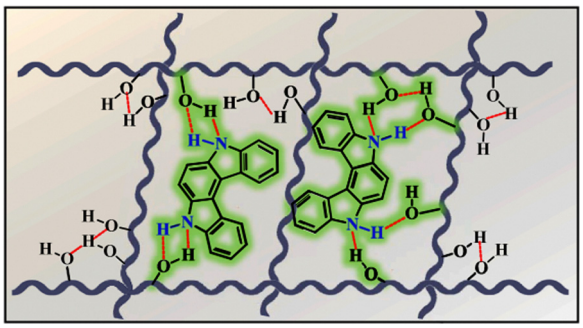

Fig. 4 Schematic illustration of intermolecular hydrogen bonding between **B9** and PVA. Reprinted from M. Jian, Z. Song, X. Chen, J. Zhao, B. Xu and Z. Chi, Afterglows from indolocarbazole families, *Chem. Eng. J.*, **429**, 132346,[20] Copyright 2023, with permission from Elsevier.

strong aggregation. Then, the captured T_1 excitons were slowly released and returned to S_0 to emit green RTP.

Although carbazole is the most widely used electroactive organic material, the indolocarbazole family remains scarcely investigated due to the solubility problems of such compounds. However, there is a high probability that they are RTP-active due to their high crystallinity and the presence of two amino groups that can readily form intermolecular non-covalent bonds, thus preventing the non-radiative loss of triplets. It was recently proved that all existing indolocarbazole isomers are indeed RTP-active when doped into a PVA matrix, and two of them (**B9** and **B10**, Fig. 5 and Table 1) were found to exhibit bright blue afterglow.[20] Compounds **B9** and **B10** revealed biluminescent behaviours with fluorescence maxima located at 390–410 nm and RTP peaking up to 494 nm. The symmetrical isomer **B9** demonstrated a τ_{RTP} of 0.76 s, which is one of the highest values among organic blue RTP emitters. In order to verify that RTP of the investigated compounds is promoted by guest–host intermolecular interactions, the NMR spectra for **B9**, PVA and **B9**/PVA mixture were recorded. For pure PVA, the –OH proton peak ranged from 4.36 to 4.76 ppm, but in the case of **B9**-PVA, it appeared to be shifted by 0.16 ppm. For pure **B9**, the signal from the –NH group was shifted to 0.16 ppm, whereas the signals of the protons of phenyl rings appeared almost at the same place (shift of 0.01 ppm).[20] This confirms the existence of intermolecular hydrogen bonding between the **B9** guest and the PVA host matrix (Fig. 4).

4. Green RTP emitters

Since the human eye is most sensitive to yellowish-green emission in the daylight, green RTP emitters are desirable for bioimaging applications that require high contrast and resolution.[21] Green RTP emitters might attract considerable attention for the development of OLEDs with high efficiency and stability. For example, they can be used for data encryption and decryption by exploiting their long-lived afterglow.

Eventually, even very small organic molecules without heavy atoms can exhibit green RTP. Han *et al.*[15] found that intramolecular rigidification on triphenylamine phenyl rotors can

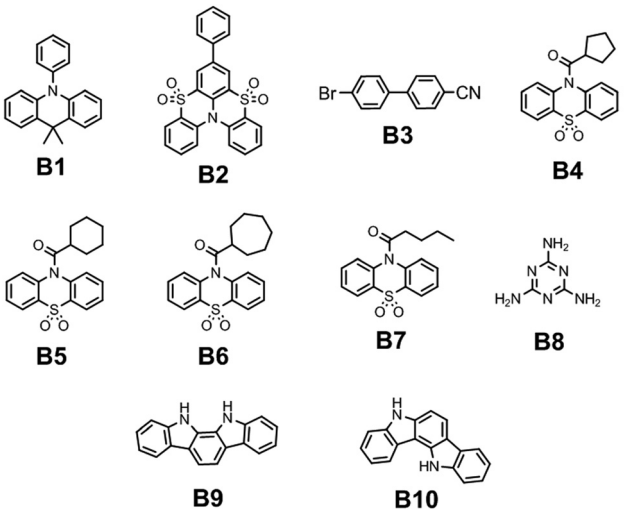

Fig. 5 Molecular structures of blue RTP-agents **B1**–**B10**.

evoke efficient RTP in the former. Locking of two phenyl rings of triphenylamine *via* an sp^3-hypridized carbon atom diminishes the rotations around C–N bonds, thus opening up a way for triplet excitons to relax radiatively. The authors[15] synthesized three derivatives of 9,10-dihydro-9,9-dimethylacridine by Buchwald–Hartwig cross-coupling: **B1** (mentioned in chapter 1, Fig. 5 and Table 1), **G1** and **G2** (Fig. 11 and Table 2). Compound **G1** which has a methyl group in the *para*-position of its unlocked phenyl ring demonstrated green RTP peaking at 529 nm (τ_{RTP} of 28 ms). It showed a PHQY of 2%. Changing the substituent from methyl- to methoxy- in **G2** results in a hypsochromic shift of the RTP peak to 508 nm and a shortening of τ_{RTP} to 18 ms. At first glance, RTP in the former compound should be more expressed due to the presence of an oxygen atom that promotes intermolecular interactions because of the electronic n-lone pair activity. The authors[15] explained such opposite RTP-behaviour by more compact and ordered molecular packing in **G1** crystals that suppressed non-radiative transitions of **G1** in comparison to **G2**.

A family of phenanthrolines, exhibiting RTP, were synthesized and investigated by Sun *et al.*[22] The suppression of molecular rotations was achieved by doping phenanthrolines **G3**, **G4**, and **G5** (Fig. 11 and Table 2) into a rigid PVA matrix. Such systems create abundant H-bonding interactions that are key to restrain the non-radiative decay of the triplet excited states. The unique property of such host–guest systems is that they can be excited from UV to visible-light to afford RTP. Compound **G4** that contains one aminogroup demonstrated the best performance among the whole family (τ_{RTP} of 229 ms and a PHQY of 19.6%). It was revealed that the RTP properties of phenanthroline derivatives strongly depend on the number of incorporated aminogroups. Apparently, in the case of unsubstituted phenanthroline **G3** doping into a PVA matrix, it did not provide the necessary amount of intermolecular interactions to facilitate RTP, and NH_2-abundant **G5** has plenty of N–H groups not attached to PVA that dissipate energy non-radiatively, resulting in a decrease of efficiency of RTP.

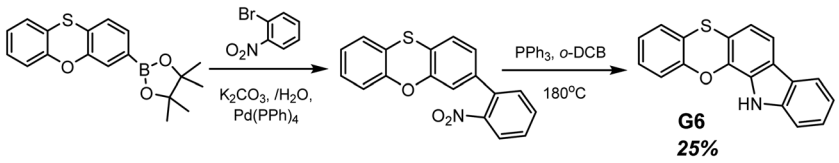

Scheme 1 Synthetic route for compound **G6**. Adapted from the literature.[23]

Another example of efficient RTP of low-molar-mass organic compounds was recently reported by Li and co-workers.[23] They synthesized a tetracyclic compound **G6** (Scheme 1, Fig. 11 and Table 2) that exhibited no RTP in the solid state but became RTP-active when molecularly dispersed in the newly developed phosphorus-containing rigid host (DIPHOS). The new host not only enabled more effective exploitation of triplet excitons of the guest **G6**, but also the ethyl chain between two phosphorus atoms provided good compatibility with surrounding guest molecules. Moreover, two phosphorus atoms of the host promote the heavy atom effect, resulting in enhanced intersystem crossing. The authors[23] managed to grow guest–host co-crystals by the evaporation of the guest–host ethanol solution with a molar ratio of 3 : 1 correspondingly. Compound **G6** itself exhibited deep-blue fluorescence in the solid state while the host was almost nonluminous with an extremely low photoluminescence quantum yield of 0.6% in the solid state. The resulting cocrystal was excited at 350 nm, which was the excitation wavelength of the guest **G6**. The host could not be excited with such irradiation. The **G6**-DIPHOS co-crystal revealed sky-blue emission at a steady state and persistent green afterglow (515 nm) with a PHQY of 25.6% and a τ_{RTP} of 32 ms.

To date, the vast majority of luminescent materials exhibiting piezochromism are attributed to purely fluorescent compounds.[24,25] However, RTP often coexists with fluorescence which makes it impossible to study RTP piezochromism separately. Yang *et al.*[26] recently reported pressure-dependent RTP properties of green organic phosphor selenanthrene **G7** (Fig. 11 and Table 2) that exhibited almost no coexisting fluorescence under ambient conditions and therefore is a perfect candidate for studying the influence of pressure on RTP. The isotopic hydrostatic pressure produced by a diamond anvil cell was applied to crystals of **G7**. With increasing pressure, the RTP of **G7** revealed two-step transformation. At the first step the pressure was increased from 1 atm to 4.15 GPa and RTP of **G7** profoundly increased, simultaneously shifting from green to greenish-yellow. The authors[26] observed the sharp shrinkage of the emission spectrum having a vibronic structure together with the appearance of a single peak at 567 nm when the pressure was increased to 4.15 GPa. At the second step, when the pressure was increased over 4.15 GPa, the emission of **G7** decreased drastically with a redshift from greenish-yellow to orange and completely ceased under 9.21 GPa. The authors[26] concluded that pressure-dependent RTP reinforcement in selenanthrene occurred due to the more folded geometry along with more intensive intermolecular interactions under high pressure, which results in an improved rate of triplet radiative transition. The shorter the intermolecular distances and the stronger the out-of-plane distortions under pressure, the more efficient the π–σ mixing; the orbital angular momentum matrix elements $\langle\sigma|\vec{l}|\pi^*\rangle$ of the SOC operator (6) increase and the influence of the heavy Se atoms get more pronounced.[6] This results in the strengthening of the SOC ME and the EDTM (9), increasing the k_p rate constant.

Selenium is a promising element for the organic halogen-free RTP agents due to its large atomic radius that results in large SOC. However, due to the high cost of selenium-containing starting materials and complex synthetic routes, such materials are not widespread. Wang *et al.*[27] developed a selenium-containing donor–acceptor compound **G8** (Scheme 2, Fig. 11 and Table 2) with the 9*H*-selenoxanthen-9-one moiety as an electron acceptor and 9-phenyl-9*H*-carbazole as an electron

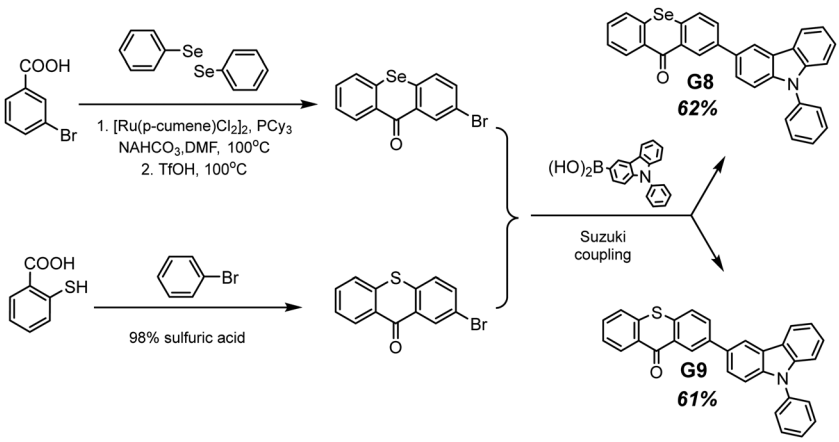

Scheme 2 Synthetic route of obtaining compounds **G8–G9**. Adapted from the literature.[27]

donor unit. They synthesized its sulfur-containing counterpart **G9** (Scheme 2, Fig. 11 and Table 2) bearing 9*H*-thioxanthene-9 as an electron-accepting moiety to brighten RTP. The presence of both a selenium heavy atom and a carbonyl group with oxygen lone electron pair promotes RTP by strengthening SOC which results in more effective non-radiative singlet–triplet transition. A photophysical investigation of 1 wt% of compounds **G8** and **G9** embedded into the polystyrene (PS) matrix revealed that both compounds exhibit a biluminescence behaviour. In the case of the molecular dispersion of compound **G8** in PS, the film exhibited bright green emission peaking at 500 nm and a shoulder at 453 nm under vacuum at room temperature. The investigation of the sample at 77 K with a delay time of 1 ms revealed complete disappearance of the mentioned shoulder, suggesting its fluorescent origin. The sulfur-containing counterpart **G2**[15] demonstrated the opposite behaviour. Its fluorescence peak at 441 nm (emission lifetime of 1.35 ns) was more intensive than the phosphorescence shoulder with emission maxima at 487 nm (τ_{RTP} of 10.38 ms). Noteworthily, the film of the molecular dispersion of **G8** in PS exhibited a high phosphorescence quantum yield of 44.3%, which is one of the highest among selenium containing RTP-materials and four times higher than that of the film of the molecular dispersion of **G9** in PS (10.1%). The authors[27] calculated the radiative rate constants of fluorescence (k_r^F) and phosphorescence (k_r^P), the intersystem crossing rate constant (k_{ISC}), and the sum of the non-radiative constant of phosphorescence (k_r^P) and the quenching rate of T_1 (k^q) of the films of **G8** and **G9** doped in PS. The theoretical calculations revealed that when sulphur is replaced with a heavier selenium atom, it results in a 1.5-fold increase in k_{ISC} and an increase in k_r^P by two orders of magnitude.

For most organic RTP-materials, crystallization enhances phosphorescent emission; however, the powder of compound **G8** exhibited a PHQY of only of 2.9%. Calculated $k_r^P + k^q$ for **G8** crystals was 200-fold higher than that of the film of the molecular dispersion in PS; therefore, in a crystalline state, the non-radiative loss of triplet excitons increased drastically, resulting in low PHQY.

The same group of researchers[27] investigated the effects of the structural isomerism on the RTP properties of compound **G8**. They synthesized three donor–acceptor isomers of **G8**, varying by the linking topology of the phenylcarbazole electron donor and selenoxanthenone electron acceptor. The film of compound **G10** (Fig. 11 and Table 2) with a phenylcarbazole moiety at C-3 position of the 9*H*-selenoxanthen-9-one ring being doped in a PS matrix has demonstrated an RTP intensity maximum at 497 nm (τ_{RTP} of 3.09 ms) and with PHQY reaching 66.7%, which is the highest value among the selenium-containining RTP materials. The isomer with a phenylcarbazole moiety at the C-4 position of the 9*H*-selenoxanthen-9-one ring exhibited blue RTP peaking at 468 nm with a PHQY of 27.3%, while the isomer with C-1 substituted position of 9*H*-selenoxanthen-9-one exhibited no RTP. It showed only green fluorescence.

Another illustrious example of the advantageous co-presence of a selenium heavy atom and a ketogroup in one molecule to maximize SOC for initiating RTP was reported in ref. 28. The simple (10*H*-phenoselenazin-10-yl)(phenyl)methanone **G11** (Fig. 11 and Table 2), where a phenoselenazine moiety is bonded with benzoyl fragment *via* an N atom, and its sulfur containing counterpart **G12** (Fig. 11 and Table 2) were synthesized. Compound **G11** did not exhibit fluorescence in a tetrahydrofuran solution at room temperature. This indicated that singlet excitons were converted into triplet excitons with almost 100% efficiency due to the enhanced SOC. Fig. 6a depicts NTO of **G12** in T_1 state. Both the HONTO and LUNTO are localized on the phenoselenazine fragment. Therefore, it can be outlined that the locally excited phenoselenazine unit vastly contributes to the phosphorescence of **G11** and the contribution of charge transfer is rather negligible. Under excitation with 365 nm the crystal of **G11** emitted bright light whereas the crystal of **G12** demonstrated faint luminescence (Fig. 6b and c). PHQYs of the crystals of **G11** and **G12** were 7.7% and close to 0%, respectively.

Derivatives of the benzothiazino-phenothiazine tetraoxide (BTPO) core were reported as a new category of organic emitters.[29] Functionalization of BTPO with different substituents enabled tuning the origin of luminescence from TADF to RTP. The BTPO skeleton was functionalized with the different moieties such as *p*-cyanophenyl-, carbazolyl- and triphenylamino to obtain compounds **G13–G15** (Fig. 11 and Table 2) in 82%. 77% and 78% yields correspondingly. Investigation of photophysical properties of the target compounds doped into a rigid PMMA matrix revealed that all of them exhibited biluminescence with obvious RTP. The RTP/PL ratio for **G14** was almost unity, whereas those for **G13** and **G15** were reduced to less than 0.5. The PHQYs were estimated to be in the range from 7.4% to 11.6%. These values are among the highest values for organic luminogens with phosphorescence lifetimes above 0.1 s. These results signify that decoration of the BTPO core with various peripheral substituents allow tuning the phosphorescence lifetime and quantum yield. The film of 5 wt% BTPO doped into the PMMA matrix exhibited no phosphorescence under ambient conditions under vacuum.[29] The S_1 and T_1 values were calculated to be 3.31 eV and 3.15 eV correspondingly, resulting in a low ΔE_{ST} of 0.16 eV. The molecular dispersions of compounds **G13–G15** in PMMA showed larger ΔE_{ST} values of 0.59, 0.7 and 0.44 eV, respectively. To verify the necessity of introduction of a phenyl ring into the BTPO core to afford efficient RTP, the authors also investigated BTPO with an extra phenyl group as a reference compound. The 5% solid solution of the reference material in PMMA showed dual emission, with a lifetime of prompt emission of 1.27 ns peaking at 391 nm, and phosphorescence peaking at 465 nm and 493 nm with the corresponding lifetimes of 658 ms and 657 ms. Thus, the triplet energy could be significantly decreased, and efficient phosphorescence could be realized by introduction of an additional aromatic substituent to the BTPO core.

BTPO serving as a favourable RTP-synthone was also used in the work.[16] BTPO was functionalized with the same substituents but at the C-7 position. Compounds **G16–G18** (Fig. 11 and Table 2) showed much brighter RTPs than compounds **G13–G15** maintaining long phosphorescence lifetimes. The 5 wt% molecular dispersions of the compounds in PMMA showed RTP with

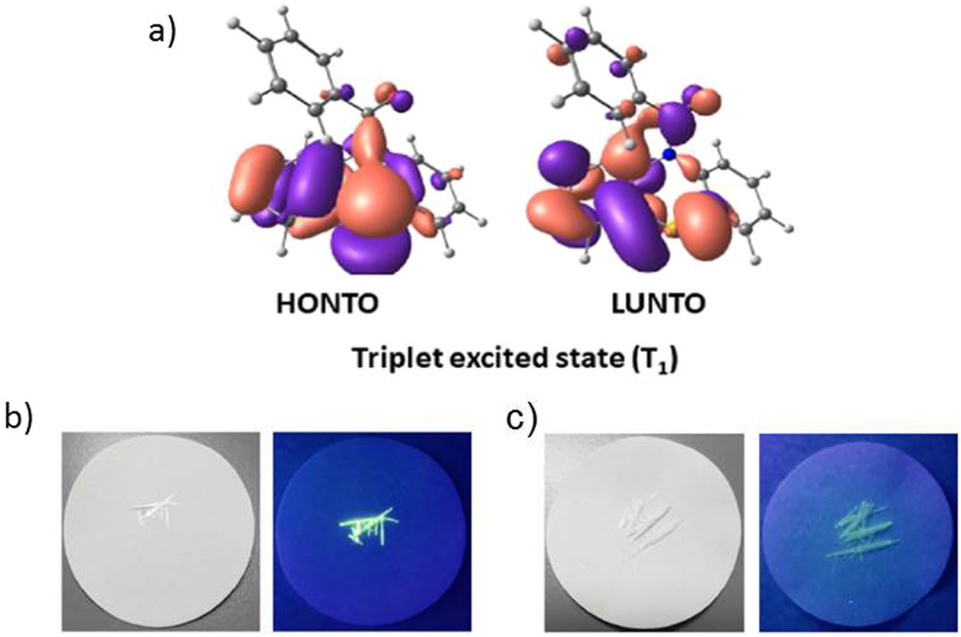

Fig. 6 (a) Natural transition orbitals of **G12** at T_1 state; (b) and (c) photographs of **G12** and **G11** under daylight and under 365 nm excitation. Reprinted from D. R. Lee, J. Park, J. Y. Lee, Metal and halogen-free purely organic room temperature phosphorescence material using heavy atom effect of phenoselenazine, *Org. Electron.*, **106**, 106534,[28] Copyright 2023, with permission from Elsevier.

obvious vibronic features of the spectra, except for the dispersion of triphenylamine-containing **G18** that revealed one emission peak. The possible explanation of this phenomenon is a more expressed CT-character of **G18** than those of **G16** and **G17**. Singlet–triplet energy gaps, calculated from the fluorescence and phosphorescence onsets, were in the range of 0.28–0.6 eV, allowing efficient ISC. The cyano-containing derivative **G16** was found to exhibit a high PHQY of 20.2% together with an ultralong phosphorescence lifetime of 818 ms. This value stands among the best results for green organic phosphors dispersed in a polymer matrix.

Planar tricoordinate boron derivatives **G19–G21** (Fig. 11 and Table 2) that are isostructural with the abovementioned BTPO derivatives, were recently reported.[30] Target compounds were obtained through lithiation reaction using *n*-BuLi at −70 °C and following borination with BBr_3 at −40 °C (Scheme 3). In a

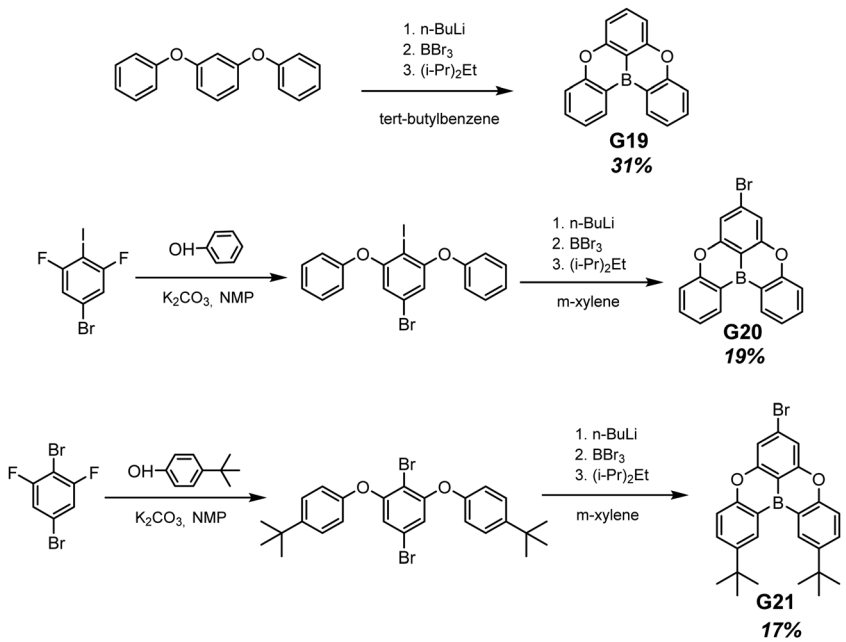

Scheme 3 Synthetic routes for compounds **G19–G21**. Adapted from the literature.[30]

crystalline state, the compounds under UV irradiation emit blue, cyan and deep-blue light with corresponding maxima at 430, 455 and 423 nm, respectively. Upon ceasing UV irradiation, luminogens **G19** and **G20** maintain green afterglow with single maxima at 476 for **G19** and double maxima at 466 and 539 for **G20**. Compound **G21**, although having a bromine atom, did not exhibit any emission from triplet states. This is due to a specific molecular packing. The incorporation of two bulky *tert*-butyl groups into a boron-centred core was performed in order to regulate the packing of the molecule and amplify intermolecular interactions (compound **G21** in Scheme 3). However, surprisingly such a molecular design failed to afford RTP. Further investigation of the **G21** crystal structure revealed antiparralel π-stacking that prohibits the radiative transition of H-aggregates and leads to the annihilation of triplet excited states. After doping into the PMMA host, luminogens **G19** and **G20** maintained the RTP properties. RTP maxima of the film of the molecular dispersion of **G19** in PMMA was blue-shifted to 415 nm whereas that of the film of the molecular dispersion of **G20** in PMMA remained at *ca.* 472 nm. For compound **G21**, even embedding into the rigid polymer matrix did not unlock the triplet radiative pathway.

The luminescence properties of the crystals of **G19–G21** were studied under hydrostatic pressure with the aid of a diamond anvil cell. When the pressure was increased from 0 atm to 10.9 GPa, the fluorescent peak of **G19** was slightly shifted to a longer wavelength area from 427 nm to 433 nm alongwith a sharp decrease in the intensity. The intensity of the phosphorescent band around 470–550 nm was gradually amplified and also exhibited a red-shift. As it was mentioned above in the case of selenanthrene **G7**, high pressure shortens the intermolecular distance, diminishing molecular vibration by reducing free molecular volume, and facilitates the overlap of electronic orbitals between neighbouring molecules.[26] The short intermolecular distances and high MO overlap between molecules lead to an increase in the σ–π intramolecular mixing and stronger SOC perturbations.[6] The processes occurring are not favourable for fluorescence but promote RTP through the enhancement of SOC and acceleration of ISC. The more intense SOC of **G20** because of the internal heavy atom effect of bromine resulted in a more expressed enhancement of phosphorescence under high pressure. With increasing pressure, the fluorescence of the crystal of **G20** also diminished sharply and red shifted from 429 nm to

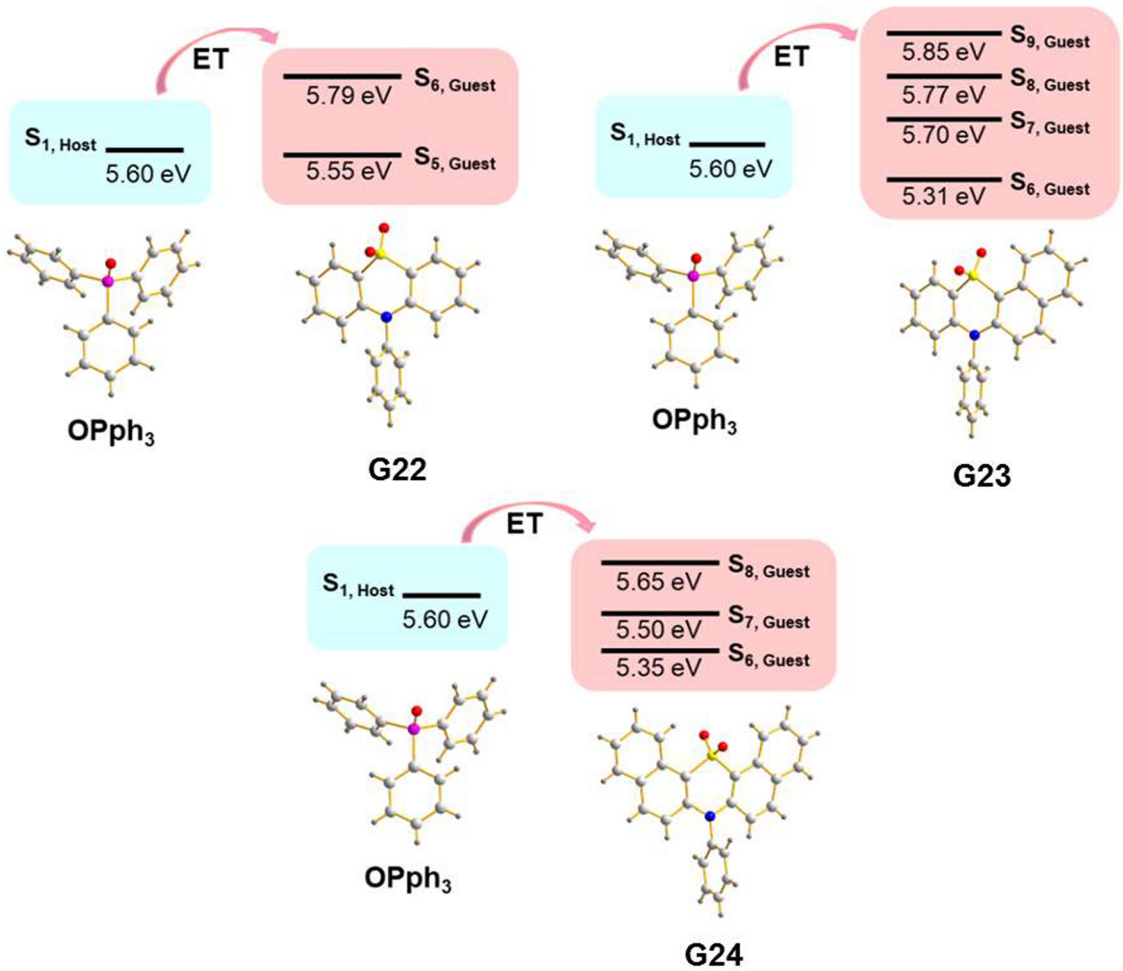

Fig. 7 Illustration of host–guest energy transfer for the molecular dispersions of **G22–G24** in $OPPh_3$. Reproduced from ref. 31 with permission from John Wiley and Sons, Copyright 2023.

437 nm. The phosphorescence intensity even outperformed fluorescence at a pressure higher than 3.1 GPa, reached its full intensity at 7.9 GPa (538 nm) and became completely quenched at 10.6 GPa. Surprisingly, high pressure released the forbidden phosphorescence in **G21** that reached its maximum at 3.0 GPa (442 nm), and gradually decreased at 9.9 GPa.

A guest–host strategy to evoke RTP in non-phosphorescent sulfone-containing homologs was proposed.[31] A family of compounds **G22–G27** (Fig. 11 and Table 2) exhibit efficient green afterglow when doped into triphenylphosphine oxide ($OPPh_3$) as a host. A strong afterglow was noticed from the co-crystal sample of **G23** (PHQY of 3.33% and τ_{PHOS} of 980 ms) whereas **G22** and **G24** revealed rather weak afterglow. To elucidate the reason of different RTP efficiency in three similar compounds in this family of compounds the authors of ref. 31 studied the photophysical properties of the solid samples of the guests and the host separately. The emission band of $OPPh_3$ was found to be significantly overlapped with the absorption bands of guest molecules that indicated a good match of their energy levels. From the output of single crystal analysis the energy levels of singlet and triplet excited states were calculated using the TD-DFT method. With the B3LYP functional and 6-31G basis set the energy of the S_1 state for $OPPh_3$ was calculated to be of 5.60 eV. The S_n states of guests with energy ±0.3 eV were enumerated. The energy transfer from $OPPh_3$ host to a guest could occur easily in such energy frame. It was found that compound **G23** had four energy levels (5.31 eV, 5.70 eV, 5.77 eV and 5.85 eV) that could match with the S_1 energy level of the host, resulting in energy transfer, whereas **G22** and **G24** exhibited only two (5.55 eV and 5.79 eV) and three (5.35 eV, 5.50 eV and 5.65 eV) matchable energy levels correspondingly (Fig. 7). The authors[31] also observed that after grinding of the guest–host samples RTP gradually rose both in intensity and the lifetime. It was explained by the decrease of the distance between the guest and host with the help of mechanical force, thus facilitating energy transfer.

Pyridine containing analogues of **G22–G24**, namely, **G25–G27** (Fig. 11 and Table 2) were obtained *via* similar synthetic pathways. When they were embedded into the $OPPh_3$ host, green afterglow was also observed and was also amplified by grinding. When the films of the molecular dispersions of pyridine-containing compounds **G25–G27** in **$OPPh_3$** films interacted with acid, their RTP was switched off as a consequence of structural change in guest molecules (Fig. 8).

Three very simple phenothiazine-based phosphors **G28–G30** (Fig. 11 and Table 2) varying by the number of phenothiazine moieties were reported by Wang *et al.*[32] The films of compounds **G28–G30** doped into the PMMA host matrix exhibited weak photoinduced RTP at initial time. The authors explained the RTP photoinduction by O_2 consunption under UV irradiation since the triplet oxygen can quench the triplet excitons of the luminophores.[11] RTP of compound **G30** that contains three phenothiazine fragments is almost negligible under initial ambient conditions, but enhances gradually with the increase in the irradiation time (λ_{irr} of 365 nm). Expressed RTP emerges after 5 s and reaches its maximum after 25 s of irradiation with

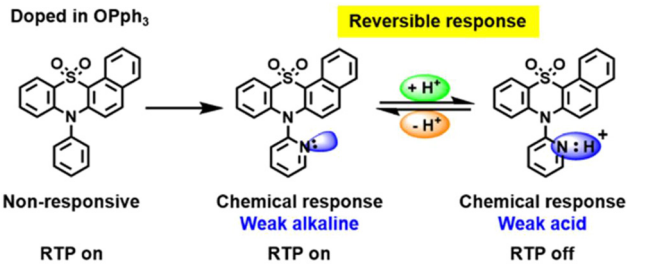

Fig. 8 Acid–base stimulus response scheme for compound **G26**. Reproduced from ref. 31 with permission from John Wiley and Sons, Copyright 2023.

a PHQY of 22% and a τ_{RTP} of 30 ms. The film returns back to a non-RTP state after heating the sample at 60 °C for 1 min or maintaining it for 30 min under ambient conditions. Compounds **G28** and **G29** also revealed reversible photoinduced phosphorescence with PHQYs of 11% and 20% respectively.

Other phenothiazine-containing conjugates with a quinoline acceptor fragment—**G31, G32** (Fig. 11 and Table 2)—were reported by Xie *et al.*[33] The special value of this work is that it demonstrated very deep theoretical insight into photophysical processes of abovementioned compounds. The authors[33] confirmed that three excited states ^{1}CT, ^{3}CT, and ^{3}LE contribute to the rISC process resulting in TADF and green RTP. For both the luminophores (**G31** and **G32**) the intermediate ^{3}CT was observed when they were molecularly dispersed in a polar matrix, that leads to TADF. RTP bands that were found to be blue-shifted with respect to charge-transfer peaks, originated from phenothiazine donor ^{3}LE, which is higher in energy than CT.

The phenothiazine-triazatruxene derivative **G33** (Fig. 11 and Table 2) demonstrated conformer-induced green RTP.[34] Triazatruxene core was decorated with three *N*-ethylphenothiazine fragments *via* C-2 position of the former. Luminescence properties of the films with 1% solid solutions of the compound in rigid Zeonex matrix were studied. Under vacuum, the investigated film demonstrated two peaks: one at 453 nm which was attributed to fluorescence and another one at 551 nm that increased the intensity of the fluorescence band by 19 times (τ_{PHOS} = 16.6 ms) was recognized as RTP band. The film demonstrated a PHQY of 54% that is among the highest values for green RTP-agents to date. The authors of ref. 34 also investigated the photophysical properties of 5% and 10% solid solutions of **G35** in Zeonex, but none of the samples revealed such an impressive RTP performance. The corresponding PLQYs were 33% and 22.5% and the RTP/PL intensities ratio were 11 and 7.5, respectively (Fig. 9). The authors[34] suggested the possibility of the existence of various types of conformations for **G32** that differ by the tilts of phenothiazine fragments. As a result, many triplet states with close, but different energies can exist and provide multichannel ISC leading to RTP.

Phenothiazine-containing phosphor **G34** (Fig. 11 and Table 2) was obtained *via* Ullmann coupling between 4,4′-diodo-2,2′-bis(trifluoromethyl)biphenyl and phenothiazine in 59% yield (Scheme 4).[35] Two trifluoromethyl groups were employed with the aim of intensifying intermolecular interactions, boosting

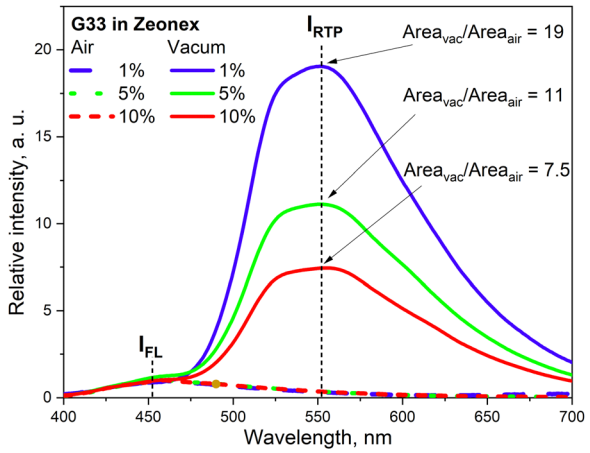

Fig. 9 RTP *vs.* fluorescence ratio for the different concentrations of **G34** in Zeonex. Reprinted from E. Skuodis, K. Leitonas, A. Panchenko, L. Volyniuk, J. Simokaitienė, R. Keruckienė, D. Volyniuk, B. F. Minaev and J. V. Gražulevičius, Very sensitive probes for quantitative and organoleptic detection of oxygen based on conformer-induced room-temperature phosphorescence enhancement of the derivative of triazatruxene and phenothiazine, *Sens. Actuators, B*, **373**, 132727,[34] Copyright 2023, with permission from Elsevier.

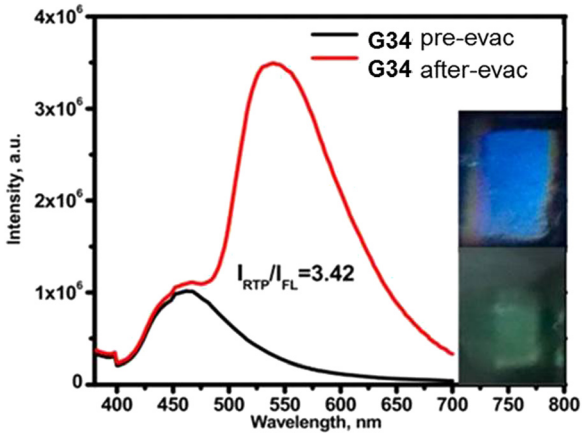

Fig. 10 Photoluminescence spectra of the film of the molecular dispersion of compound **G34** in Zeonex before and after evacuation. Reproduced from R. Keruckiene, N. Kusas, L. Dvylys, E. Skuodis, V. E. Matulis, E. G. Ragoyja, D. A. Lyakhov, I. Klymenko and J. V. Grazulevicius, Derivatives of Bis(trifluoromethyl)biphenyl and Various Donor Moieties Exhibiting Dual State Emission, *J. Luminescence*, **241**, 118502,[35] Copyright 2023, with permission from Elsevier.

thermal stability and enhancing ISC and obtaining efficient radiative simultaneous decay of singlet and triplet excited states. Under vacuum, 1 wt% of compound **G34** dispersed in a Zeonex rigid matrix revealed dual emission with fluorescence peaking at 456 nm and RTP peaking at 533 nm (τ_{PHOS} of 1 μs). The ratio between the RTP intensity and fluorescence intensity of evacuated and air-equilibrated samples was 3.42 (Fig. 10).

Multi-twisted organic compounds that have many rotational bonds possess great potential to be used in molecular machines, sensors *etc.* However, the abundance of rotational freedom that results in non-radiative energy loss makes it hard to achieve RTP for such molecules. Shen *et al.*[36] introduced an elegant solution for this problem by engineering appropriate hosts for highly twisted compounds. They designed and synthesized three asterisk-like sulfur containing luminophores **G35–G37** (Fig. 11 and Table 2) and proposed an individual host for each compound to afford efficient RTP. Hosts **H35–H37** (Fig. 11 and Table 2) were designed taking into account the structural peculiarities of the guest compounds to ensure not only restriction of molecular motions but also compatibility of energy levels. All the guest compounds did not exhibit RTP after being doped into the PVA matrix, confirming that RTP of the guest–host solid mixtures is driven by energy transfer rather than by restriction of rotational freedom. All the guest–host solid mixtures exhibited RTP peaking at *ca.* 550 nm with a τ_{RTP} of 80.4 ms for **G35–H35**, 3.85 ms for **G36–H36** and 59.44 for **G37–H37**. The authors[36] attributed the short RTP of the **G36–H36** solid mixture to the fast triplet–triplet energy transfer from the **H36** host to the **G36** guest, which was further proven by theoretical calculations, revealing that $\Delta ET_{HOST} - T_{GUEST}$ was only 0.18 eV.

5. Orange/red RTP agents

The field of organic red light-emitting materials is thriving at this point in time since there is still a high demand for such materials to be utilized in optical sensors, displays, lighting devices, security probes and night vision devices.[38,39] Organic red-emitting materials are exclusively used in medical applications, *i.e.*, bioimaging, drug tracking, and especially, tumour diagnosis

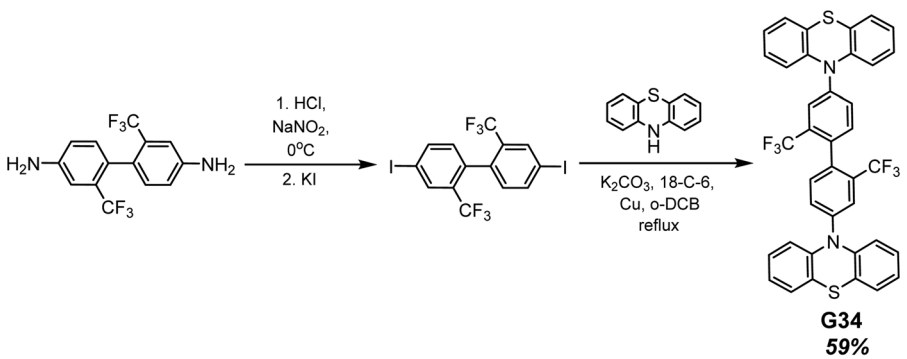

Scheme 4 Synthesis of compound **G34**. Adapted from the literature.[35]

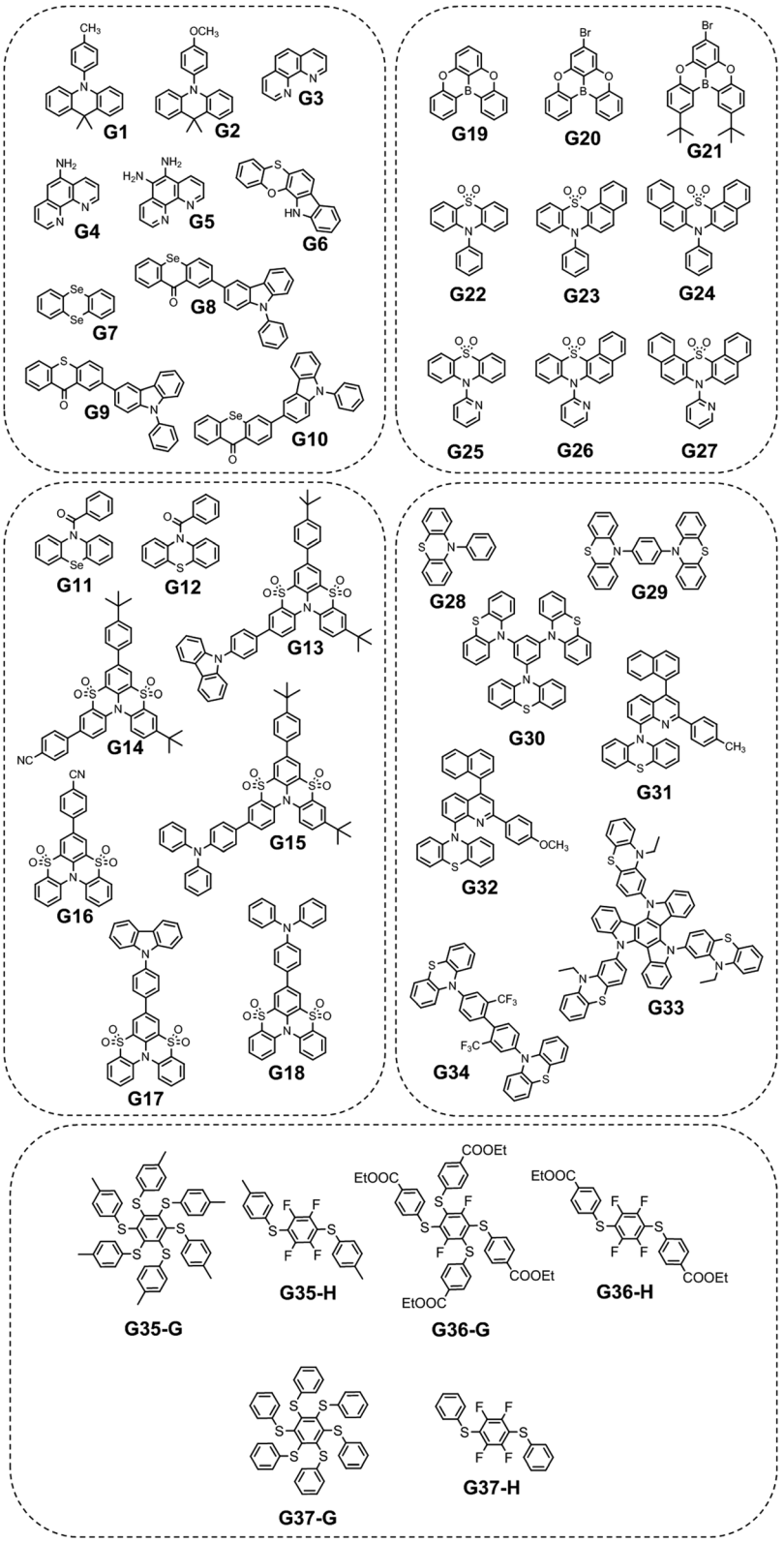

Fig. 11 Molecular structures of green RTP-agents **G1**–**G37**.

and treatment.[40] Emitters with a wavelength shorter than 580 nm cannot be applied for achieving the abovementioned goals because their high photon energies can damage live tissues instead of penetrating them.[41] Moreover, organic compounds have obvious advantages over their inorganic counterparts and metal complexes such as low toxicity, good biocompatibility, the

Table 3 Photophysical parameters of red RTP-agents **R1**–**R45**

Compound	λ_{FL}, nm	T_{PL}, ns	FLQY, %	λ_{RTP}, nm	τ_{RTP}, ms	PHQY, %	Host	Ref.
R1	448	2.32	0.4	648	0.585	3.7	—	46
R1	426	—	—	642	—	—	PMMA	46
R2	422	2.34	0.4	629	0.233	1.8	—	46
R3	426	23.1	1	559	0.110	1.6	—	46
R4	402	0.48	2.4	555	0.073	0.5	—	46
R5	—	5	—	575	1.9	0.21	—	47
R6	510	0.29	0.19	605	1.57	13.43	*p*IA	48
R7	512	0.31	2.34	611	830	15.96	*p*IA	48
R8	610	25.54	—	625	0.029	—	—	49
R9	620	9.25	—	636	0.027	—	—	49
R10	622	3.03	—	628	0.017	—	—	49
R11 r-cr.	433	—	—	615	2.24	4.56	—	50
R11 g-cr.	559	1.79	—	—	—	—	—	50
R11 g-cr.	—	—	—	580	0.685	—	PVK	50
R11 g-cr.	—	—	—	580	0.006	13.9	PMMA[a]	50
R12-B	398	3.3, 8.08 × 10^5	1.4	546	2.1	6.7	—	52
R12-Y	398	4.5, 8.42 × 10^5	75.2	—	—	—	—	52
R13	—	—	—	549	280	5	—	53
R14	—	—	—	570,620	140	11	—	53
R15	635	7.2 × 10^5	8.2	789	0.72	1.8	PVA	54
R16	637	5.8 × 10^5	13.9	793	0.78	2.6	PVA	54
R17	665	2.7 × 10^5	15	819	0.27	3	PVA	54
R18	400	2.70	—	576	10.5	26[b], 28.7[c]	—	56
R18	400	2.11	—	480	1.4	18, 54.7	PMMA 1%	56
R18	—	—	—	650	5.2	17.5, 23.5	PMMA 50%	56
R19	400	2.75	—	585	0.61	48[b], 68.2[c]	-	56
R19	400	2.57	—	487	0.006	2, 2.4	PMMA 1%	56
R19	—	—	—	650	0.32	30,45.9	PMMA 50%	56
R20^{cr}	—	—	—	655	0.087	3.4[d]/7.8[e]	—	55
R20$^{cr.\,pw.}$	—	—	—	652	0.010	1.8[d]/5[e]	—	55
R20^{film}	—	—	—	649	0.007	0.8[d]/2.8[e]	—	55
R21$^{cr.}$	—	—	—	664	0.011	11.8[d]/15.1[e]	—	55
R20$^{cr.\,pw.}$	—	—	—	664	0.012	6.8[d]/10.8[e]	—	55
R20^{film}	—	—	—	662	0.01	3.8[d]/4.5[e]	—	55
R22	403	—	27.6	541	403	4.2	*o*-Phthalic acid	58
R22	425	—	—	569	373	4.6	*m*-Phthalic acid	58
R22	451	—	—	649	337	1.8	*p*-Phthalic acid	58
R23	443	2.86	0.3	573	79	—	—	59
R24	412, 432	18.4, 18.55	—	552, 600	423, 414	0.3	—	60
R25	411, 431	13.74, 13. 68	—	552, 596, 650	753, 731, 715	0.7	—	60
R26	411, 432	5. 36, 5. 43	—	553, 602, 664	383, 335, 313	7	—	60
R27	415, 441, 466	9.10, 8.25, 7.59	—	555, 604	6.7, 4.4	0.03	—	60
R28	—	—	—	560	170	2.3	—	62
R28				560	420[f]	3.8[f]	—	62
R29	—	—	—	530	40	2.3	—	62
R29				530	760[f]	5.1[f]	—	62
R30	—	—	—	531	190	1.5	—	62
R30				531	460[f]	3.9[f]	—	62
R31	415	1.43	14.2	600, 657	327, 324	9.2	BP	64
R32	424	2.03	13.4	623, 680	215, 210	8	BP	64
R33	440	1.98	15.2	643, 697	201, 198	6.3	BP	64
R34	471	2.19	12.3	657, 713	180, 175	5.4	BP	64
R35	483	2.32	16.1	681, 732	106, 102	4.2	BP	64
R36	—	—	—	679, 736	0.032	11	—	65
R37	474	0.3	—	654, 702	0.018	1.2	—	65
R38	448	—	—	540	299.3	8.3	BP	70
R39	417	—	—	540	120.3	3.6	BP	70
R40	418	—	—	541	244.7	11.2	BP	70
R41	468	—	—	551	4.4	6.6	BP	70
R42	440	—	—	544	26.8	4.1	BP	70
R43	467	—	—	553	240.4	18.6	BP	70
R44	418	—	—	548	165.7	13.4	BP	70
R45	422	—	—	544	93.0	7.2	BP	70

λ_{FL} – the wavelength of fluorescence maxima, τ_{PL} – fluorescence lifetime, FLQY – fluorescence quantum yield, λ_{RTP} – the wavelength of room temperature phosphorescence maxima, τ_{RTP} – RTP lifetime, and PHQY – phosphorescence quantum yield. [a] After UV irradiation for 40 s. [b] Under ambient conditions. [c] Under vacuum. [d] Excitation wavelength = 450 nm. [e] Excitation wavelength = 400 nm. [f] After photoactivation, cr. – crystal, and cr. pw. – crystalline powder.

vast variety of possible materials and cost efficiency of the synthesis. However, in terms of luminescence lifetimes and quantum yields, the inorganic orange/red emitters are still superior.[42] Fluorescence organic materials are not sufficiently efficient because of the limitation imposed by spin statistics. In addition, the lifetimes of fluorescence are usually in the range of nanoseconds. Room-temperature phosphorescence, *i.e.*, emissive relaxation from the triplet excited state to the ground state at a temperature higher than 290 K has considerable advantages against fluorescence both in terms of efficiencies and lifetimes.

While developing red-emissive organic compounds, researchers have encountered several challenges:

(1) in order to generate emission in the long-wavelength region of the spectrum, a compound has to have a low optical bandgap;

(2) in order to harvest energy not only from singlet excitons but also from triplet excited states, a compound has to have high-lying triplet energy levels. Generally, extension of the π-conjugation system results in a shift in emission to longer wavelengths, but it also increases the number of rotational bonds that results in lower emission quantum yield. Highly planar and rigid π-conjugated compounds such as pyrene and coronene derivatives have low-lying triplet energy levels which make it hard for these compounds to harvest energy from them *via* ISC;[43]

(3) An additional problem arises when it comes to RTP quenching. For triplet excitons to relax radiatively, non-emissive pathways of energy dissipation have to be blocked. It can be easily achieved *via* dispersing small amounts of the compound into a rigid host matrix, but it is almost impossible to observe RTP of liquid solutions, where molecular motions are intensive. Therefore, in cases when triplet energy levels of compounds are low, the major challenges in achieving red RTP refer to the enhancement of the ISC rate and suppression of the non-radiative decay of excitons.

A simple and efficient method of initiating RTP in the long-wavelength region of the spectrum is to functionalize the compounds that are used as acceptor units in fluorescent/TADF donor–acceptor-type organic emitters with heavy halogen atoms to promote intersystem crossing and populate triplet excitons. The 2,1,3-benzothiadiazole (**BTD**) moiety, a very common electron-accepting constituent of organic fluorescent red/NIR emitters is RTP-inactive when unsubstituted, while its RTP properties can be easily evoked by introducing heavy halogen atoms.

Long-wavelength RTP of bihalogenated derivatives of **BTD** was previously observed.[44,45] Recently, Ishi-e *et al.* studied the impact of methoxy-groups and halogen heavy atom co-presence on RTP of **BTD** derivatives.[46] Compounds **R1**–**R4** (Fig. 17 and Table 3) were synthesized starting from *o*-dimentoxybenzene in moderate yields (Scheme 5). First, the nitration of *o*-dimethoxybenzene was performed by heating it with fuming nitric acid to afford 1,2-dimethoxy-4,5-dinitrobenzene. Then the nitro groups were reduced to amino groups using palladium on the carbon catalyst and ammonium acetate at room temperature. Dimethoxy-2,1,3-benzothiadiazole **R1** was synthesized by treating the amino derivative with pyridine and thionylchloride. Bromination of **R1** using bromine resulted in the formation of compound **R2** with 43% yield. Condensation of 4,5-dimethoxybenzene-1,2-diamine with glyoxal afforded compound **R3** that was transformed into **R4** after treating it with bromine.

In the solid state, the compounds emitted blue light with fluorescence maxima ranging from 402 nm to 448 nm. The observed phosphorescence under ambient conditions ranged from 555 to 648 nm. The highest PHQY (3.7%) as well as the longest τ_{RTP} (585 μs at 648 nm) were observed for compound **R1** having two methoxy groups incorporated into the benzothiadiazole core. The analogous compound **R2** with fluorine atoms instead of methoxy groups exhibited phosphorescence in a shorter wavelength region peaking at 629 nm, with a reduced PHQY (1.8%) and τ_{RTP} (233 μs), pointing out that methoxy-groups are superior to fluorine atoms in amplification of RTP of 4,7-dibromo-2,1,3-benzothiadiazole. The authors[46] also examined the photophysical properties of compound **R4** which is similar

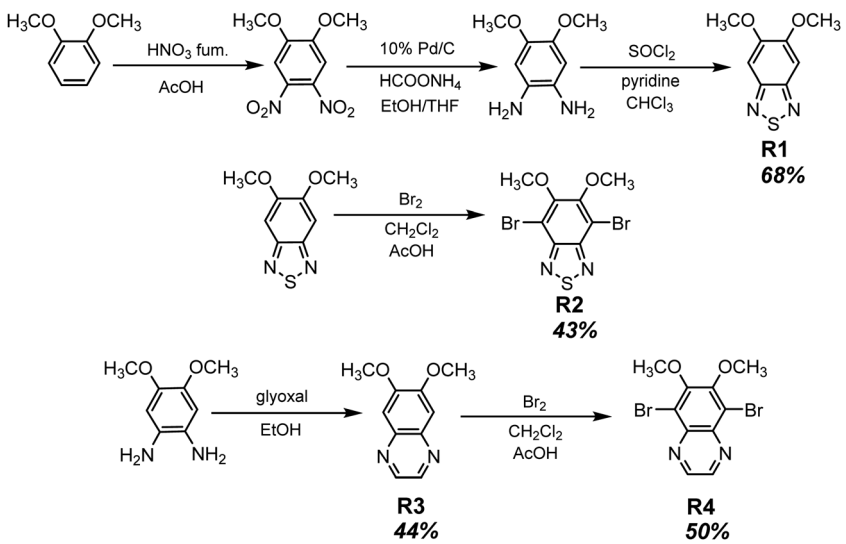

Scheme 5 Synthetic routes for compounds **R1–R4**. Adapted from the literature.[46]

to **R1** but being without bromine atoms. Based on the significantly reduced PHQY (0.5%) and τ_{RTP} (73 μs) of the former, they came to the conclusion that the co-presence of both methoxy groups and bromine heavy atoms is important for phosphorescence of BTD derivatives. To shed light on the triplet harvesting origin of the **BDT** derivatives, the authors[46] investigated compound **R1** in more detail. By doping 1% **R1** into the rigid PMMA matrix, RTP was observed with intensity maximum at 642 nm. The shape of the spectrum was very similar to that observed for the crystalline sample. The similarity of the RTP properties of **R1** in the crystalline state, where molecular packing is tight and in the PMMA matrix where intermolecular interactions are minimized, indicates that RTP of **BDT** derivatives arises not only from the formation of intermolecular aggregates but also from inherent monomeric characteristics.

Compound **R5** (Fig. 17 and Table 3) that has thionyl units fused with a quinoline ring was obtained *via* Suzuki–Miyaura coupling between 3,4-dibromoisoquinoline and 2-methylbenzo[*b*]thiophene pinacol boronic ester and next methylation with subsequent anionic exchange in 84% yield.[47] Steady state investigations of the film of **R5** revealed green fluorescence with a lifetime of 5 ns. The PL spectrum of the film of **R5** with a delay of 120 μs revealed the disappearance of fluorescence and appearance of red-shifted emission with the maximum at 575 and a lifetime of 1.9 ms, which was recognized as RTP. The authors of ref. 47 supposed that the formation of a boron complex was the key factor that helped in achieving RTP for **R5**. The cation–anion interactions between the aromatic unit and the $[BF_4]^-$ anion apparently isolated the emissive thiophene-quinoline core from molecular oxygen and promoted harvesting the energy from triplets. To verify the assumption, a non-complexed precursor of **R5** was investigated and no RTP was observed. Quantum chemical simulations of collision complexes between O_2 and organic chromophore models[6,12] support this assumption.

Stabilization of sulfur-containing boronic complexes with an appropriate rigid host matrix can not only improve RTP but also make it pH-sensitive. Xiao *et al.*[48] designed and synthesized compounds **R6** and **R7** (Fig. 17 and Table 3) in a three-step synthetic pathway (Fig. 12a and c). The formation of the corresponding boronic complexes was achieved by a treatment of intermediates possessing a free NH-group with boron trifluoride diethyletherate in DCM. Both resulting compounds were RTP-inactive in the crystalline form; however, red RTP was observed after doping of 1 wt% of **R6** and **R7** into a *p*-iodoaniline (*p*-$IPhNH_2$) matrix. X-ray analysis revealed the built-in halogen bonds between the cyano-group of **R6** and the iodine atom of *p*-$IPhNH_2$ host molecules and between the iodine atoms of **R7** guest molecules and the amino-group of the *p*-$IPhNH_2$ host. The molecules of the guests became strongly restricted in motion that allow triplet excited states to relax radiatively. After treatment with hydrochloric acid the concurrent formation of complexes *p*-$IPhNH_2$·HCl takes place, thus disrupting the iodine-NH_2 guest–host bonding in the **R7**-*p*-$IPhNH_2$ system and consequently turning off the red RTP (Fig. 12d). In the case of RTP, persistent luminescence of the assembled **R6**-*p*-$IPhNH_2$, where intermolecular bonding does not involve NH_2-groups, remained unchanged (Fig. 12b).

Three boron-containing organic complexes that show RTP in aqueous media were reported by Wang *et al.*[49] Difluoroboron β-diketonate derivatives **R8**–**R10** (Fig. 17 and Table 3) were obtained *via* two-step synthesis from acetyl-carbazole intermediates and the corresponding naphthalic acid methyl esters. All the complexes in an aqueous solution exhibited fluorescence and RTP upon excitation with visible light (470 nm). The longest living RTP (29 μs) was observed for halogen-free compound **R8**. The mostly red-shifted phosphorescence peaking at 636 nm was observed for **R9** that has a naphthyl fragment substituted with a bromine atom. The authors[49] managed to achieve RTP of **R8–R10** even under NIR excitation. The compounds exhibited maximum emission by femtosecond laser excitation in the wavelength range of 780–820 nm. The examination of the photophysical properties of dilute THF solutions of the compounds revealed that the corresponding luminescence maxima were significantly blue-shifted. The phosphorescence intensity maxima observed at 77 K also were blue-shifted with respect to those observed at room temperature. It was assumed that RTP of all these compounds may arise from some form of aggregates rather than from monomeric species.[49] The single-crystals of **R9** and **R10** were obtained and it was revealed that the neighbouring molecules are in close proximity to each other. On the basis of the obtained crystallographic data quantum chemical calculations were performed for the monomeric and dimeric structures of **R9** and **R10**. The calculated energy gap between the lowest singlet and triplet excited state of the dimer was substantially lower than those of the monomeric forms (Fig. 13). Therefore, in the case of dimers with lower energies ISC was promoted and efficient intermolecular interactions were enabled, which resulted in efficient RTP. These lower energy dimers acted as the ISC channels between S and T states, resulting in the decrease of ΔE_{ST}. Thus, they enabled multiple intermolecular interactions which resulted in the appearance of efficient RTP in aqueous media.

Huand *et al.* decided to decorate the phenanthrene fragment with bromine and cyano groups with the aim of not only facilitating ISC but also obtaining tighter molecular packing by enchancing intermolecular contacts.[50] The luminophore **R11** (Fig. 17 and Table 3) was obtained from 2-(4-bromophenyl)acetonitrile in two steps (Scheme 6). The steady state and time-resolved luminescence spectra of **R11** in the crystalline form exhibited intensity maxima at 615 nm with a PHQY of 4.56% and a luminescence lifetime of 2.24 ms indicating that the nature of luminescence was RTP. When the crystal of **R11**, namely, **R11-r** was left under ambient conditions for 24 hours, its colour changed from red to yellow (**R11-g**), along with the emission colour altering to green. Furthermore, the steady-state spectra recorded showed that the mentioned green emission (559 nm) had nanosecond-range lifetimes, pointing out its fluorescence origin. These authors decided to evacuate the **R11-r** crystal for 25 min and obtained the same change in colour and emission. When the the **R11-g** crystal was annealed for 6 min with DMF vapor, the red emission was restored, while green fluorescence significantly shrinked in intensity. Further experiments proved that the process was reversible and can be repeated more than 10 times. The crystal of non-brominated dicyanophenanthrene

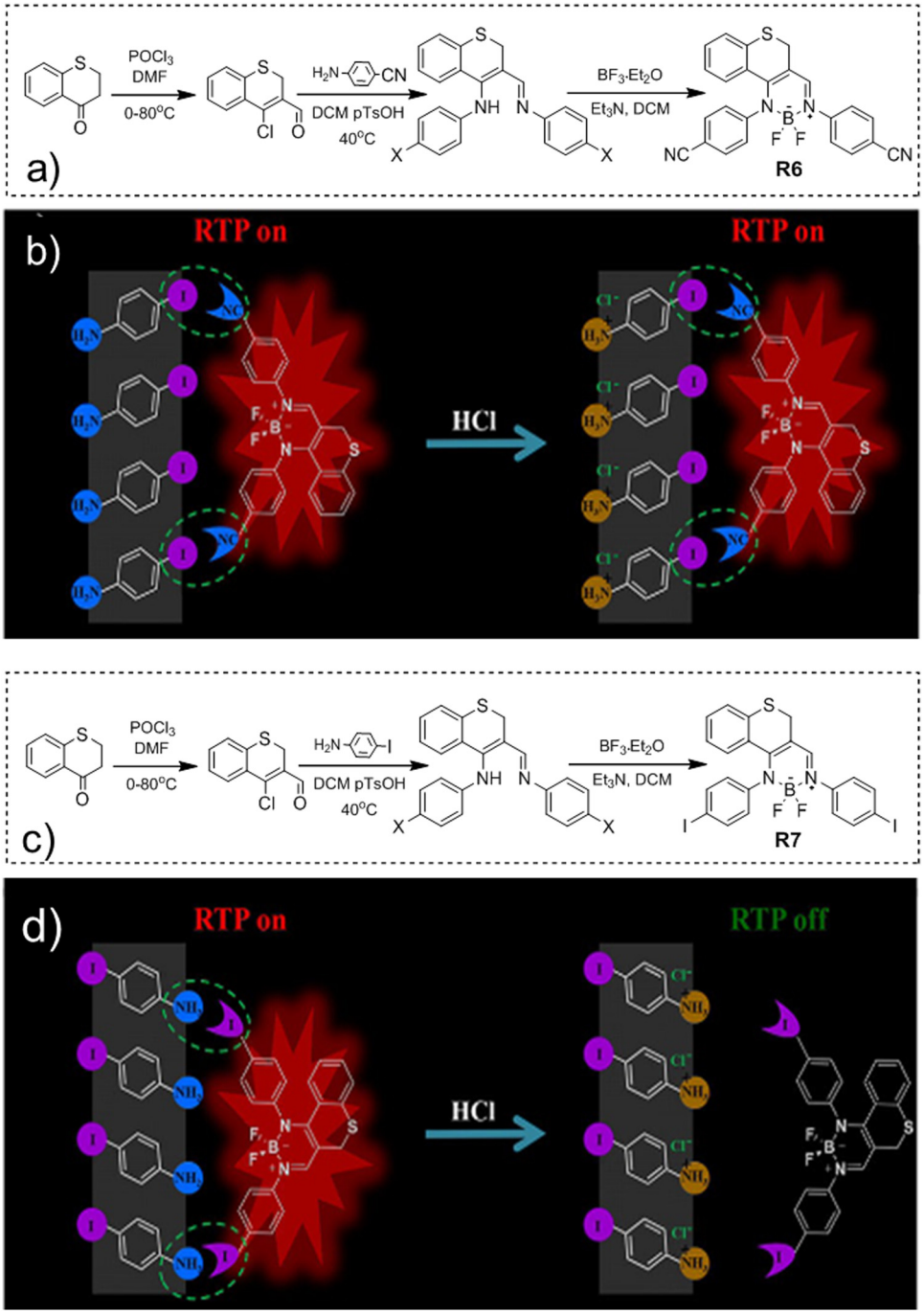

Fig. 12 (a) Synthetic route for the synthesis of compound **R6**, (b) schematic mechanism of HCl-sensitive behaviour of **R6**, (c) synthetic route for the synthesis of compound **R7**, and (d) schematic mechanism of HCl-sensitive behaviour of **R7**. Reproduced from ref. 48 with permission from John Wiley and Sons, Copyright 2023.

showed no red phosphorescence itself, proving that the bromine heavy atoms are essential to initiate phosphorescence. However, it was reported that DMF can decompose into *N*,*N*-dimethylamine upon heating.[51] Therefore, it was speculated that the substitution product of **R11** by *N*,*N*-dimethylamine, namely **N-R11** may be present in the **R11-r** crystal. To prove the assumption, **N-R11** was synthesized according to the route reproduced in Scheme 6. After that, a co-crystal of **N-R11** and **R11** was grown and investigated. It emitted in the very same way as compound **R11-r**, losing RTP after evacuation and restoring it after fumigation with DMF. X-ray analysis revealed that in the case of **R11-r** red phosphorescence occurred from the host–guest system cluster of **R11** and **N-R11**, in which DMF stabilized the crystal lattice by providing abundant intermolecular interactions.

Although crystallization is quite a facile strategy to promote RTP by tightening molecular packing, for a single compound

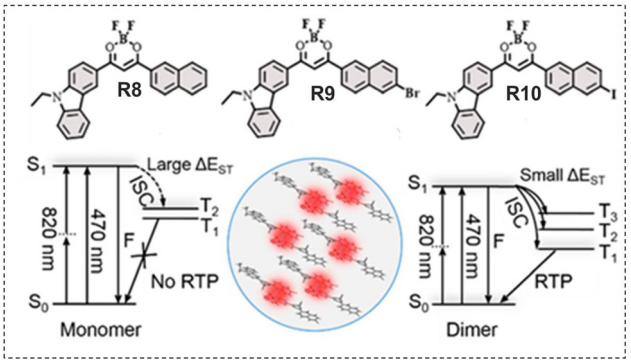

Fig. 13 Molecular structures of compounds **R8–R10** and Jablonski diagram illustrating the origin of RTP from their dimers. Adapted with permission from ref. 49. Copyright 2023, American Chemical Society.

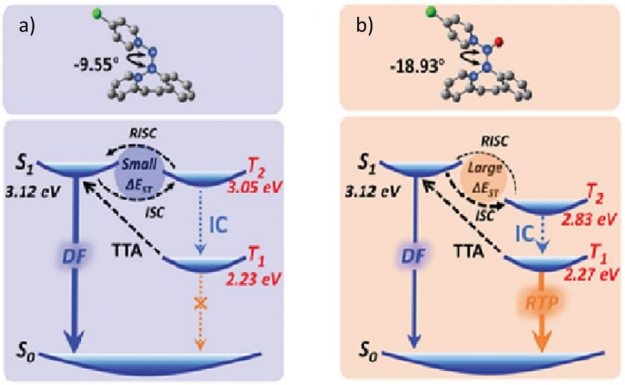

Fig. 14 Geometries and schematically drawn mechanisms of delayed fluorescence in **R12-B** (a) and **R12-Y** (b) types of crystals. Reproduced from ref. 52 with permission from Royal Society of Chemistry, Copyright 2023.

with polymorphism one crystalline form may demonstrate RTP while another may be RTP-inactive. The work of Wen *et al.* is an illustrious example.[52] Compound **R12** (Fig. 17 and Table 3) that has a structure very similar to common organic RTP luminophores was synthesized in one step from iminostilbene and *p*-chlorobenzoyl chloride in 68% yield. Two types of crystals were obtained by different methods: **R12-B** crystals were obtained by sublimation and **R12-Y** crystals were obtained by slow evaporation of the **R12** DCM solution. The **R12-B** crystals showed a rare highly efficient near-ultraviolet emission with the intensity maximum at 398 nm, accompanied with a very high PLQY of 75.2% The PL decay of the **R12-B** crystal exhibited prompt (4.5 ns) and delayed (842.0 μs) components. The **R12-Y** crystals exhibited yellowish emission with a PLQY of 8.1%. Two bands contributed to the resulting emission: a weak band at 398 nm (τ_{PF} of 3.3 ns, τ_{DF} of 808.3 μs) and a major band peaking at 546 nm (τ of 2.1 ms) that had obvious RTP character. Single crystal X-ray analysis was performed for both types of crystals and it was revealed that **R12-B** crystals exhibited a donor iminostylbene fragment rotation by 9.55° with respect to the acceptor fragment. The corresponding angle for **R12-Y** crystals was 18.9° (Fig. 14). Thus, molecular packing and the degree of intermolecular interaction were different. Based on the difference in the crystal structure, theoretical and experimental investigations were further performed to elucidate the emission mechanism of the crystals of **R12**. Singlet–triplet energy splittings were calculated to be too large, enabling rISC, therefore, TADF as a mechanism of blue emission in both crystal forms was excluded. The delayed component in blue emission originated from triplet–triplet annihilation (TTA), which was proved experimentally by recording the photoluminescence spectra of crystals under different excitation powers. Additionally, participation of upper triplet state T_2 was confirmed for **R12-Y** crystals by recording their PL spectra at different temperatures. A new emission band appeared at *ca.* 438 nm at 80 K with a long lifetime of 71.1 ms. Thus, it was demonstrated that this new emission peak originated from the high-lying excited state T_2.

It was further predicted by calculations[52] that in the case of **R12-B**, when the donor–acceptor twist angle is small, only TTA

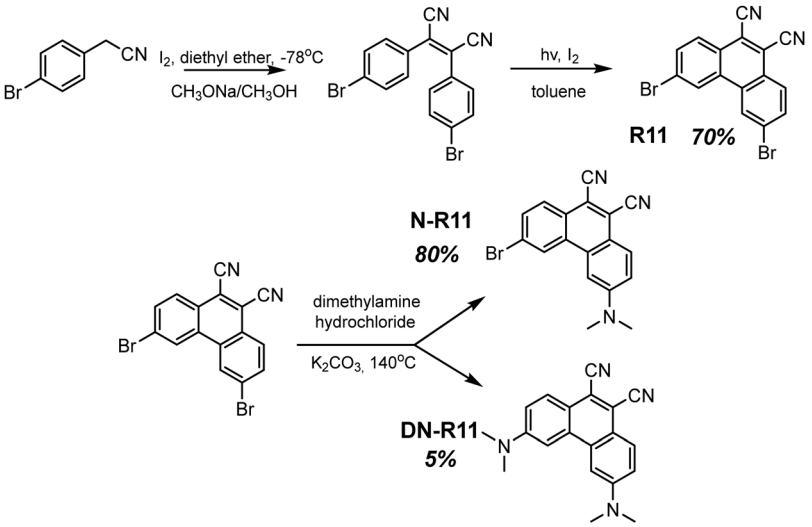

Scheme 6 Synthetic route for obtaining compounds **R11**. Adapted from the litetature.[50]

is achieved through the rISC between the T_2–S_1 process due to the small $\Delta E_{S_1-T_2}$. With an increase in the twist angle, the energy level of the T_2 state is lowered and therefore RTP is achieved for **R12-Y** crystals from the T_1 excited state *via* a more competitive internal conversion (T_2–T_1) process in comparison to the slower rISC (T_2–S_1) process. The tighter molecular packing contributed to the RTP-dominated emission of the **R12-Y** crystal in addition to more effective ISC for triplet exciton population.

The effect of incorporation of a long alkyl chain into the RTP-luminophore on molecular packing was studied by Fateminia *et al.*[53] A soft alkoxy spacer group was introduced between the moieties of, already reported by that time, RTP agent **R13** (Fig. 17 and Table 3) aiming to prolong the emission lifetimes and enhance PHQY. A butoxy spacer helped to separate carbazole and the 4-bromobenzophenone groups, thus affording a new luminogen **R14** (Fig. 17 and Table 3) with a more versatile conformational behaviour. Compound **R14** was obtained from *p*-bromobenzoyl chloride in 90% yield. X-ray analysis revealed that the distance between carbazole and bromobenzophenone units in compound **R14** was shortened, compared to those observed in **R13**. That indicated stronger intermolecular interactions and more efficient RTP. Due to the crystal packing differences, even the effect of the bromine heavy atom was different. The C–Br bond in the crystal of **R13** is far from the carbazolyl fragment. It was arranged nearly parallel to it, weakening the effect of the heavy halogen atom on the carbazolyl unit and resulting in weaker RTP. Taking into account of the observed long phosphorescence lifetime of 0.14 s for **R14**, it can be characterized as one of the most efficient red-emissive persistent RTP materials reported so far.

By incorporating multiple bromine atoms into the well-known organic acid–base indicator phenolsulfonephthaleine, Sun *et al.*[54] recently managed to achieve near-infrared RTP. They doped the **R15**–**R17** derivatives with different amounts of bromine atoms into a rigid PVA matrix. It was reported earlier[55] that the **R15**–**R17** derivatives were highly sensitive to the acidity of the media and undergo structural transformation in acidic and neutral aqueous solutions (Fig. 15). In acidic media, sulfogroups of compounds **R15**–**R17** were found in a close-ring structural form while in neutral and alkaline media, the anionic form prevailed, resulting in ring opening. The authors[54] prepared two types of the films of the molecular dispersions of **R15**–**17** in PVA. The films of the first type were prepared under acidic conditions and the films of the other one were fabricated under neutral conditions. The films, fabricated under acidic conditions, were light-yellow, whereas those fabricated under neutral conditions were dark-blue, manifesting that compounds **R15**–**R17** appeared in the different forms in the differently prepared films. Photophysical investigation revealed that the neutral films exhibited TADF with the intensity maxima at 600–700 nm and RTP peaking above 750 nm. Eventually, the film of the molecular dispersion of **R17** in PVA exhibited the reddest RTP peaking at 819 nm with τ_{RTP} of 0.27 ms. The films prepared under acidic conditions exhibited only red fluorescence and no RTP was observed.

Aromatic imides, such as naphthalene monoimide and phthalimide derivatives are well-known to exhibit orange-red RTP even in the presence of oxygen. Garain *et al.*[56] reported the derivatives of arylene diimide **R18** and **R19** (Fig. 17 and Table 3) functionalized with heavy halogen atoms not only as RTP agents in the long-wavelength spectral region but also as very rare examples of air-persistent RTP. In order to harvest triplet excitons by diminishing the non-radiative energy dissipation the authors[56] dispersed 1 wt% of **R18** and **R19** in a PMMA rigid medium. A strong cyan emission was witnessed for the films of the dispersions of both **R18** and **R19** with the corresponding maxima at 480 (τ_{RTP} = 1.4 ms) and 487 nm (τ_{RTP} = 6.25 μs). In air, the corresponding PHQY values were 18% and 2%, but in a vacuum the **R18** containing film exhibited a remarkably high PHQY of 54%. Interestingly, while increasing the ratio of PMMA to 50%, triplet excitons did not become quenched by the intensified molecular motions but the RTP maxima were shifted to orange-red region peaking at 576 (τ_{RTP} = 5.2 ms) nm and 585 nm (τ_{RTP} = 0.32 ms) for **R18** and **R19** (Fig. 16). The authors[56] assumed that the presence of abundant non-covalent interactions in the aggregated state helps to stabilize the triplet energy. This assumption was further supported by the

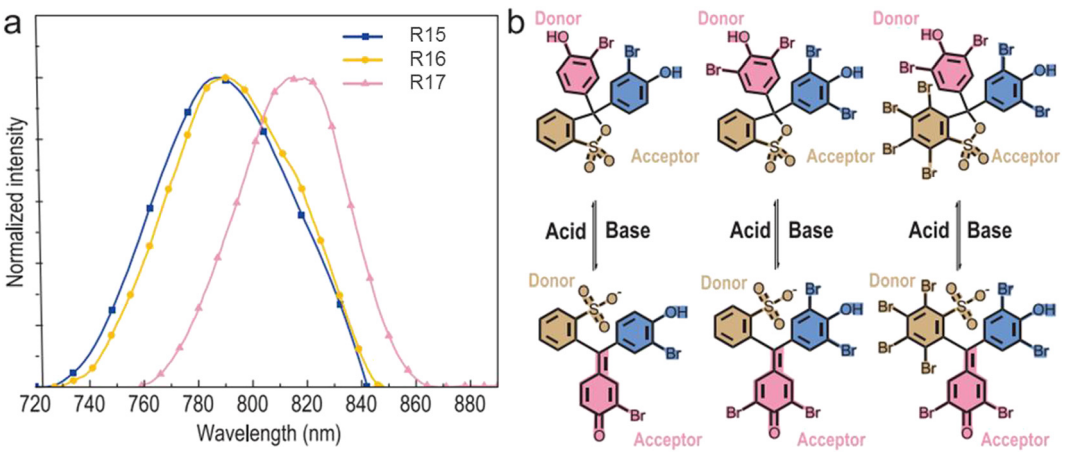

Fig. 15 (a) The RTP profiles of molecular mixtures of compounds **R15–R17** with PVA; (b) structural transformation of **R15–R17** in an aqueous solution with differing pH values. Reproduced from ref. 54 with permission from Oxford University Press. Copyright 2023.

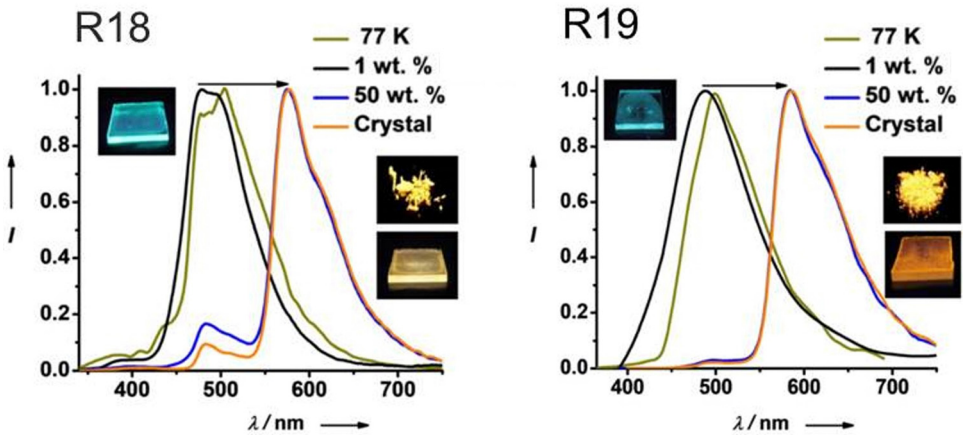

Fig. 16 Phosphorescence spectra of the solutions of **R18** and **R19** in frozen THF recorded at 77 K of the films of molecular dispersions in PMMA with the concentrations of the phosphors of 1 wt % and 50 wt % and of the crystals. Reproduced from ref. 56 with permission from John Wiley and Sons. Copyright 2023.

investigation of the photophysical properties of the single crystals of **R18** and **R19** that exhibited orange-red RTP with maxima at 576 and 585 nm for **R18** and **R19**, indicating the similarity to the phenomena observed for 50% molecular dispersions of the compounds in PMMA. Both the crystals of **R18** and **R19** demonstrated high PHQYs of 26% and 48% in air, which are among the highest PHQY values reported for the orange-red RTP emitters.

A limited number of organic crystals exhibiting RTP persistent under high humidity conditions have been reported.[57] Interaction with water is destructive for RTP since water molecules easily destroy the original intermolecular bonding in crystals and form hydrogen bonds. Furthermore, molecular oxygen present in water quenches triplet excitons. Wang *et al.* reported halogenated maleimide derivatives **R20** and **R21** (Fig. 17 and Table 3) as efficient RTP-agents in the near infrared region.[55] Their RTP demonstrated unique resistivity to water. Yellow crystals of **R20** and **R21** emitted bright red light under a UV lamp. Upon excitation at 450 nm their emission spectra revealed broad unstructured peaks *ca.* 650 nm. The emission lifetimes were found to be 87 μs and 11 μs for **R20** and **R21**, respectively. For compound **R20**, the excitation spectrum revealed four excitation peaks at 385 nm, 405 nm, 450 nm, and 530 nm. Upon all these excitations, compound **R21** demonstrated very similar phosphorescence decay profiles with constant lifetimes, indicating that RTP of **R20** originates from one emission centre. The authors of ref. 55 also studied the impact of morphology of the solid samples on RTP of **R20** and **R21**, fabricating their thin films with a thickness of *ca.* 465 nm. Due to the low thickness, some light penetrated the surface before getting absorbed by it. The films demonstrated photophysical behaviour very similar to that of the crystalline samples confirming that red RTP of **R20** and **R21** is stable and independent of the morphology of the samples. PHQYs of the films were lower than those of the crystals. This observation can be attributed to the degradation of the crystalline lattice to some extent that facilitates the molecular motions and leads to nonradiative energy losses. In order to establish whether the RTP properties of maleimides **R20** and **R21** originate from the single molecules or from aggregates, a single crystal X-ray analysis was performed. It was revealed that the molecules of both **R20** and **R21** are packed in a quite stable 2D-layered structure, that is stabilized by abundant intermolecular interactions. No π–π stacking was observed that indicated the absence of J-type and H-type aggregates and proved that the RTP properties of **R20** and **R21** originated from single molecules. Amazingly, after soaking the **R20** crystal in water for one hour, the phosphorescence remained almost unchanged. The authors of ref. 55 explained such a high water stability by a stiff layered structure stabilized by halogen bonds, preventing the diffusion of water into the crystalline lattice.

Wang *et al.*[58] succeeded in evoking RTP from 1,8-naphthalimide **R22** (Fig. 17 and Table 3) by doping it into isomeric dicarboxylic acids. Planar and rigid **R22** is reported to be an efficient fluorescent material without any hints of delayed emission at room temperature due to its large singlet–triplet energy splitting. The authors[58] considered the aromatic dicarboxylic acids as favourable hosts for **R22** to activate RTP because of their high PHQYs, long phosphorescence lifetimes and high singlet and triplet energy levels which ensure efficient energy transfer to the **R22** guest. Additionally, plentiful intermolecular interactions can be formed between the carboxylic groups of the aromatic acid and the imidyl group of **R22** that results in a stable molecular framework. Guest–host films of **R22** and *ortho*-, iso- and terephthalic acid were prepared. All the films exhibited a bright yellow afterglow after ceasing the UV irradiation. The best RTP-performance was demonstrated by the film of the molecular mixture of **R22** isophthalic acid with a τ_{RTP} of 1.169 s and a PHQY of 5.9%. The authors of ref. 58 also investigated the impact of guest concentration on RTP. After increasing the molar ratio of the **R22** guest from 0.02 to 1 mol%, the relative RTP intensity significantly decreased. That could be caused by triplet quenching. A concentration lower than 0.02 mol% resulted in inefficient energy transfer that again led to inefficient phosphorescence.

The essential role of intermolecular interactions in evoking RTP in organic systems was proved by Chen *et al.*[59] The

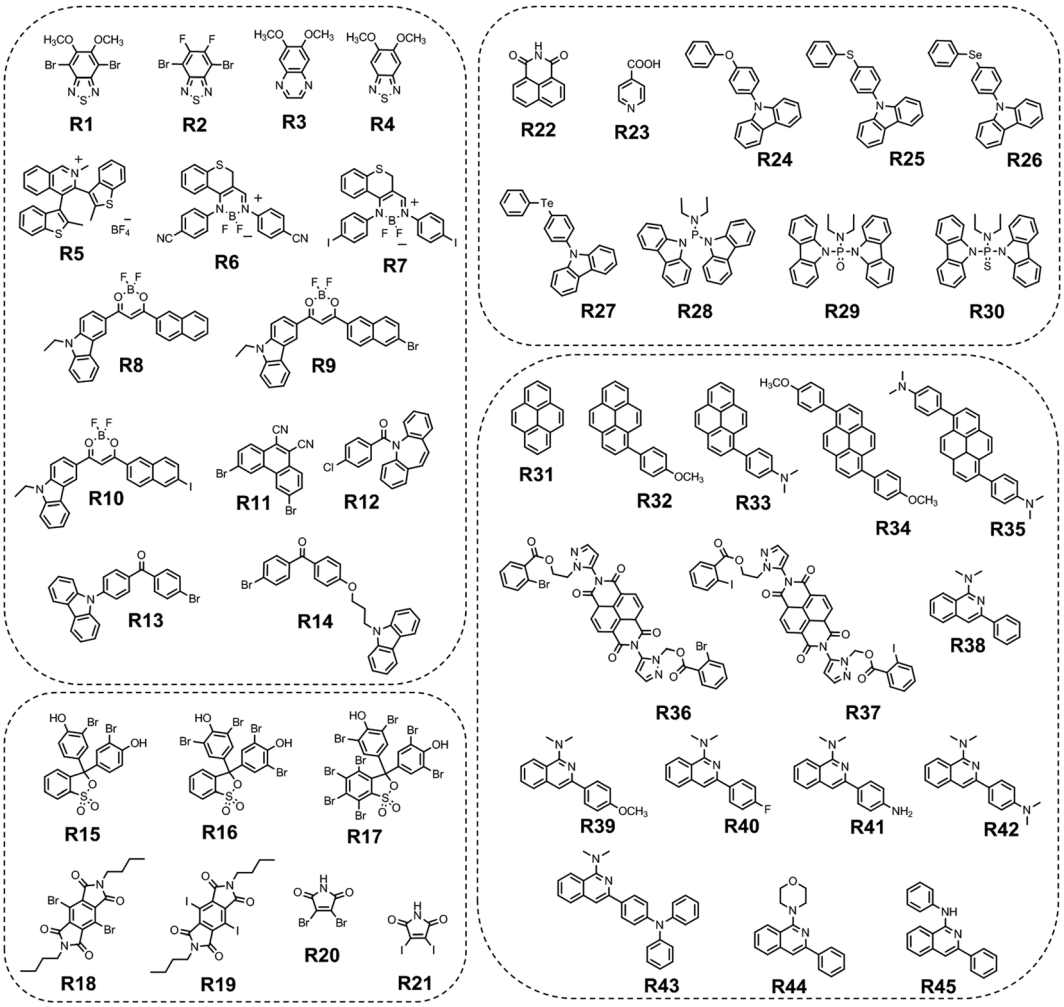

Fig. 17 Molecular structures of red RTP-agents **R1**–**R45**.

isonicotinic acid **R23** (Fig. 17 and Table 3) was found to be an excellent RTP agent being in the crystalline state but lost its RTP properties when dispersed in the rigid PMMA matrix. Under excitation two luminescence bands were observed for the crystals of isonicotinic acid **R23**. The fluorescence band peaked at 443 nm while the RTP band peaked at 573 nm (τ_{RTP} = 79 ms). After doping isonicotinic acid into the PMMA matrix it did not exhibit RTP. This observation suggested that RTP of **R23** crystals was initiated by hydrogen bond interactions between the carboxyl group and the pyridine nitrogen atom.

Xu *et al.* studied the impact on RTP of heavy chalcogen atoms by combining a chalcogen-linked diphenyl fragment with the carbazolyl donor unit (**R24**–**R27**, Fig. 17 and Table 3).[60] The simplicity of the structure made it possible to tune the RTP properties by incorporating chalcogen atoms with different sizes something that made it possible to study the mechanism of RTP at a single-molecular level. All the compounds in the crystalline state demonstrated structured fluorescence peaking in the range of 400–470 nm. For selenium-containing **R26** an additional band appeared at 525–675 nm. After switching off the excitation source, all the samples emitted yellow light with maxima at 525–675 nm. The similarity of emission profiles of the compounds indicates that they had similar T_1 energies. Nevertheless, the PHQYs and τ_{RTP} were different: 0.3% and 423 ms for **R24**; 0.7% and 753 ms for **R25**; 7% and 380 ms for **R26** and 0.03% and 7 ms for **R27**. The phosphor **R27** exhibited one of the longest phosphorescence lifetimes among the reported tellurium-containing compounds. A single crystal X-ray analysis revealed that molecular conformations as well as the crystal packing were similar for all the compounds, indicating that differences in the RTP-behaviour were predetermined by the individual chalcogen atom. In the case of compounds **R24**–**R25** the low values of spin–orbit coupling were predicted indicating a rather weak ISC for these compounds. In contrast, compounds **R26**–**R27**, featuring heavier selenium and tellurium atoms, have high spin orbit coupling indicating that an electron can be easily moved from S_1 to T_n. **R27** exhibited the largest SOC constant that resulted in the shortest phosphorescence lifetime among the compounds of the series.

Tao *et al.*[61] synthesized three photoresponsive organic luminophores containing phosphorus atoms **R28**–**R30** (Fig. 17 and Table 3). Steady-state luminescence spectra revealed orange

ultralong organic phosphorescence for the powders of compounds **R28** and **R30**. Considerably shorter RTP with a lifetime of 40 ms was measured for the sulfur-containing compound **R30**. When the powders of all three compounds were irradiated with 365 nm UV light, their phosphorescence lifetimes as well as phosphorescence quantum yields profoundly increased. A most significant change in PHQY by a factor of 18.5 was observed for compound **R29**.[62] Pyrene is widely used in the design and synthesis of electroactive materials due to the high population of triplet excitons.[63] Xiao *et al.*[64] recently proposed a facile method of activating RTP in pure pyrene **R31** (Fig. 17 and Table 3) as well as in its mono- and di-substituted derivatives **R32–R35** (Fig. 17 and Table 3) by doping them into a benzophenone host matrix. Highly conjugated pyrene-based guests had T_1 energy levels sufficiently low to afford RTP in the red/NIR area. The authors[64] chose benzophenone as a host with the aim of promoting exciton transfer from the guest to the host and to diminish their non-radiative transitions by suppressing molecular motions. Resulting RTP was observed in the range of 600–732 nm together with long τ_{RTP} ranging from 102 ms to 324 ms. Through this smart guest–host architecture, the authors[64] managed to achieve both long τ_{RTP} and emission in the NIR area, which is a perfect combination for biomedical applications. The stability of guest–host films containing **R31** and **R33** was studied. After soaking in water for 24 h, the films still had a strong red afterglow. Their phosphorescence remained almost unchanged after keeping under ambient conditions for a month.

Near-infrared RTP derivatives of naphthalene diimide (NDI) were reported by Ono *et al.*[65] Similarly, to its hydrocarbon relative pyrene, NDI has low-lying triplet energy levels that result in large ΔE_{ST}.[66] Efficient RTP was realized in metalorganic complexes where NDI acted as a ligand. The intermediate NDI-derivative was synthesized in 58% yield by the reaction between 1,4,5,8-naphthalenetetracarboxylicdianhydride and 5-amino-1-(2-hydroxyethyl)pyrazole.[65] Compounds **R36** and **R37** (Fig. 17 and Table 3) were obtained *via* coupling of an intermediate with the corresponding halobenzoates. The NDI-derivative with a 3-chlorodenzoate unit exhibited only fluorescence while a compound bearing a 3-bromobenzoate unit (**R36**) afforded both green fluorescence and orange RTP. Surprisingly, two out of three iodine-containing compounds that have an iodine atom introduced at C-3 and C-4 positions of the benzene ring exhibited no RTP while compound **R37** that has the C-2 position occupied by iodine demonstated bright NIR RTP with a lifetime of 11 μs. At first glance, there is a trend in RTP performance of the series determined by the heavy atom effect that promotes ISC. While the chlorine-containing derivative showed no RTP, the bromine containing compound showed both RTP and fluorescence. To clear up why there was no RTP observed for the two iodine-containing isomers, the authors[65] performed single X-ray analysis for the compounds containing iodine atoms. It was revealed that the compounds formed open structures originating from a flexible linker at the NDI core and halobenzoate fragments. In the case of compound **R37**, the NDI core and 2-iodobenzoate packed closely and formed face-to-face intermolecular stacking. The authors[65] assumed that such packing promoted CT interaction between molecules, which resulted in RTP. This assumption was confirmed by quantum chemical calculations.

Isoquinoline derivatives are widely used in organic optoelectonics due to their high photostabitity and a great possibitity of structural modifications.[67–69] Chen *et al.*[70] reported isoquinoline-based compounds **R38–R45** (Fig. 17 and Table 3) which exhibited persistent yellow afterglow at room temperature when doped in a benzophenone matrix. They suggested a simple and cost-effective method of obtaining isoquinoline derivatives using copper catalysts such as copper(I) iodide. Compounds **R38–R45** containing different peripheral moieties were doped into the benzophenone host (molar ratio 1 : 100). A persistent yellow afterglow was observed for all the films after ceasing the excitation source at 418–468 nm but with very different lifetimes. Phosphorescense lifetimes and PHQYs were lower for compounds **R39**, **R41**, and **R42**, indicating that functionalizing the isoquinoline core with electron-donating groups results in a lower RTP performance. Triphenylamine-containing compound **R43** exhibited the highest PHQY and one of the longest τ_{RTP} among the whole family.

6. White RTP agents

The fabrication of white solid-state light-emitting devices is a challenging task.[71] A conventional strategy to generate white emission is to appropriately adjust emissive layers with complementary blue/orange or primary blue/green/red colours of emission in a multi-layered device.[72] This approach has a series of drawbacks, including unavoidable phase separation that appears as a consequence of a multi-layered structure and results in unstable luminescence. An intuitive strategy to overcome the issue is to fabricate a device that consists of one white light-emitting layer. This means the necessity of obtaining of a combination of several emission bands in a single molecule. As long as white light is composed of emission with different wavelengths, it is practically impossible to reach an RGB spectrum with the same excitation wavelength and with the same photoluminescence lifetime using one compound. If three different types of chromophores (*i.e.*, blue, green and red) are combined in a single molecule, the resulting emission arises from the red moiety. For the single molecule, the emissive spectral coverage of 400–700 nm (the spectral coverage of white light) is not consistent with Kasha's rule that states that the photons can only be emitted from the lowest excited state.[73] Various approaches are explored with an attempt to achieve single-molecule white emission, *e.g.*, aggregation-induced emission enhancement (AIEE), molecular excited-state intramolecular proton transfer (ESIPT), excimer and electroplex formation.[74] In particular, harvesting of triplet emission imposes a vast contribution to the above-listed phenomena. A balanced white spectrum can be achieved either from blue fluorescent material by carefully adjusting the suitable host that induces orange afterglow or from the co-existence of blue fluorescence and complementary orange RTP in a single molecule. The latter seems to be more

challenging but advantageous from a technological perspective. It is possible to outline a number of general strategies for the design of purely organic molecules with dual excited state emission to afford white light:

(1) The singlet excited state should not be converted into a triplet excited state ultimately, because in the opposite case we will have only phosphorescence. Therefore, ISC should be rather balanced, not too rapid, to achieve both fluorescence and phosphorescence because for white light, we are interested in both.

(2) Singlet–triplet energy splitting has to be *ca.* 0.2 eV. Too large splittings will not be efficient in evoking triplet excited states, while too small splittings may initiate thermally activated delayed fluorescence.

(3) The structure of the emitter has to be sterically hindered to suppress the non-radiative energy dissipation.

The first statement is essential for white light generation whereas the 2nd and the 3rd ones are general rules for the initiation of RTP in pure organic compounds.

Along the path of searching for organic white-emitting materials, Yang *et al.*[26] came across an interesting finding. By studying the pressure effect on RTP, they discovered that the well-known yellow RTP-agent thianthrene is an uncommon white emitter.[26] The authors[26] compared the pressure-responsive emission of thianthrene **W1** with that of selenanthrene **G7** (Fig. 11 and Table 2). Both thianthrene and selenanthrene are RTP-active due to the presence of heavy atoms and a folded structure that facilitates spin–orbit coupling. However, in the case of heavier selenanthrene, SOC is strengthened and only pure RTP was observed, whereas thianthrene **W1** showed dual-emission, *i.e.*, minor blue fluorescence and the dominating yellow RTP (Fig. 18a). Isotropic hydrostatic pressure was applied to the powder of **W1** with the aid of a diamond anvil cell. As the pressure was increased, more molecular interactions occurred which effectively suppressed restrictions of molecular motions and non-radiative quenching of triplet excitons. Interestingly, for thianthrene **W1**, high pressure did not close up a fluorescence radiative way by shortening the intermolecular distances and promoting ISC, but intensified it to the point comparable with RTP (Fig. 18b). The authors[26] explained such unusual enhancement by the prevalence of nonradiative molecular motions over the ISC process. Consequently, both RTP and fluorescence were enhanced profoundly, which resulted in the change of the emission colour from yellow to white (Fig. 18c). The most intense white emission was achieved at a pressure of 4.55 GPa. At a higher pressure the emission shrunk drastically.

Two unique examples of the smallest single-molecular white emitters were reported by Zheng *et al.* in 2021.[75] One of the first attempts to develop tiny single-molecular white emitters was made by Zhang and co-workers, who reported derivatives of triazole with intrinsic broadband white light emission in 2017.[76] However, the white emission of the mentioned derivatives did not include RTP but originated from supramolecular aggregates and involved several processes, like excited-state intramolecular proton transfer (ESIPT), synergetic emission from a monomer and excimer/exciplex, aggregation-induced emission (AIE), delayed fluorescence, and simultaneous emission from singlet and triplet states of a single monomer.

Rigid and planar compounds **W2** and **W3** (Fig. 20 and Table 4) both of which feature electron-rich sulfur atoms were obtained from commercially available thiophene-3,4-dicarboxylic acid with yields of 68.3% and 85%, respectively.

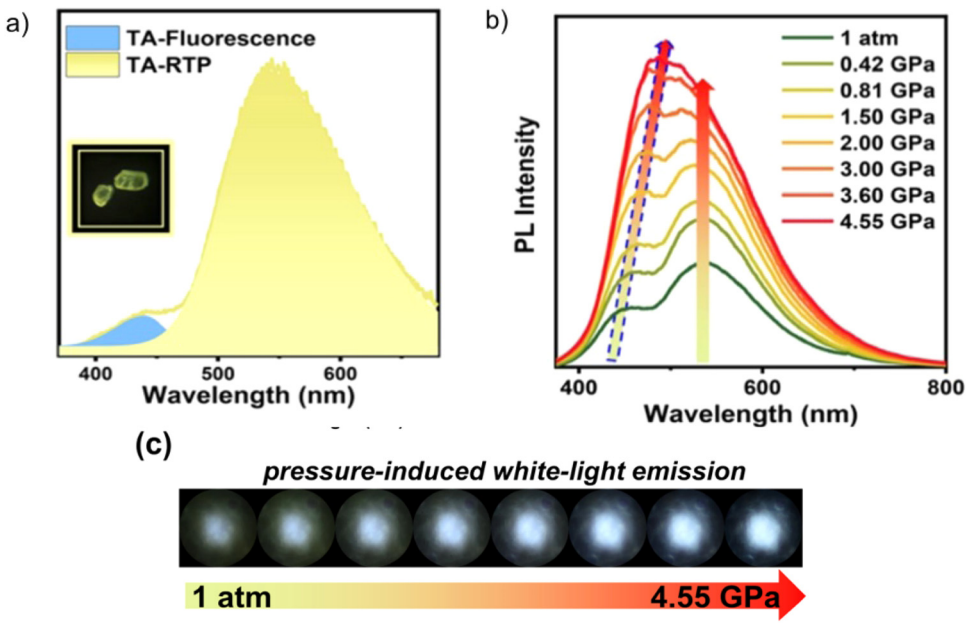

Fig. 18 (a) Emission spectra of the crystal of **W1** observed under ambient conditions, (b) pressure-responsive luminescence spectra of the single crystal of **W1**; and (c) luminescence photographs of the single crystals of **W1** under different pressures. Reproduced from ref. 26 with permission from Royal Society of Chemistry, Copyright 2023.

Table 4 Photophysical parameters of white RTP-agents **W1**–**W16**

Compound	λ_{FL}, nm	τ_{PL}, ns	FLQY, %	λ_{RTP}, nm	τ_{RTP}, ms	PHQY, %	Host	CIE coord.	CRI index	Ref.
W1	*n*/*m*	*n*/*m*	*n*/*m*	*n*/*m*	*n*/*m*	*n*/*m*	*n*/*m*	*n*/*m*	—	26
W2	—	—	—	585	39	—	—	(0.26, 0.30)	85[a]	75
W3	—	—	—	587	44	—	—	(0.32, 0.42)	—	75
W4	386	0.4	—	519	35.6	—	—	(0.24, 0.26)	—	77
W5	388	0.7	—	549	0.007	—	—	(0.27, 0.27)	—	77
W6	455	1.75, 6730	—	571	4.16	—	—	(0.33, 0.33)		78
W7	393	2.71	31.0	546	626	1.7	PVA	—	—	79
W7^{film}	—	—	—	543	328	2.5	—	—	—	79
W8	413	2.70	3.2	562	480	5.5	PVA	—	—	79
W8^{film}	—	—	—	546	356	5	—	(0.33, 0.34)	87[a]	79
W9	422	2.07	0.5	547	142	1.6	PVA	—	—	79
W9^{film}	—	—	—	546	150	0.5	—	—	—	79
W10	455	89×10^6	50.68	542, 592	280	10.92	—	(0.30, 0.35)	—	80
W11	402	1.53	2.9	547	134	7.4	—	(0.33, 0.34)	—	81
W12	405	0.7	1.6	544	219	11.3	—	—	—	81
W13	410	3.4	6.34	567	204	2.85	—	(0.27, 0.26)	—	82
W14	431	3.4	3.6	546	79	5.5	—	(0.30, 0.31)	—	83
W15	448, 475, 550	4.7, 5.6, 4.5	—	575	370	—	—	(0.28, 0.31)	—	84
W16	467	—	42	564	13.67	42	Zeonex	(0.32, 0.39)	79	85

λ_{FL} – the wavelength of fluorescence maxima, τ_{PL} – fluorescence lifetime, FLQY – fluorescence quantum yield, λ_{RTP} – the wavelength of room temperature phosphorescence maxima, τ_{RTP} – RTP lifetime, PHQY – phosphorescence quantum yield, CIE – Commission Internationale d'Eclaraige, CRI – colour rendering index, and *n*/*m* – not mentioned. [a] Estimated for the fabricated device.

Compound **W3** possesses the unique ability of emitting white light both in solution and in crystalline states. The origin of white emission in DMF is the emission enhancement caused by the formation of aggregates with different sizes, while emission in the solid state exhibits orange RTP. Investigation of the photophysical properties of DMF solutions of **W3** in DMF led to the conclusion that the luminescence intensity of **W3** depends on the concentration and increases considerably with the increase in the concentration from 5×10^{-3} M to 0.25 M.[75] In addition, the change in the colour of emission from blue to green, and finally to yellow-white was observed. A conclusion was made that compounds **W2** and **W3** are AIE-active. However, their AIE-activity is different from that of the conventional AIE agents, rich in rotational fragments. The lack of the latter in **W2** and **W3** allowed the authors[75] to deduce that the AIE mechanism of their emission does not refer to a restriction of molecular rotations but to space-conjugation of the aggregates. At a concentration of **W3** in DMF of 0.25 M the excitation at 340 nm afforded a wide white emission with CIE coordinates of (0.30, 0.36). In the case of compound **W2** the intermolecular interaction of its aggregates at high concentrations was found to be weaker than that of **W3** which was explained by the absence of a nitrogen heteroatom. As a result, white emission of its DMF solution was not observed. The crystals of **W2** and **W3** were easily grown from toluene and methanol solutions. They showed yellow RTP after turning off the 365 nm light source. The crystals of **W2** showed emission intensity maximum at 585 nm and a lifetime of 39 ms, while the RTP of the crystal of **W3** peaked at 587 nm with a lifetime of 44 ms. Their photoluminescence spectra covered the whole visible light region. The crystal of **W2** demonstrated cold white luminescence with CIE coordinates of (0.26, 0.30), while that of **W3** displayed white light with CIE coordinates of (0.32, 0.42). On the basis of theoretical calculations, the authors[75] concluded that RTP of the crystals of **W2** and **W3** originated from a certain kind of specific aggregate and that it had no obvious excitation wavelength dependence.

Two efficient dual-emissive compounds **W4** and **W5** (Fig. 20 and Table 4) were synthesized by Xu *et al.*[77] Butterfly-type luminogens **W4** and **W5** were obtained *via* a Suzuki cross-coupling reaction from the corresponding arylbromide and dibenzo[*b*,*d*]thiophen-4-yl-boronic acid in 76% and 78% yields, respectively. Their solutions exhibited only blue fluorescence, but in the solid state, both compounds were found to exhibit biluminescence that included orange RTP with the CIE coordinates of (0.24, 0.26) and (0.27, 0.27), respectively. The authors[77] observed that phosphorescence of the crystals of both the compounds shrank significantly after applying a mechanical force. Fluorescence also underwent minor red shifts from 385 nm to 392 nm in the case of the crystal of **W4** and from 400 nm to 414 nm in the case of **W5**. Thus, their emission is easily tuneable from white to deep blue even with a minor mechanical treatment or hand grinding. Based on the single crystal analysis the authors[77] concluded that mechanochromism appeared as a result of a transition from the crystalline phase to the amorphous one that destroyed intermolecular interactions thus opening up a way for triplet excitons to relax nonradiatively. By fuming the films of both the compounds with dichloromethane vapor, the yellow phosphoresce of **W4** and **W5** was revitalized again and the emission colors were restored to white. Interestingly, the authors[77] also discovered that thermal annealing also caused a change in the emission colour of **W5** from white to blue with CIE coordinates of (0.18, 0.11). Emission of the annealed sample was found to return back to the white colour after the fumigation with DCM vapour.

One more white-emitting dibenzothiophene derivative **W6** (Fig. 20 and Table 4) was reported by Zhang *et al.*[78] They attached pyrimidine to dibenzothiophene *via* Suzuki coupling

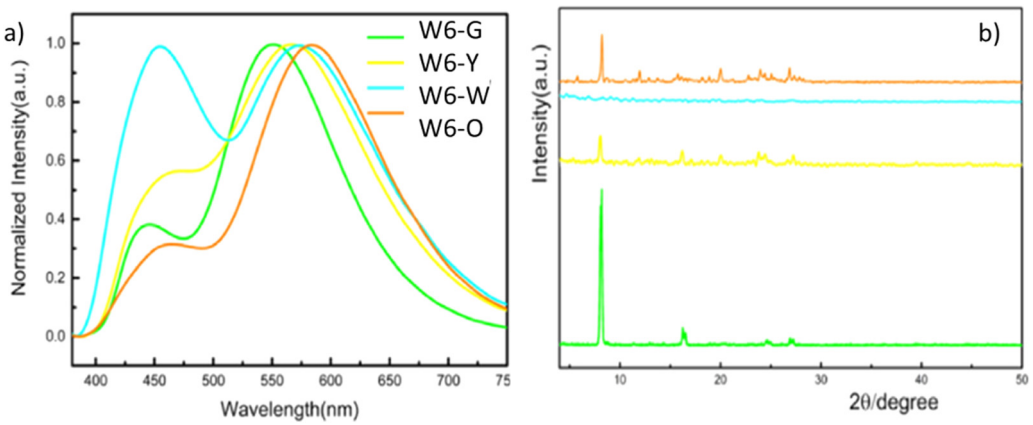

Fig. 19 PL spectra (a) and powder X-ray diffraction (b) of compound **W6** in different solid states. Reprinted from Y. Sun, H. Qu, J. Zhang, X. Duan and X. Zhang, Room temperature phosphorescence, thermally activated delayed fluorescence and multicolor mechanochromic luminescence of emitters through molecular interaction and conformational modulations, *Tetrahedron*, **110**, 132692,[78] Copyright 2023, with permission from Elsevier.

between 4-chloropyrimidine hydrochloride and dibenzo[*b*,*d*]-thiophen-4-yl-boronic acid. The PL spectra of crystalline powder of **W6** displayed dual emission with the peaks at 455 nm (1.75 ns, 6.73 μs) and 571 nm (1.16 ms). Similarly to **W4** and **W5**,[77] the emission of compound **W6** also exhibited stimuli responsiveness. The fluorescence peak shifted after grinding, and the phosphorescence peak significantly decreased. The authors[78] managed to grow yellow-green crystals of **W6**, namely **W6-G** by slow evaporation of the hexane/DCM mixture. The PL spectrum of **W6-G** demonstrated a dominant peak of phosphorescence at 550 nm, and a minor peak of fluorescence at 443 nm. When slightly ground in a mortar, the **W6-G** crystals transformed into a **W6-Y** type of crystal along with an RTP colour shifting from yellow-greenish to yellow (565 nm). After continuing grinding, the **W6-Y** crystals underwent another transformation into **W6-W** powder, and its emission peaks were further red-shifted to 454 nm and 574 nm, with almost equal intensities (Fig. 19). The CIE coordinates of **W6-W** were calculated to be (0.33, 0.33), confirming its pure white light emission. The process was reversible. It could be repeated several times.

Crystalline materials usually suffer from poor processability and reproducibility. In particular, the preparation of their thin films is always a critical and challenging task, while thin films with desirable optical properties are highly desired for many important practical applications. Shu *et al.*[79] studied the impact of heavy chalcogen atoms on RTP of three asterisk-shaped molecules **W7–W9** (Fig. 20 and Table 4). The heavy atom effect and large steric hindrance led to the appearance of RTP not only in crystalline forms, but also in neat and host-containing films. The compounds were obtained *via* a nucleophilic aromatic substitution reaction between carbazole and the corresponding tetrafluorinated chalcogene-containing intermediate in the moderate yields of 60–75%. The most effective k_{ISC} in the series was observed for compound **W9** containing the selenium atom. Unlike most organic RTP materials, all three compounds demonstrate RTP even in neat films peaking at 543, 546, and 546 nm, respectively. This is due to high steric hindrance of

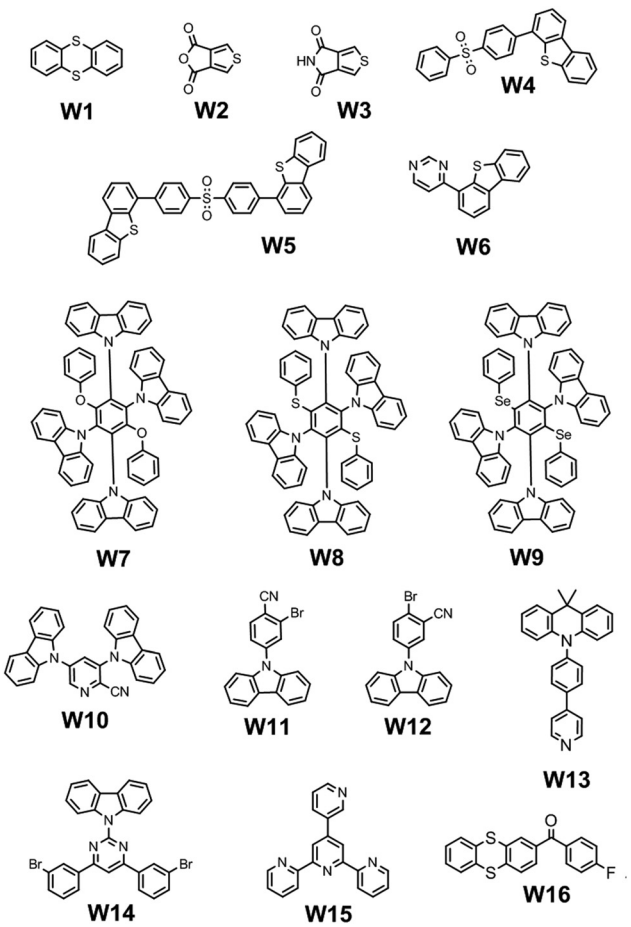

Fig. 20 Molecular structures of white RTP-agents **W1–W16**.

star-shaped structures that suppress non-radiative electronic transitions. The neat film of compound **W8** showed the longest lived RTP with τ_{PHOS} of 356 ms. This was the highest τ_{PHOS} value among all reported low-molar-mass organic molecules. Although compound **W7–W9** exhibited complementary blue-yellow emissions, the authors[79] managed to generate white

emission only from compound **W8**. This compound doped into DPEPO was used for the preparation of an emitting layer of a solution processed WOLED with white electroluminescence and CIE colour coordinates of (0.36, 0.38).

Liu *et al.*[80] reported RTP-containing white afterglow of the molecule containing no heavy halogen or chalcogen atoms. Compound **W10** (Fig. 20 and Table 4) that consists of a pyridine ring, to which two carbazole moieties are linked at the *meta*-positions and a cyano group linked at the *ortho*-position, was easily obtained *via* nucleophilic substitution between carbazole and 4-cyano-3,5-difluoropyridine. The presence of two carbazolyl donor units led to a decrease in ΔE_{ST} and a promotion of ISC and rISC. Under excitation at 365 nm, the crystal of compound **W10** exhibited blue emission with white afterglow. The white emission of **W10** consisted of TADF (λ_{max} = 455 nm, τ = 89 ms), distinguishable thermally activated delayed phosphorescence (λ_{max} = 483 nm) and organic ultralong phosphorescence from the stabilized triplet state T_1^* (λ_{PHOS} = 542 nm, 592 nm, and τ_{RTP} = 240 ms). This is the first and only example of a molecule's white afterglow which appears from multi-mode triplet emissions.

RTP has a tendency to cease when the temperature of the environment is increased. The molecular packing tightens as temperature decreases, leading to the enhancement of intermolecular interactions. When the temperature increases, molecular movement becomes more intensive, resulting in weaker intermolecular interactions. Bi *et al.*[81] reported two isomeric compounds **W11** and **W12** (Fig. 20 and Table 4) that are similar to **W10** in structure but have a bromine heavy atom instead of one carbazole moiety. The compounds were reported to be the first examples of materials with stable RTP at elevated temperatures. The introduction of bromine helps not only to enhance the RTP efficiency but also to increase the thermal stability and most importantly resistance of RTP of **W11** and **W12** to the elevated temperatures. The authors[81] explained this observation by the co-presence of bromine atoms and cyano groups, facilitating abundant intermolecular interactions. The solid powders of both the compounds **W11** and **W12** demonstrated biluminescence with fluorescence maxima in the deep-blue region of the spectrum (at 402 nm for **W11**, 405 nm for **W12**), and an RTP peaking in the 523–683 nm range for **W11** and in the 520–689 nm range for **W12**. Both compounds still exhibited double emission in the crystalline state. Compared to the emission of the solid powders, the fluorescence maxima did not change, but τ_{FL} and PHQY significantly increased. At the same time, FLQY and τ_{RTP} were found to be significantly diminished as they were competing processes. The isomers **W11** and **W12** exhibited temperature-dependent emission both as solid powders and in the crystalline state. For a balanced fluorescence-RTP intensity ratio with the help of temperature changing, almost pure white light with the CIE coordinates of (0.33, 0.34), could be achieved for compound **W11**. In addition, a significant RTP peak was still present at 380 K (τ_{RTP} of 4 ms and a PHQYof 3.9%). To the best of our knowledge, these are the first compounds reported in which RTP shows resistance to such temperatures. In addition to the temperature-dependent luminescence, the authors[81] revealed the dependence of the emission on the intensity of the excitation light for both compounds. With the constant growth of excitation intensity, the intensity of fluorescence increased two to three times faster than that of phosphorescence resulting in a modulated multicolour luminescence that includes pure white light (CIE coordinates 0.33, 0.33).

An illustrious example of pure organic RTP of the different morphological forms is compound **W13** (Fig. 20 and Table 4), designed and synthesized by Du *et al.*[82] Luminophore **W13** consists of an electron donating 9,9-dimethyl-9,10-dihydroacridine moiety, an electron accepting 4-phenylpyridine unit and a phenyl linker between them. The authors[82] managed to obtain two crystalline forms of **W13: W13-B** that was afforded by the evaporation of the solvents from the solution of **W13** in a DCM–acetonitrile mixture and **W13-W** that was obtained by diffusing hexane vapour into a DCM solution of **W13**. The PL spectrum of **W13-B** crystals revealed a blue fluorescence peak at 402 nm with a τ_{FL} of 3 ns. The time resolved luminescence spectrometry revealed yellow RTP peaking at 567 nm with a τ_{RTP} of 118 ms. Despite the presence of two complementary emission colours, the authors in ref. 82 failed to obtain white emission from the corresponding crystalline form due to its low PHQY of only 1.07%. Meanwhile, the **W13-W** crystal revealed single-molecular white emission that consisted of blue fluorescence at 410 nm (τ_{FL} of 3.4 ns) and orange RTP at 567 nm (τ_{RTP} of 204 ms) with a PHQY of 2.85%. Consequently, white light with CIE coordinates of (0.27, 0.26) was afforded. The authors[82] performed single X-ray analysis for each polymorph. The molecules in both crystals were characterized by similar dihedral angles between the donor fragment and the phenyl linker, but the dihedral angle between the pyridine acceptor and benzene ring was smaller in the case of **W13-B** crystals. This provides more efficient intramolecular charge transfer in the **W13-B** polymorph. Additionally, **W3-W** crystals were found to form more abundant intermolecular interactions than **W13-B** crystals. Surprisingly, the film of compound **W13** doped in the rigid PMMA matrix also afforded white emission with CIE coordinates of (0.26,0.30) that consisted of two fluorescence components with maxima around 430 nm and 540 nm and an RTP component peaking around 500 nm. The sample was characterized by a PLQY of 40.2%.

Ishi-I *et al.*[83] demonstrated that if a compound exists in two polymorph forms and both of them exhibit dual fluorescence-RTP behaviour, reversible switching can be achieved with the aid of external stimuli. They synthesized a bromine-containing carbazole–pyrimidine conjugate **W14** with a yield of 76% (Fig. 20 and Table 4), which was found to crystallize in two different polymorphs.[83] White crystals of **W14-A** were obtained by the evaporation of the solvent from the chloroform solution of **W14**, while yellow crystals of **W14-B** were grown from a hexane/chloroform mixture. Upon excitation, the **W14-B** crystalline form demonstrated very weak RTP peaking at 546 nm (τ_{RTP} of 8 ms), and fluorescence peaking at 476 nm. Meanwhile, the **W14-A** crystals showed blue fluorescence with the maximum at 431 nm and intensive yellow afterglow (λ_{RTP} of 546 nm and τ_{RTP} of 77 ms). Almost pure white emission, (0.30, 0.31), could be generated by heating **W14-A** crystals above their melting point

(210 °C) and then cooling to room temperature. The obtained crystalline form **W14-W** demonstrated enhanced RTP with PHQY raised to 5.5% together with the decrease of FLQY to 3.6%. The process was reversible and could be repeated. The authors[83] concluded that the heating–cooling cycle of the sample **W14-A** helped to increase its crystallinity that promoted ISC, and therefore in the obtained **W14-W** crystalline form, the phosphorescence intensity increased whereas the fluorescence decreased.

The unique excitation-dependent luminescence was observed by Ma *et al.*[84] from the simple terpyridine derivative **W15** (Fig. 20 and Table 4). After being excited at 254–330 nm, the **W15** film demonstrated two emission peaks at 372 nm and 550 nm. After an increase in the excitation wavelength to 365 nm, a slight decrease in intensity of the peak at 550 nm was observed, but the appearance of three additional peaks at 448 nm and 475 nm and 575 was noticed. The last peak was characterized by a luminescence lifetime of 0.73 s and was recognized as RTP. The resulting emission had CIE coordinates of (0.28, 0.31) which can be described as cold white light. After a further increase in the excitation wavelength to 380 nm, the emission peaks at 448, 475, and 550 nm increased in intensity, but the white emission was still observable (CIE coordinates of (0.30, 0.37)). After increase of the excitation wavelength to 420 nm, the peaks at 448 and 475 nm still increased and a minor peak at 505 nm emerged, while the peak at 550 nm almost disappeared.

Our group recently reported high-quality white emission from a single heavy-atom-free molecule.[85] State-of-the-art monomolecular white emission with a PLQY of 84%, a CRI of 79, a T_C of *ca.* 5100 K, and CIE 1931 colour coordinates of (0.32, 0.39) close to that of the natural white colour (0.33, 0.33) was observed for compound **W16** (Fig. 20 and Table 4). The concept of monomolecular white emission was proved after the investigation of twelve compounds containing thianthrene and benzoyl moieties with different arrangements of halogen atoms. All the compounds were obtained in good yields *via* Fridel–Crafts acylation of thianthrene with differently substituted benzoyl chlorides. The structural peculiarities of the compounds are responsible for their efficient fluorescence and RTP. Taking into account the results of X-ray analyses and the theoretical study, the high PLQY values of the thianthrene derivatives are attributed to the absence of π–π intermolecular interactions and the low amount of weak van der Waals intermolecular stacking due to the strong bending of the heterocyclic thianthrene moiety and due to the high dihedral angle between thianthrene and benzoyl moieties. The valence ⩽C–S–C angle of the thianthrene fragment based on a 1,4-dithiin structural moiety is *ca.* 102°. In the case of the investigated compounds, the theoretically calculated dihedral bending angle between the two planes of the 1,4-dithiin structural moiety *via* the S···S axis was 140.6°. Such dihedral bending of the rigid heterocyclic thianthrene can prevent the formation of π–π intermolecular interactions. Among all twelve compounds, only the **W16** derivative with a fluorine atom in the *para*-position to the carbonyl fragment was found to exhibit almost pure white emission. Such emissive properties originate from well-balanced rates of radiative transition from singlet states (3.24×10^7 s^{-1}) and intersystem crossing (3.09×10^7 s^{-1}).

7. Applications of organic triplet emitters

Organic RTP materials have been used in chemical sensors, anticounterfeiting, molecular oxygen and temperature sensors, for *in vivo* bioimaging, lighting applications, multicolor displays, chemical qubits, optical memory, luminescence printing, 3D printing, information storage in programmable luminescent tags, quantum computers, microfluidic devices, and optoelectronic devices, to mention some examples.[86–88] Multifunctional applications of organic RTP compounds are discussed in many research articles.[89–91] The most widespread applications of organic RTP materials are discussed in review articles.[92–97] Therefore, we will highlight only the recent records and the unique applications of organic RTP materials.

From the point of view of colour purity and efficiency, very attractive applications of organic RTP-agents have been recently reported by Zou *et al.*[98] The authors developed high-colour-purity afterglow materials and demonstrated their potential applications in afterglow displays, information encryption, identification, *etc.* (Fig. 21a–e). For the development of high-colour-purity afterglow materials, phosphorescent chromophores 4,4′-biphenol (BP), 1,1′-bi-2-naphthol (BNP), and 1,8-naphthalimide (NPI) were used as as electron-donating moieties. Rhodamine derivatives (BCA, BPH, R123, RdB, and R101) were used as electron-accepting compounds with narrow-band fluorescence spectra. Both donor and acceptor compounds were dispersed in the polyvinyl alcohol (PVA) matrix. The rigidity of this matrix enabled the prevention of non-radiative transitions of organic RTP-agents and fluorescent derivatives of rhodamine. The efficient Förster resonance energy transfer was observed in donor–acceptor molecular mixtures owing to large emission-absorption spectral overlap of the co-doped donor and acceptor in the PVA polymeric matrix (Fig. 21f). Such systems showed long-lived afterglow at room temperature. The authors[98] investigated a series of narrowband polymeric afterglow materials with high colour purity. By optimization of the donor–acceptor pairs, colours of narrowband polymeric afterglow materials were tuned from green to red. The resulting organic afterglow materials exhibited narrow full width at half-maximum (FWHM) approaching 23 nm, and a long lifetime of 721.22 ms at room temperature (Fig. 21g).

A record external quantum efficiency of 15.8% for host-free OLEDs exhibiting aggregation-induced organic room temperature electrophosphorescence was reported by Xu *et al.*[99] The device efficiency is superior in comparison to that of OLEDs based on previously reported organic RTP emitters.[100,101] The authors[99] designed donor-oxygen-acceptor-type compounds containing an acridine moiety as a donor, a triazine unit as an acceptor and oxygen as the bridge between the acridine and triazine moieties. They claimed that such a molecular structure caused effective ISC resulting in efficient RTP. The neat emitting layers exhibited PLQYs of up to 77.5% under an inert

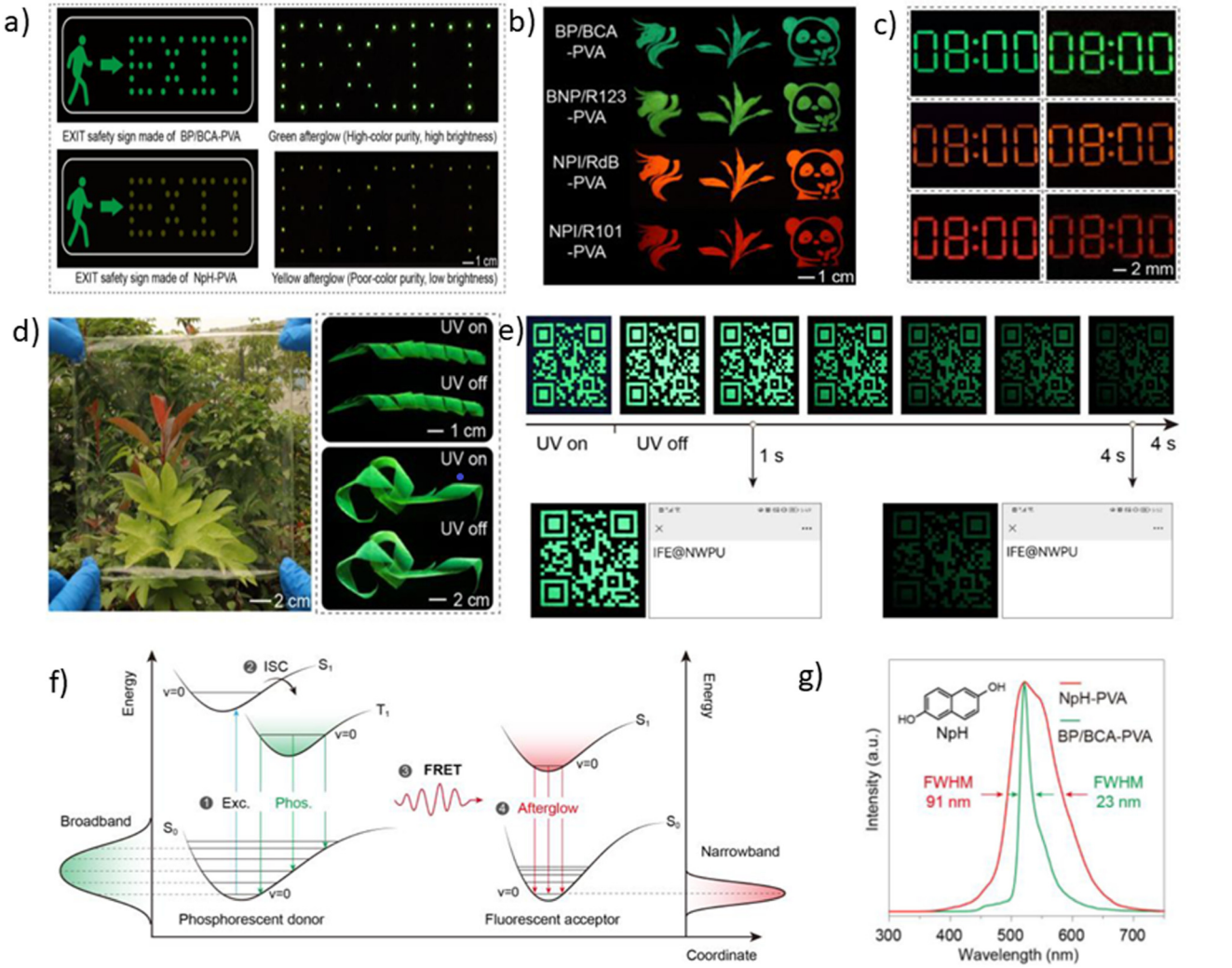

Fig. 21 Examples of applications of narrowband polymeric afterglow materials based on electron-donating RTP-agents for safety sign afterglow displays (a); afterglow photographs with multicolor patterns (b); miniature display patterns in different colors (c); and large-area transparent and flexible film applications under on/off UV excitation at a wavelength of 254 nm (d). QR code before and after switching off the UV excitation at 310 nm (e). Schematic visualisation of the emission mechanism of narrowband polymeric afterglow materials based on electron-donating RTP-agents (f) and delayed photoluminescence spectra of narrowband polymeric afterglow materials and reference films BP/BCA-PVA and NpH-PVA recorded under ambient conditions (g). Reproduced from ref. 98 with permission from John Wiley and Sons, Copyright 2023.

atmosphere. The donor-oxygen-acceptor type RTP compounds were used as the hosts for multiple resonance emitters facilitating the fabrication of pure colour OLEDs with a maximum EQE of 26.4% and narrow electroluminescence spectra approaching FWHMs of 26 nm. In our group, white host-free OLEDs based on organic RTP emitters were developed[102] (Fig. 22a). White electroluminescence of the fabricated devices resulted from the overlapping of blue fluorescence and orange RTP of 2-(3,7-di-*tert*-butyl-phenothiazin-10-yl)thianthrene (PTZ-^{t}Bu-TA).[102] The maximum external quantum efficiencies of the devices did not exceed 1% because of the low PLQY of the neat films of PTZ-^{t}Bu-TA. Meannwhile, the PMMA hosting of PTZ-^{t}Bu-TA leads to intensive green RTP with high oxygen sensitivity described by a high Stern–Volmer constant of 21×10^{-4} ppm^{-1} (Fig. 22b).

Reineke *et al.*[103] used 4,4-dithianthrene-1-yl-benzophenone (BP-2TA) exhibiting RTP with PHQY up to 20% for the fabrication of photonic devices, such as programmable luminescent labels or tags. BP-2TA showed much better performance in programmable luminescent labels in comparison to Ir(III) and Pt(II) complexes (Fig. 23a). The advantages of BP-2TA are mainly attributed to the ratio of Φ_{RTP} and Φ_F (P2F = Φ_{RTP}/Φ_F), which shows a better contrast of the tags than those of tags based on organometallic complexes. Compound BP-2TA demonstrates a P2F value of 21. The same group[104] proposed an interesting application of BP-2TA as the active material of organic thin-film wavelength sensors for accelerating wavelength tracking of inorganic light-emitting diodes under heating. Such applications of BP-2TA were also possible due to its P2F parameter, resulting in the production of mostly triplet excited states due to efficient ISC under absorption of irradiation.

RTP is detectable not only under optical and electrical excitations but also under X-ray excitation, resulting in various

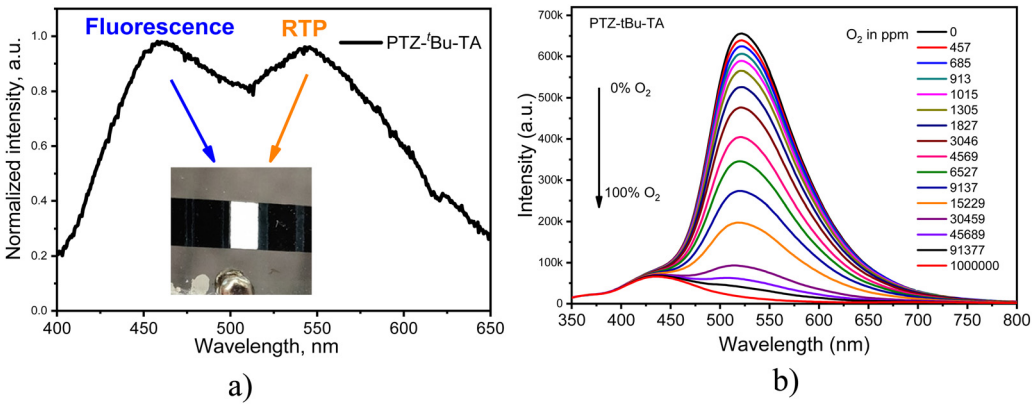

Fig. 22 Electroluminescence (EL) spectra of host-free devices based on the organic RTP emitter PTZ-^{t}Bu-TA (a) and PL spectra of PTZ-^{t}Bu-TA dispersed in the PMMA matrix at different concentrations of oxygen (b). Reprinted from K. Leitonas, A. Tomkeviciene, G. Baratte, A. Dabuliene, S. M. Punniyakoti, D. Volyniuk and J. Vidas Grazulevicius, oxygen sensing properties of thianthrene and phenothiazine derivatives exhibiting room-temperature phosphorescence: Effect of substitution of phenothiazine moieties, *Sens. Actuators, B*, **345**, 130369,[102] Copyright 2023, with permission from Elsevier.

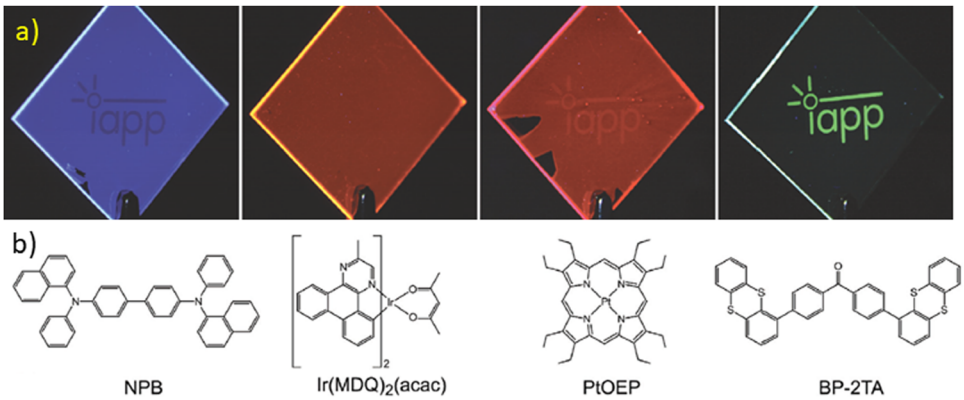

Fig. 23 Programmable luminescent tags with readability under continuous-wave illumination (a) and molecular structure of PRT fluorophores used for their fabrication: NPB, Ir(MDQ)$_2$(acac), PtOEP, and BP-2TA (b). Reproduced from ref. 103 with permission from John Wiley and Sons, Copyright 2023.

applications of organic RTP materials such as radiation detection, X-ray imaging, radiotherapy, non-destructive testing, and X-ray astronomy.[105,106] (Fig. 24a). Gan *et al.*[105,106] obtained amorphous copolymers through the copolymerization of bromine-containing RTP-agents and acrylic acid for organic phosphorescent scintillation and the related emissive processes under X-ray irradiation (Fig. 24b and c). The developed polymeric scintillators were able to efficiently respond to X-rays and have a respectable PHQY of up to 51.4% at room temperature. To achieve simultaneous X-ray absorption and ISC, heavy atoms such as bromine and iodine are used in the design of X-ray detectable organic RTP materials (Fig. 24d and e).

At the end of this review, we have to mention that energy transfer from the singlet oxygen to solvent vibrations is an important temperature dependent process.[6,12,107] Since the RTP quenching by O_2 is accompanied by the singlet oxygen generation and quenching, all the temperature dependence studies should be considered in cooperation. In this respect, the role of high-frequency C–H, N–H and O–H vibrations could be considered since they determine the most active energy-accepting vibrational modes in the singlet oxygen quenching by solvents. The same vibrations could be important for the organic RTP quenching by matrixes and solvents (especially for orange and red RTP). This aspect of the RTP problem needs additional analysis.[12,107]

We also want to stress an important SOC peculiarity, which is almost forgotten in the vast modern literature on RTP problems. The quantum-chemical modelling of intermolecular interactions in host–guest (H–G) organic crystals indicates that at the typical H–G distances, even weak overlap between H–G molecular orbitals can induce the σ–π mixing inside the electronic shell of the planar phosphorescent guest molecule, which is sufficient for increasing SOC ME and notably diminishing the phosphorescence lifetime.[108,109] This internal magnetic effect is due to the appearance of one-centre contributions to the SOC integrals $\langle S_{\pi\pi^*}|H_{SO}|T_{\pi\pi^*}\rangle$.[108] High pressure and tight interactions in the polymer matrix led to shorter contacts and higher intermolecular overlap of the H–G orbitals, which increases the σ–π intramolecular mixing and induces stronger SOC perturbations inside the G chromophore responsible for the RTP.[6,108,109]

8. Conclusion and outlook

Organic RTP materials offer numerous benefits, such as energy-saving and environmental benefits. They can harvest emissive

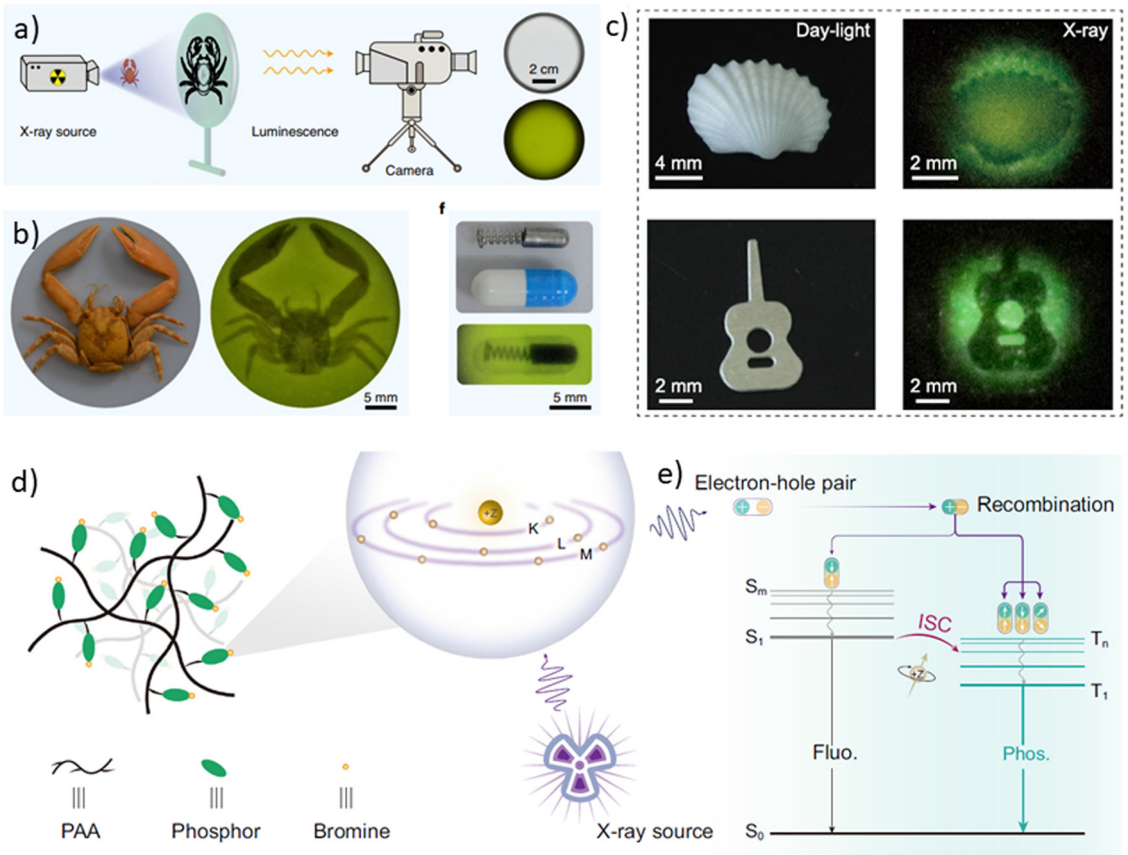

Fig. 24 Schematic visualization of a radiography set up (a), examples of the aplication of RTP-agent-based X-ray detectors containing RTP-agents with heavy atoms such as bromine or iodine (b) and (c), design strategy of X-ray detecteble organic RTP materials (d) and schematic mechanism of X-ray-irradiated RTP (e). Reproduced from ref. 105 and 106 with permission from Springer Nature. Copyright 2023.

triplets and do not contain any hazardous elements. These benefits allow the prediction of the usage of organic RTP materials in many fields of human activities including sensing and X-ray detection as well as lighting and photonic information technologies. However, in order to expand the fields of application of organic RTP materials, their efficiency, stability, and simplicity, there are still challenges that must be resolved.

Although fluorophores that have a phosphorescence quantum yield higher than 50% have been developed, many organic RTP materials have low efficiency because of weak spin–orbit coupling and high non-radiative decay rates of triplet states. Even the best examples exhibit phosphorescence quantum yields significantly lower than 100%. There are various methods to improve the efficiency of RTP luminophores, especially in the solid-state. For example, a polymer can interact with the molecules of a luminophore through specific non-covalent interactions, thereby facilitating the vibronic confinement of the luminophores. The most frequently exploited non-covalent perturbations are host–guest and charge-transfer interactions, hydrogen bonding, isolation from oxygen, and suppression of internal vibrational movements. The latter type of perturbation can shift vibration frequency and destroy resonances that are typically associated with free luminophores. All confinements produced by polymer matrices or by other hosts introduce perturbations to the electronic–vibrational coupling and thus a subtle regulation of non-radiative relaxation processes. At a higher pressure and tighter interactions in the polymer matrices the shorter contacts and the higher intermolecular MO overlap occur, which increases the σ–π intramolecular mixing and leads to stronger SOC perturbations inside the RTP chromophore.

Significant attention should be paid to the role of a host matrix in ensuring/improving/tuning the RTP properties of a guest compound. The main task of hosts for RTP luminophores is to provide an environment rigid enough to suppress molecular vibrations and to stabilize triplet excitons. For this reason, rigid polymers such as Zeonex, PS, PMMA, *etc.* are employed as hosts. This approach seems to be the simplest and the most easily available one.

More advanced technologies exploit hosting of RTP agents in supramolecular systems such as cucurbituril and cyclodextrin that act as cavities into which the guest molecules can fit. However, the role of a host matrix for organic RTP guests is not limited by the rigidification only. Engineering of host–guest systems to initiate energy/charge transfer seems to be the least studied. While the roles of hosts that promote charge/energy transfer to fluorescent and TADF emitters are widely investigated and discussed, the host–guest interactions in organic RTP systems are studied to considerably less extent. It is established

that triplet–triplet energy transfer (Dexter energy transfer determined by exchange interaction, eqn (1)) usually occurs when host and guest molecules have closely located triplet energy levels. Charge transfer in host–guest RTP systems is provided by closely located ^{1}CT and ^{3}CT excited states. Such systems are very scarce, because in this case rISC can easily prevail above ISC, thus initiating TADF instead of RTP; therefore, deeper theoretical insights as well as more experimental data are needed.

There are numerous problems related to organic RTP materials which have to be addressed in the future. For instance, these materials have limited RTP colours, mainly in the deep-blue to blue region due to colour purity issues arising from the broad emission spectra and overlap of fluorescence and phosphorescence. For lighting applications, efficient white emissions of organic RTP emitters with colour coordinates close to that of natural white (0.33, 0.33) have to be developed. In several instances, it is possible to achieve white emission of organic RTP emitters by applying external stimuli such as pressure or oxygen quenching.

Most organic RTP materials are prone to being quenched by molecular oxygen and moisture, which leads to the deactivation of the triplet states and a reduction in both phosphorescence lifetime and intensity.[105] In order to improve the efficiency of organic RTP materials, it is important to develop hosts with low oxygen and water permeability and effective encapsulation methods. On the other hand, utilizing intricate fabrication techniques such as crystallization, polymerization, or rigid matrix formation to achieve efficient RTP emission can result in poor processability and reproducibility.

Low stability and durability are also issues associated with organic RTP materials. Many RTP materials are prone to degradation under ambient conditions or UV excitation, which can affect their phosphorescence efficiency and lifetime. The mechanism of RTP of organic materials is still not fully understood since it can be affected by several factors such as molecular structure, intermolecular interactions, energy transfer, and exciplex formation. Extensive research has still to be conducted on RTP compounds to gain a better understanding of how their structure and properties are related.

In this article, we reviewed the fluorescence and phosphoresence quantum yields, lifetimes, colour purity, and the wavelengths of intensity maxima of organic RTP materials. However, it is difficult to directly compare the photophysical parameters of the reported compounds since they were investigated under different conditions (in either an amorphous or a crystalline phase, in hosts or in neat films, and in air or in an inert atmosphere). To date, there has been no unified standard or method for the estimation and comparison of RTP of different organic materials. The terms phosphorescence, long pristine luminescence, long-lived afterglow, ultralong organic phosphorescence, ultralong organic luminescence, and room temperature phosphorescence are often used for the characterization of the same phenomenon.

Poor water solubility and biocompatibility of many hydrophobic and insoluble in water RTP materials limits their applications in aqueous environments and biological systems. Many RTP materials have low RTP efficiency and stability in solutions due to the collisional quenching, molecular motions, and oxygen diffusion. Some RTP compounds have low photostability and photobleaching resistance due to the photochemical degradation or oxidation of the chromophores under prolonged or intense irradiation. This can reduce their phosphorescence intensity and lifetime over time. These factors can reduce the intersystem crossing rate and increase the non-radiative decay rate of the triplet state. In addition, certain RTP materials possess cytotoxic or phototoxic properties that can cause damage to living cells or tissues, limiting bioimaging applications.

Although organic RTP materials have shown promise in chemical and physical sensors, such as optical sensors of oxygen and temperature, many of these materials exhibit a weak or non-existent response to external stimuli such as pH, metal ions, and biomolecules. This limitation reduces their potential applications in sensing and imaging. Moreover, some RTP materials are characterized by poor reversibility or reproducibility of their response, which affects the accuracy and reliability of the devices. Many RTP materials have similar molecular structures or design strategies, which limit their diversity and functionality.

We anticipate that the efficiency, stability, and cost-efficiency of the synthesis of organic RTP materials will be improved, enabling the discovery of chemical and physical approaches to better meet the requirements of both the known and forthcoming applications.

Conflicts of interest

There are no conflicts to declare.

Acknowledgements

This work has received funding from the Research Council of Lithuania (LMTLT), agreement no. S-MIP-23-50, from the Ministry of Science and Education of Ukraine (project 0122U000760), the Swedish Wenner-Gren Foundations (project no. GFU 2022-0036) and the Swedish Natural Science Research Council (Dnr 2022-03405).

References

1 R. C. Sharma, R. Nandal, N. Tanwar, R. Yadav, J. Bhardwaj and A. Verma, *J. Phys.: Conf. Ser.*, 2023, **2426**, 012008.
2 K. J. Yu, Z. Yan, M. Han and J. A. Rogers, *npj Flexible Electron.*, 2017, **1**, 1–14.
3 M. A. Baldo, D. F. O'Brien, Y. You, A. Shoustikov, S. Sibley, M. E. Thompson and S. R. Forrest, *Nature*, 1998, **395**, 151–154.
4 J. Gibson, A. P. Monkman and T. J. Penfold, *ChemPhysChem*, 2016, **17**, 2956–2961.
5 Kenry, C. Chen and B. Liu, *Nat. Commun.*, 2019, **10**, 1–15.
6 G. Baryshnikov, B. Minaev and H. Ågren, *Chem. Rev.*, 2017, **117**, 6500–6537.
7 Y. Gong, J. Yang, M. Fang and Z. Li, *Cell Rep. Phys. Sci.*, 2022, **3**, 100663.

8 Y. Patil, C. Demangeat and L. Favereau, *Chirality*, 2023, **35**(7), 390–410.
9 M. Singh, K. Liu, S. Qu, H. Ma, H. Shi, Z. An and W. Huang, *Adv. Opt. Mater.*, 2021, **9**, 2002197.
10 H. E. Hackney and D. F. Perepichka, *Aggregate*, 2022, **3**, e123.
11 B. F. Minaev, *Chem. Phys.*, 2017, **483–484**, 84–95.
12 H. Uoyama, K. Goushi, K. Shizu, H. Nomura and C. Adachi, *Nature*, 2012, **492**, 234–238.
13 A. Monkman, *ACS Appl. Mater. Interfaces*, 2022, **14**(18), 20463–20467.
14 C. R. Wang, Y. Y. Gong, W. Z. Yuan and Y. M. Zhang, *Chin. Chem. Lett.*, 2016, **27**, 1184–1192.
15 M. Han, Z. Xu, J. Lu, Y. Xie, Q. Li and Z. Li, *Mater. Chem. Front.*, 2021, **6**, 33–39.
16 L. Deng, Z. Ma, J. Zhou, L. Chen, J. Wang, X. Qiao, D. Hu, D. Ma, J. Peng and Y. Ma, *Chem. Eng. J.*, 2022, **449**, 137834.
17 N. Xie, H. Yu, J. Wang, Z. Li, J. Wei and Y. Wang, *J. Phys. Chem. C*, 2021, **125**, 27489–27496.
18 Z. Cong, M. Han, Y. Fan, Y. Fan, K. Chang, L. Xiao, Y. Zhang, X. Zhen, Q. Li and Z. Li, *Mater. Chem. Front.*, 2022, **6**, 1606–1614.
19 Y. Miao, L. Ma, J. Lv, S. Liu, W. Yang and J. Li, *Anal. Chem.*, 2021, **93**, 4075–4083.
20 M. Jian, Z. Song, X. Chen, J. Zhao, B. Xu and Z. Chi, *Chem. Eng. J.*, 2022, **429**, 132346.
21 Y. Zhang, H. Li, M. Yang, W. Dai, J. Shi, B. Tong, Z. Cai, Z. Wang, Y. Dong and X. Yu, *Chem. Commun.*, 2023, **59**, 5329–5342.
22 W. Sun, B. Shi, Z. Xia and C. Lü, *Mater. Today Chem.*, 2023, **27**, 101297.
23 M. Li, X. Cai, Z. Chen, K. Liu, W. Qiu, W. Xie, L. Wang and S. J. Su, *Chem. Sci.*, 2021, **12**, 13580–13587.
24 B. He, Z. Chang, Y. Jiang, X. Xu, P. Lu, H. S. Kwok, J. Zhou, H. Qiu, Z. Zhao and B. Z. Tang, *Dyes Pigm.*, 2014, **106**, 87–93.
25 Y. Dai, H. Liu, T. Geng, R. Duan, X. Li, Y. Liu, W. Liu, B. G. He, L. Sui, K. Wang, B. Zou, B. Yang and Y. Qi, *J. Mater. Chem. C*, 2023, **11**, 4892–4898.
26 Z. Yang, Z. Fu, H. Liu, M. Wu, N. Li, K. Wang, S.-T. Zhang, B. Zou and B. Yang, *Chem. Sci.*, 2023, **14**, 2640–2645.
27 S. Wang, H. Shu, X. Han, X. Wu, H. Tong and L. Wang, *J. Mater. Chem. C*, 2021, **9**, 9907–9913.
28 D. R. Lee, J. Park and J. Y. Lee, *Org. Electron.*, 2022, **106**, 106534.
29 Z. Ma, Z. Yang, L. Mu, L. Deng, L. Chen, B. Wang, X. Qiao, D. Hu, B. Yang, D. Ma, J. Peng and Y. Ma, *Chem. Sci.*, 2021, **12**, 14808–14814.
30 L. Tu, Y. Fan, C. Bi, L. Xiao, Y. Li, A. Li, W. Che, Y. Xie, Y. Zhang, S. Xu, W. Xu, Q. Li and Z. Li, *Sci. China: Chem.*, 2023, **66**, 816–825.
31 Y. Tian, J. Yang, Z. Liu, M. Gao, X. Li, W. Che, M. Fang and Z. Li, *Angew. Chem., Int. Ed.*, 2021, **60**, 20259–20263.
32 Y. Wang, J. Yang, M. Fang, Y. Gong, J. Ren, L. Tu, B. Zhong Tang, Z. Li, Y. Wang, J. Yang, M. Fang, Y. Gong, J. Ren, L. Tu, B. Z. Tang and Z. Li, *Adv. Funct. Mater.*, 2021, **31**, 2101719.
33 N. Acharya, M. Hasan, S. Dey, S.-C. Lo, E. B. Namdas and D. Ray, *Adv. Photonics Res.*, 2021, **2**, 2000201.
34 E. Skuodis, K. Leitonas, A. Panchenko, L. Volyniuk, J. Simokaitienė, R. Keruckienė, D. Volyniuk, B. F. Minaev and J. V. Gražulevičius, *Sens. Actuators, B*, 2022, **373**, 132727.
35 R. Keruckiene, N. Kusas, L. Dvylys, E. Skuodis, V. E. Matulis, E. G. Ragoyja, D. A. Lyakhov, I. Klymenko and J. V. Grazulevicius, *J. Lumin.*, 2022, **241**, 118502.
36 S. Shen, G. V. Baryshnikov, Q. Xie, B. Wu, M. Lv, H. Sun, Z. Li, H. Ågren, J. Chen and L. Zhu, *Chem. Sci.*, 2023, **14**, 970–978.
37 S. Wang, Z. Cheng, X. Han, H. Shu, X. Wu, H. Tong and L. Wang, *J. Mater. Chem. C*, 2022, **10**, 5141–5146.
38 J. H. Kim, J. H. Yun and J. Y. Lee, *Adv. Opt. Mater.*, 2018, **6**(18), 1800255.
39 L. Tu, Y. Xie, Z. Li and B. Tang, *SmartMat*, 2021, **2**, 326–346.
40 Z. Liu, W. Shi, G. Hong, W. Chen, B. Song, X. Peng, X. Xiong and F. Song, *J. Controlled Release*, 2019, **310**, 1–10.
41 A. Amaro-Ortiz, B. Yan and J. A. D'Orazio, *Molecules*, 2014, **19**, 6202.
42 Q. Zhang, X. Wang and Y. Wang, *Inorg. Chem. Front.*, 2020, **7**, 1034–1045.
43 L. Li, Q. Zhang, C. Han, X. Sun, T. Xing, M. Wang, M. Wu, N. Weeranoppanant and W. Wu, *J. Phys. Chem. C*, 2023, **127**, 12586–12592.
44 G. D. Gutierrez, G. T. Sazama, T. Wu, M. A. Baldo and T. M. Swager, *J. Org. Chem.*, 2016, **81**, 4789–4796.
45 H. Shi, L. Zou, K. Huang, H. Wang, C. Sun, S. Wang, H. Ma, Y. He, J. Wang, H. Yu, W. Yao, Z. An, Q. Zhao and W. Huang, *ACS Appl. Mater. Interfaces*, 2019, **11**, 18103–18110.
46 T. Ishi-I, R. Kichise, I. S. Park, T. Yasuda and T. Matsumoto, *J. Mater. Chem. C*, 2023, **11**, 3003–3009.
47 Z. Xu, Q. T. Liu, X. Wang, Q. Liu, D. Hean, K. C. Chou and M. O. Wolf, *Chem. Sci.*, 2020, **11**, 2729–2734.
48 L. Xiao, Y. Wu, Z. Yu, Z. Xu, J. Li, Y. Liu, J. Yao and H. Fu, *Chem. – Eur. J.*, 2018, **24**, 1801–1805.
49 X. F. Wang, H. Xiao, P. Z. Chen, Q. Z. Yang, B. Chen, C. H. Tung, Y. Z. Chen and L. Z. Wu, *J. Am. Chem. Soc.*, 2019, **141**, 5045–5050.
50 Y. Huang, X. Zheng, Z. Yao, W. Lv, S. Xiang, Q. Ling and Z. Lin, *Chem. Eng. J.*, 2022, **444**, 136629.
51 L. Dziewit, M. Dmowski, J. Baj and D. Bartosik, *Appl. Environ. Microbiol.*, 2010, **76**, 1861–1869.
52 Y. Wen, S. Xiao, H. Liu, X. Tian, J. De, T. Lu, Z. Yang, D. Zou, Y. Lv, S. T. Zhang, Q. Su and B. Yang, *J. Mater. Chem. C*, 2021, **9**, 17511–17517.
53 S. M. A. Fateminia, Z. Mao, S. Xu, Z. Yang, Z. Chi and B. Liu, *Angew. Chem., Int. Ed.*, 2017, **56**, 12160–12164.
54 S. Sun, L. Ma, J. Wang, X. Ma and H. Tian, *Natl. Sci. Rev.*, 2022, **9**(2), nwab085.
55 S. Wang, J. Wang, Q. Huang, X. Zheng, Z. Yao, S. Xiang, Q. Ling and Z. Lin, *ACS Appl. Mater. Interfaces*, 2022, **14**, 14703–14711.
56 S. Garain, S. Kuila, B. C. Garain, M. Kataria, A. Borah, S. K. Pati and S. J. George, *Angew. Chem., Int. Ed.*, 2021, **60**, 12323–12327.

57 H. Sun and L. Zhu, *Aggregate*, 2023, **4**, e253.
58 X. Wang, Z. Wang, H. Feng, C. Lin, H. Shi, Z. An, Z. M. Su and F. S. Liang, *Chem. Commun.*, 2022, **58**, 3641–3644.
59 Y. Chen, Y. Xie and Z. Li, *J. Phys. Chem. Lett.*, 2022, **13**, 1652–1659.
60 L. Xu, G. Li, T. Xu, W. Zhang, S. Zhang, S. Yin, Z. An and G. He, *Chem. Commun.*, 2018, **54**, 9226–9229.
61 Y. Tao, C. Liu, Y. Xiang, Z. Wang, X. Xue, P. Li, H. Li, G. Xie, W. Huang and R. Chen, *J. Am. Chem. Soc.*, 2022, **144**, 6946–6953.
62 Y. Tao, C. Liu, Y. Xiang, Z. Wang, X. Xue, P. Li, H. Li, G. Xie, W. Huang and R. Chen, *J. Am. Chem. Soc.*, 2022, **144**, 6946–6953.
63 T. M. Figueira-Duarte and K. Müllen, *Chem. Rev.*, 2011, **111**, 7260–7314.
64 F. Xiao, H. Gao, Y. Lei, W. Dai, M. Liu, X. Zheng, Z. Cai, X. Huang, H. Wu and D. Ding, *Nat. Commun.*, 2022, **13**, 1–10.
65 T. Ono, K. Kimura, M. Ihara, Y. Yamanaka, M. Sasaki, H. Mori and Y. Hisaeda, *Chem. – Eur. J.*, 2021, **27**, 9535–9541.
66 A. Nowak-Król, K. Shoyama, M. Stolte and F. Würthner, *Chem. Commun.*, 2018, **54**, 13763–13772.
67 Y. Li, X. Li, T. Yu, W. Su, Y. Wang, Y. Zhao and H. Zhang, *Dyes Pigm.*, 2020, **172**, 107803.
68 Ł. Balewski, F. Sączewski, M. Gdaniec, A. Kornicka, K. Cicha and A. Jalińska, *Molecules*, 2019, **24**, 4070.
69 J. Wang, G. Zhang, Z. Liu, X. Gu, Y. Yan, C. Zhang, Z. Xu, Y. Zhao, H. Fu and D. Zhang, *Tetrahedron*, 2013, **69**, 2687–2692.
70 L. Chen, W. Xiong, Y. Ma, J. Y. Ge, N. Lv, X. Wu, J. Chen and Z. Chen, *Chem. – Eur. J.*, 2023, **29**, e202202909.
71 S. Reineke, M. Thomschke, B. Lüssem and K. Leo, *Rev. Mod. Phys.*, 2013, **85**, 1245–1293.
72 H. Liu, Y. Fu, B. Z. Tang and Z. Zhao, *Nat. Commun.*, 2022, **13**, 1–11.
73 J. C. Del Valle and J. Catalán, *Phys. Chem. Chem. Phys.*, 2019, **21**, 10061–10069.
74 V. Anand, R. Mishra and Y. Barot, *Dyes Pigm.*, 2021, **191**, 109390.
75 X. Zheng, Y. Huang, D. Xiao, S. Yang, Z. Lin and Q. Ling, *Mater. Chem. Front.*, 2021, **5**, 6960–6968.
76 N.-N. Zhang, C. Sun, X.-M. Jiang, X.-S. Xing, Y. Yan, L.-Z. Cai, M.-S. Wang, G.-C. Guo and R. Li, *Chem. Commun.*, 2017, **53**, 9269.
77 B. Xu, H. Wu, J. Chen, Z. Yang, Z. Yang, Y. C. Wu, Y. Zhang, C. Jin, P. Y. Lu, Z. Chi, S. Liu, J. Xu and M. Aldred, *Chem. Sci.*, 2017, **8**, 1909–1914.
78 Y. Sun, H. Qu, J. Zhang, X. Duan and X. Zhang, *Tetrahedron*, 2022, **110**, 132692.
79 H. Shu, L. Chen, X. Wu, T. Wang, S. Wang, H. Tong and L. Wang, *J. Mater. Chem. C*, 2022, **10**, 1833–1838.
80 J. Liu, Z. Ma, Z. Li, Y. Liu, X. Fu, H. Jiang, Z. Ma and X. Jia, *J. Mater. Chem. C*, 2021, **9**, 3257–3263.
81 X. Bi, Y. Shi, T. Peng, S. Yue, F. Wang, L. Zheng, Q.-E. Cao, X. Bi, Y. Shi, S. Yue, L. Zheng, Q. Cao, T. Peng and F. Wang, *Adv. Funct. Mater.*, 2021, **31**, 2101312.
82 M. Du, Y. Shi, Q. Zhou, Z. Yin, L. Chen, Y. Shu, G. Y. Sun, G. Zhang, Q. Peng and D. Zhang, *Adv. Sci.*, 2022, **9**(5), 2104539.
83 T. Ishi-I, H. Tanaka, I. S. Park, T. Yasuda, S. I. Kato, M. Ito, H. Hiyoshi and T. Matsumoto, *Chem. Commun.*, 2020, **56**, 4051–4054.
84 X. Ma, L. Jia, B. Yang, J. Li, W. Huang, D. Wu and W. Y. Wong, *J. Mater. Chem. C*, 2021, **9**, 727–735.
85 L. Volyniuk, D. Gudeika, A. A. Panchenko, B. F. Minaev, M. Mahmoudi, J. Simokaitiene, A. Bucinskas, D. Volyniuk and J. V. Grazulevicius, *ACS Sustainable Chem. Eng.*, 2023, **11**, 16914–16925.
86 H. Thomas, D. L. Pastoetter, M. Gmelch, T. Achenbach, A. Schlögl, M. Louis, X. Feng, S. Reineke, H. Thomas, M. Gmelch, T. Achenbach, A. Schlögl, M. Louis, S. Reineke, D. L. Pastoetter and X. Feng, *Adv. Mater.*, 2020, **32**, 2000880.
87 M. Louis, H. Thomas, M. Gmelch, F. Fries, A. Haft, J. Lindenthal and S. Reineke, *Adv. Opt. Mater.*, 2020, **8**, 2000427.
88 Z. Yang, S. Zhao, X. Zhang, M. Liu, H. Liu and B. Yang, *Front. Chem.*, 2022, **9**, 810304.
89 Y. Li, G. V. Baryshnikov, F. Siddique, P. Wei, H. Wu and T. Yi, *Angew. Chem., Int. Ed.*, 2022, **61**, e202213051.
90 H. Liu, W. Ye, Y. Mu, H. Ma, A. Lv, S. Han, H. Shi, J. Li, Z. An, G. Wang, W. Huang, H. Liu, Y. Mu, S. Han, J. Li, G. Wang, W. Ye, H. Ma, A. Lv, H. Shi, Z. An and W. Huang, *Adv. Mater.*, 2022, **34**, 2107612.
91 X. Yao, H. Ma, X. Wang, H. Wang, Q. Wang, X. Zou, Z. Song, W. Jia, Y. Li, Y. Mao, M. Singh, W. Ye, J. Liang, Y. Zhang, Z. Liu, Y. He, J. Li, Z. Zhou, Z. Zhao, Y. Zhang, G. Niu, C. Yin, S. Zhang, H. Shi, W. Huang and Z. An, *Nat. Commun.*, 2022, **13**, 1–8.
92 J. Wang, X. Y. Lou, Y. Wang, J. Tang and Y. W. Yang, *Macromol. Rapid Commun.*, 2021, **42**, 2100021.
93 Z. Wang, X. Cheng, Y. Xie, S. Liu, M. Dong, J. Zhao, F. Liang, Z. An and W. Huang, *CCS Chem.*, 2023, **5**, 292–309.
94 X. Wei, J. Yang, L. Hu, Y. Cao, J. Lai, F. Cao, J. Gu and X. Cao, *J. Mater. Chem. C*, 2021, **9**, 4425–4443.
95 L. Ma and X. Ma, *Sci. China: Chem.*, 2022, **66**, 304–314.
96 M. Ji and X. Ma, *Ind. Chem. Mater.*, 2023, **1**, 582–594.
97 S. Guo, W. Dai, X. Chen, Y. Lei, J. Shi, B. Tong, Z. Cai and Y. Dong, *ACS Mater. Lett.*, 2021, **3**, 379–397.
98 X. Zou, N. Gan, M. Dong, W. Huo, A. Lv, X. Yao, C. Yin, Z. Wang, Y. Zhang, H. Chen, H. Ma, L. Gu, Z. An and W. Huang, *Adv. Mater.*, 2023, **35**, 2210489.
99 L. Xu, Y. Mo, N. Su, C. Shi, N. Sun, Y. Zhang, L. Duan, Z. H. Lu and J. Ding, *Nat. Commun.*, 2023, **14**, 1–9.
100 H. F. Higginbotham, M. Okazaki, P. De Silva, S. Minakata, Y. Takeda and P. Data, *ACS Appl. Mater. Interfaces*, 2021, **13**, 2899–2907.
101 T. Hosono, N. O. Decarli, P. Z. Crocomo, T. Goya, L. E. de Sousa, N. Tohnai, S. Minakata, P. de Silva, P. Data and Y. Takeda, *J. Mater. Chem. C*, 2022, **10**, 4905–4913.
102 K. Leitonas, A. Tomkeviciene, G. Baratte, A. Dabuliene, S. M. Punniyakoti, D. Volyniuk and J. V. Grazulevicius, *Sens. Actuators, B*, 2021, **345**, 130369.

103 M. Gmelch, T. Achenbach, A. Tomkeviciene, S. Reineke, M. Gmelch, T. Achenbach and S. Reineke, *Adv. Sci.*, 2021, **8**, 2102104.

104 A. Kirch, T. Bärschneider, T. Achenbach, F. Fries, M. Gmelch, R. Werberger, C. Guhrenz, A. Tomkevičienė, J. Benduhn, A. Eychmüller, K. Leo, S. Reineke, A. Kirch, T. Bärschneider, T. Achenbach, F. Fries, M. Gmelch, R. Werberger, A. Tomkevičienė, J. Benduhn, K. Leo, S. Reineke, C. Guhrenz and A. Eychmüller, *Adv. Mater.*, 2022, **34**, 2205015.

105 X. Wang, H. Shi, H. Ma, W. Ye, L. Song, J. Zan, X. Yao, X. Ou, G. Yang, Z. Zhao, M. Singh, C. Lin, H. Wang, W. Jia, Q. Wang, J. Zhi, C. Dong, X. Jiang, Y. Tang, X. Xie, Y. Yang, J. Wang, Q. Chen, Y. Wang, H. Yang, G. Zhang, Z. An, X. Liu and W. Huang, *Nat. Photonics*, 2021, **15**, 187–192.

106 N. Gan, X. Zou, M. Dong, Y. Wang, X. Wang, A. Lv, Z. Song, Y. Zhang, W. Gong, Z. Zhao, Z. Wang, Z. Zhou, H. Ma, X. Liu, Q. Chen, H. Shi, H. Yang, L. Gu, Z. An and W. Huang, *Nat. Commun.*, 2022, **13**, 1–8.

107 M. Bregnhøj, M. Westberg, B. F. Minaev and P. R. Ogilby, *Acc. Chem. Res.*, 2017, **50**, 1920–1927.

108 B. F. Minaev and A. F. Terpugova, *Soviet Phys. J.*, 1969, **12**, 1260–1263.

109 H. Wu, L. Gu, G. V. Baryshnikov, H. Wang, B. F. Minaev, H. Ågren and Y. Zhao, *ACS Appl. Mater. Interfaces*, 2020, **12**, 20765–20774.

